[redacted]

111 p.

Code [redacted]

OPTICAL CONSTANTS OF METALS IN THE FAR ULTRAVIOLET AND THEIR RELATION TO ENERGY BAND STRUCTURE

written by

Luke Steven Gournay

Principal Investigator: William A. Rense

UNIVERSITY OF COLORADO
Laboratory for Atmospheric and Space Physics
Boulder, Colorado

2047009

SCIENTIFIC REPORT NO. 1

Air Force Contract No. AF 19(628)-287

N.A.S.A. Contract No. NASr 86

1 May 1963

Period covered

June, 1962 - May, 1963

Prepared for

ELECTRONIC SYSTEMS DIVISION
AIR FORCE SYSTEMS COMMAND
LAURENCE G. HANSCOM FIELD
BEDFORD, MASSACHUSETTS

and

NATIONAL AERONAUTICS AND SPACE ADMINISTRATION
WASHINGTON 25, D. C.

[redacted]

ABSTRACT

~~14573~~ 16327

The real and imaginary components of the indices of refraction, the optical constants, of silver, a silver-indium alloy, gold, gold-aluminum alloys, and aluminum have been studied in the wavelength range of 304 to 1671 A.

Electrical conductivity as derived from the optical constants is shown to be related to interband transitions in these metals. A model has been constructed which permits computation of conductivity on the basis of these transitions and the energy band structure of the metal. The effectiveness of this model is shown for the metals studied.

Analysis of results for silver indium alloys indicate a breakdown of the rigid band concept. A Fermi surface which has less contact at the Brillouin zone faces and a less distorted shape is indicated for the alloy. The modified energy band structure is presented and discussed.

The relation between the energy gap at Brillouin zone faces and the interband transition probability is developed and data are presented which demonstrate its relative importance.

Author

OPTICAL CONSTANTS OF METALS IN THE FAR ULTRAVIOLET
AND THEIR RELATION TO ENERGY BAND STRUCTURE

written by

Luke Steven Gournay

Principal Investigator: William A. Rense

UNIVERSITY OF COLORADO
Laboratory for Atmospheric and Space Physics
Boulder, Colorado

SCIENTIFIC REPORT NO. 1

Air Force Contract No. AF 19(628)-287

N.A.S.A. Contract No. NASr 86

1 May 1963

Period covered

June, 1962 - May, 1963

Prepared for

ELECTRONIC SYSTEMS DIVISION
AIR FORCE SYSTEMS COMMAND
LAURENCE G. HANSCOM FIELD
BEDFORD, MASSACHUSETTS

and

NATIONAL AERONAUTICS AND SPACE ADMINISTRATION
WASHINGTON 25, D. C.

[redacted]

ACKNOWLEDGMENTS

The author wishes to acknowledge the constant encouragement and guidance of Professor William A. Rense, not only in the course of this research but also throughout the period of graduate study. Sincere appreciation is also extended to Professors W. F. Love and S. C. Miller and Dr. E. A. Todd for helpful discussions and to Mr. Jim Austin of the Laboratory for Atmospheric and Space Physics for his kind assistance and advice in the production of thin films.

Research funds for part of this work were made available under Air Force Contract No. AF 19(628)-287 and N.A.S.A. Contract No. NASr 86.

Special acknowledgment is extended to the management of the Socony Mobil Oil Company and the Field Research Laboratory for the grant of an Incentive Fellowship which made this educational opportunity possible.

TABLE OF CONTENTS

CHAPTER		PAGE
	ACKNOWLEDGMENTS	iii
I.	INTRODUCTION	1
II.	THEORY - CLASSICAL	4
	A. Maxwell's Equations and Optical Constants	4
	B. Drude, Zener, Kronig Free Electron Gas	9
III.	QUANTUM MECHANICAL TREATMENT OF OPTICAL PROPERTIES	14
	A. Free Electron Model	14
	B. Band Theory and Brillouin Zones	18
	C. Interaction Between Electron and Electromagnetic Radiation	27
	D. Band Structure and Optical Constants	30
IV.	EXPERIMENTAL RESULTS AND DISCUSSION	38
	A. Results for Pure Silver	38
	B. Silver-Indium Alloy	52
	C. Results for Gold	69
	D. Gold-Aluminum Alloys	79
	E. Results for Aluminum	89
	F. Possible Future Work	96
V.	EXPERIMENTAL APPARATUS AND METHODS	97
	A. Monochromator and Reflectometer	97
	B. Thin Film Production	98
	C. Data Reduction and Analysis	100
BIBLIOGRAPHY		103

LIST OF TABLES

TABLE PAGE

I. Silver Reflectivity Data. 40

II. Data Used in Silver Computation (Equation 66). 47

III. Electron/Atom Ratio at α-Phase Boundary for Several Alloys. 53

IV. Silver-Indium Reflectivity Data 59

V. Data Used in Ag-In Computation (Equation 66) 67

VI. Gold Reflectivity Data 72

VII. Data Used for Gold Computation (Equation 66, Figure 23) 76

VIII. Gold Reflectivity at 304A, $\phi = 10°$, for Various Concentrations of Aluminum. 80

IX. Gold-Aluminum Reflectivity Data (Au-Al-8, 3.38 wt % Al) 85

X. Gold-Aluminum Reflectivity Data (Au-Al-10, 4.3 wt % Al) 87

XI. Data Used in Aluminum Computation (Equation 66) 93

LIST OF FIGURES

FIGURE PAGE

1. Optical constant curves for two choices of polarization of incident beam 8
2. Reflectivity vs. extinction coefficient at normal incidence. 10
3. Relation between n and k for constant reflectivity and normal incidence. 11
4. Kronig-Penney one-dimensional model. 20
5. The allowed values of βa given by equation (30) for a fixed value of P 20
6. First brillouin zone for face-centered cubic lattice 24
7. "Vertical" transitions in reduced zone scheme. 28
8. Discs in k-space from which inter-band transitions can occur. 32
9. Conductivity vs. wavelength for a monovalent metal having free electrons. 36
10. Reflectivity of silver vs. wavelength for four angles of incidence 39
11. Silver conductivity vs. wavelength 42
12. Energy band structure for silver 44
13. Fermi surface for silver from Segall's calculations 45
14. $(1 - \frac{m}{3m^*})$ for two zone directions in silver. 49
15. Conductivity of silver vs. wavelength. 50
16. Density of states, g(E), for fcc and bcc lattices, as a function of energy. 54
17. Optical absorptivity vs. wavelength. 56

FIGURE PAGE

18. Reflectivity of AgIn alloy (10 at .% In) vs. wavelength 58
19. Conductivity of Ag and AgIn alloy vs. wavelength. 61
20. Conductivity of AgIn alloy and free electron model 63
21. Estimated Fermi surface for AgIn alloy. 65
22. AgIn conductivity vs. wavelength 66
23. Reflectivity of gold vs. wavelength 71
24. Conductivity of gold vs. wavelength 74
25. Energy band structure for gold 75
26. Fermi surface for gold from ultrasonic attenuation measurements 77
27. Reflectivity of film #AuAl-8, (22.6 at .%Al) vs. wavelength. 81
28. Reflectivity of film #AuAl-10, (24.6 at .%Al) vs. wavelength 82
29. Conductivity of Au and AuAl alloy vs. wavelength 84
30. Fermi surface for aluminum 90
31. Fermi surface for aluminum 91
32. Conductivity of aluminum vs. wavelength. 92
33. Conductivity of aluminum film as a function of age of film. 95
34. Effect of errors in reflectivity on n-k curves for silver at 1671A. 101

CHAPTER I

INTRODUCTION

In the region of visible radiation most metals can be described optically as having high reflectivity and low transmissivity. These properties can be defined in a more quantitative manner with the introduction of two quantities: the index of refraction, n, and the extinction coefficient, k. The index, n, is usually defined as the ratio of the velocity of light in vacuo to the velocity of propagation in the medium under consideration, while the coefficient k is related to the rate of absorption of energy from the incident beam of radiation.

In most non-conductors k is essentially zero, but in metals it is usually the dominant factor of reflectivity and may assume values much greater than n. These optical constants have attracted considerable attention from the time of the formulation of Maxwell's equations. Indeed, the latter can be written to include these constants in a complex index of refraction defined as $N = n - ik$. It should be noted that the appellation "optical constant" is somewhat a misnomer because both n and k are distinctly functions of the frequency of radiation.

When Maxwell's equations are written in terms of the complex index, an expression for the electric field inside the metal is obtained which includes an exponential attenuation factor:

$$(1) \quad \overrightarrow{E(\vec{r})} = \vec{E}_o(\vec{r})\, e^{-\frac{k\omega}{c}\vec{r}\cdot\hat{q}}\; e^{-i\omega\frac{n}{c}\vec{r}\cdot\hat{q}}\; e^{i\omega t}$$

where $\hat{q}$ is a unit vector in the direction of propagation. Since the intensity of the electromagnetic wave goes as the square of the electric vector, the decay of intensity with distance is given by the exponent

$4\pi k/\lambda$ where λ is the free space wavelength. This exponent is often referred to as the absorption coefficient.

Further manipulation of Maxwell's equations produces expressions for conductivity and dielectric constant in terms of the optical constants:

(2) $\sigma = nk\nu$, and $\kappa = n^2 - k^2$.

A determination of these constants therefore permits an evaluation of two important electrical quantities. However, conductivity and dielectric constant were also derived by Drude, Zener and Kronig[1] starting with the equation of motion for a free electron in an oscillating electric field. This strictly classical approach was found to give satisfactory results at wavelengths in the far infrared, but the theoretical predictions do not agree with experimental results in the region of visible and shorter wavelengths. At these frequencies, n and k are usually determined by means of absorption or reflection measurements and are then used to evaluate conductivity and dielectric constant by means of Equation (2).

In the far ultraviolet it is not unusual to find conductivities which exceed the Drude value by factors of several hundred, and we must resort to some other approach for an explanation of the observed phenomena.

The advent of quantum theory and the introduction soon thereafter of concepts such as energy bands in solids provided the foundation for radically new approaches to many physical problems, including that of the optical properties at short wavelengths. The work of Bloch, especially, supplied the basis for a quantum formulation of optical phenomena in solids. Chapter III presents a development of this formulation and suggests means of applyingit to quantities such as conductivity.

---

[1] F. Seitz, Modern Theory of Solids, McGraw-Hill Book Co., New York, 1940.

Although the quantum mechanical approach to this problem appears basically sound, its practical application has been hampered by the difficulties attendant to writing the wave function for the system of electrons in a metal. It is only in recent years that credible wave functions and energy level schemes have been devised for other than the simplest metals. The results discussed in Chapter IV are based on theoretical band structures which were calculated in the last two years.

The investigations presented here are those of the optical properties of several metals and their alloys and the relationship of these properties to the energy band structure of the metals. Included are measurements of n and k in the wavelength range where interband transitions occur and the calculation of conductivity from these constants. A model is introduced which permits the computation of conductivity from quantum mechanical principles and a comparison of the two results is used to analyze the band structure of the metals.

CHAPTER II

THEORY - CLASSICAL

A. Maxwell's Equations and Optical Constants

Consider a plane, electromagnetic wave traveling in the positive X direction, with $\vec{E} = E_y \hat{j}$, and $\vec{H} = H_z \hat{k}$, and assume a time dependence for $\vec{E}$ such that $\vec{E} = \vec{E}(x)\, e^{-i\omega t}$. Then the general wave equation can be written in MKS units as[1]

$$(1) \qquad \frac{\partial^2 \vec{E}}{\partial x^2} = -(\mu \epsilon \omega^2 + i\omega\mu\sigma)\vec{E} = -K^2\vec{E}, \text{ where,}$$

$\epsilon = \kappa\epsilon_o$, κ = the dielectric constant

$\mu = \kappa_m \mu_o$, κ_m = relative permeability

$K = \alpha - i\beta$.

As a solution to Equation (1) we have

$$(2) \qquad \vec{E} = \vec{E}_o\, e^{i(Kx - \omega t)} = \vec{E}_o\, e^{-\beta x}\, e^{i(\alpha x - \omega t)} .$$

The last equation can be written in terms of a complex index of refraction, N, by using the following relations

$$K = \frac{\omega}{c} N = \frac{2\pi}{\lambda_o} N$$

λ_o = free space wavelength

$K = (n - ik)$ = complex index of refraction

k = extinction coefficient .

---

[1]W. K. H. Panofsky and M. Phillips, Classical Electricity and Magnetism, Addison-Wesley Publishing Co., Reading, Mass., Chapter 11.

Then, in terms of a complex index, the electric and magnetic fields are

(3) $\vec{E} = \vec{E}_o\, e^{-i\omega(t - \frac{N}{c}x)}$, $\vec{H} = \vec{H}_o\, e^{-i\omega(t - \frac{N}{c}x)}$.

Recalling Maxwell's equations in the form

(4) $\vec{\nabla} X \vec{H} = \sigma E + \kappa\epsilon_o \frac{\partial \vec{E}}{\partial t}$

$\vec{\nabla} X \vec{E} = -\kappa_m \mu_o \frac{\partial \vec{H}}{\partial t}$

we can substitute for $\vec{E}$ and $\vec{H}$ in (4) from (3) and obtain

(5) $-i\omega \frac{N}{c} \vec{H} = (\sigma - i\omega\kappa\epsilon_o)\vec{E}$, and $i\omega \frac{N}{c} \vec{E} = i\omega\kappa_m \mu_o \vec{H}$.

If κ_m is set equal to unity, as is possible for many media, and the two equations in (5) are combined, the following relation results

(6) $\sigma - i\omega\kappa\epsilon_o = 2\omega\epsilon_o nk - i\omega\epsilon_o (n^2 - k^2)$.

Upon equating real and imaginary parts we obtain expressions for the conductivity and the dielectric constant of the medium:

(7) $\sigma = 2nk\epsilon_o\omega \qquad \kappa = n^2 - k^2$.

In cgs units these quantities are given as

(8) $\sigma = nk\nu \qquad \kappa = n^2 - k^2$.

Thus, the real and imaginary parts of the index of refraction are basic to both conductivity and dielectric constant.

Further application of Maxwell's equations with appropriate boundary conditions leads to the generalized Fresnel equations. For homogeneous, isotropic, semi-infinite media, these can be written as[2]

(9) $\frac{E''_s}{E_s} = - \frac{n\cos\theta - \cos\phi}{n\cos\theta + \cos\phi} = - \frac{\sin(\phi - \theta)}{\sin(\phi + \theta)}$

---

[2] Panofsky and Phillips, op. cit., p. 178.

(10) $$\frac{E''_p}{E_p} = -\frac{n\cos\phi - \cos\theta}{n\cos\phi + \cos\theta} = \frac{\tan(\phi - \theta)}{\tan(\phi + \theta)}$$

where

- s = that component of E perpendicular to plane of incidence
- p = that component of E parallel to plane of incidence
- ϕ = angle of incidence
- θ = angle of refraction .

Unprimed terms denote the incident electric field components and primed terms denote the reflected field components. Noting that the intensities of the reflected and refracted beams are proportional to the square of the wave amplitudes, the Fresnel equations can be used to obtain reflectivity in terms of the angle of incidence and the two components of the index of refraction, namely

(11) $$R_s = \frac{(a - \cos\phi)^2 + b^2}{(a + \cos\phi)^2 + b^2}$$

$$R_p = R_s \frac{a^2 + b^2 - 2a\sin\phi\tan\phi + \sin^2\phi\tan^2\phi}{a^2 + b^2 + 2a\sin\phi\tan\phi + \sin^2\phi\tan^2\phi}$$

where

- R_s = reflectivity of that component of $\vec{E}$ perpendicular to the plane of incidence
- R_p = reflectivity of that component of $\vec{E}$ parallel to the plane of incidence

$$a = \frac{1}{2}\left[(n^2 - k^2 - \sin^2\phi)^2 + 4n^2k^2\right]^{1/2} + \frac{1}{2}\left[n^2 - k^2 - \sin^2\phi\right]^{1/2}$$

$$b = \frac{1}{2}\left[(n^2 - k^2 - \sin^2\phi)^2 + 4n^2k^2\right]^{1/2} - \frac{1}{2}\left[n^2 - k^2 - \sin^2\phi\right]^{1/2} .$$

At normal incidence $\sin\phi = 0$ and we have

(12) $$R_s = R_p = \frac{(n-1)^2 + k^2}{(n+1)^2 + k^2} .$$

With these relations, therefore, one can obtain n and k for a medium if reflectivity measurements are performed at least at two different angles of incidence.

Inasmuch as algebraic solutions of these equations for n and k is not possible, various graphical and geometrical solutions have been proposed. In this work, the method of Tousey[3], as extended by Cole[4], was used to obtain n and k, given R and ϕ. Graphs of R versus n for constant k and ϕ were used to obtain pairs of values in an n-k plane. Plots of these values of n and k for two or more angles of incidence reveal a unique pair of n and k which satisfy the Fresnel equations.

For these results to be valid, the degree of polarization must be taken into consideration. We defined the degree of polarization of the incident beam as

$$P = \frac{I_p - I_s}{I_p + I_s} \tag{13}$$

and adopted a trial and error method in the solution of Equation 11 using various values of P. Experimentally, R was measured at four values of ϕ, (70°, 50°, 30°, and 10°), and n-k pairs were obtained for various choices of P. It was found that a most constant multiple intersection of the n-k curves resulted with a unique value of P. This value of P was then used to define the optical constants. Figure 1 shows two n-k graphs for gold at 1671A and demonstrates the effect of varying the value of P. Since the intersections of these four curves were influenced by errors of experiment and graphical interpolation, an average value was taken for the point of intersection with the most probable P.

Reflectivity as a quantity does not uniquely characterize a particular medium as to its conductivity, nor can the converse notion be

---

[3] R. J. Tousey, J. Opt. Soc. Am. <u>29</u>, 235, (1939).

[4] T. T. Cole, <u>Thesis</u>, University of Colorado, 1961.

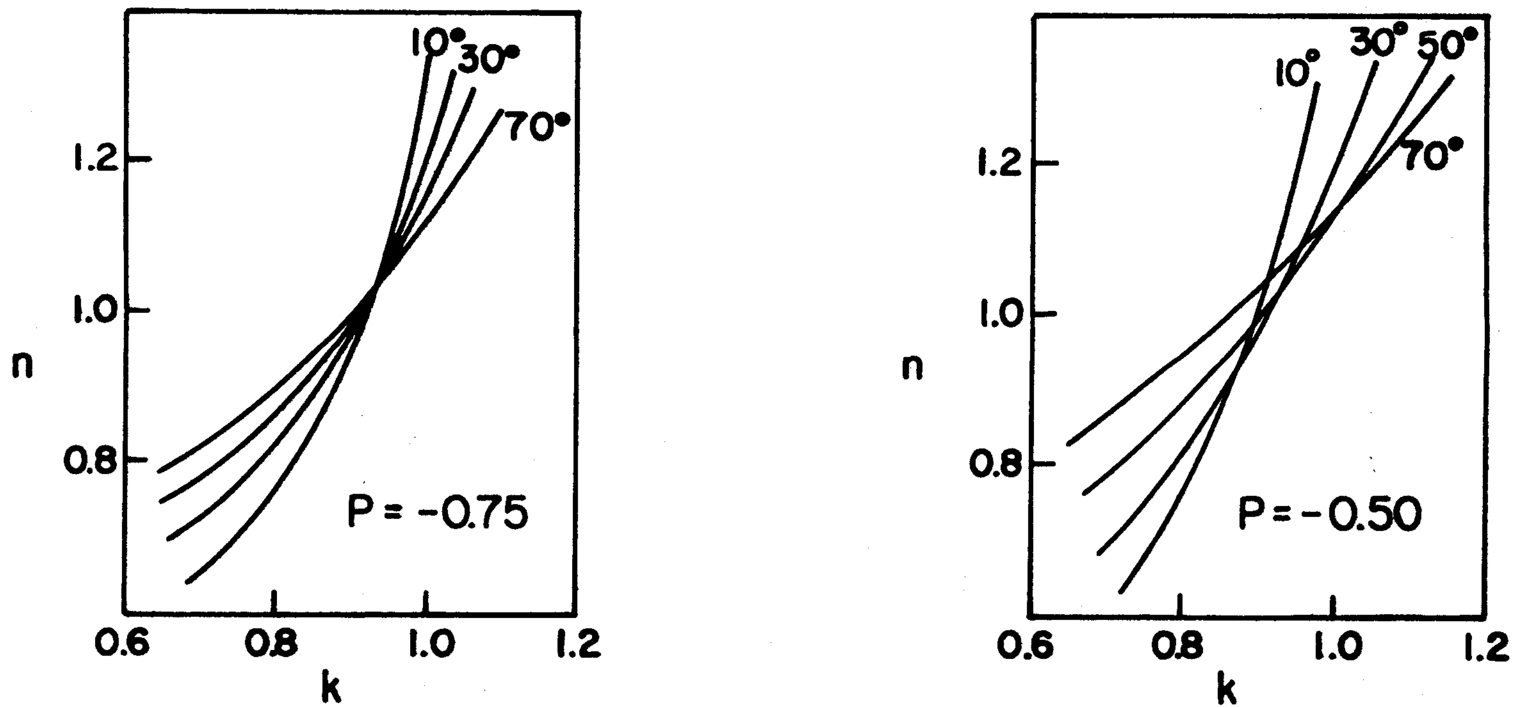

Figure 1
Optical Constant Curves for Two Choices of Polarization
of Incident Beam.

accepted. The quantities n and k appear to be more fundamental in this respect. Let us consider the expressions derived for conductivity and for reflectivity at normal incidence, equations (8) and (12). Using these relations, one can calculate R as a function of k for fixed n, and then construct a family of curves, each for a different value of n as in Figure 2. From this construct one can devise curves of iso-reflectivity for various combinations of n and k as in Figure 3. The two dashed curves represent lines of constant nk product, or lines of constant conductivity. In Figure 3 we can compare two media, A and B, which have different conductivities. In the example chosen, A has a lower conductivity than B but higher reflectivity, in contrast to the intuitive feeling that increased conductivity should lead to higher reflectivity. The same results can also be obtained for reflectivity at other than normal incidence.

B. Drude, Zener, Kronig Free Electron Gas

In this concept, the conduction electrons in a metal are assumed to be perfectly free and to move in a random manner. Their velocity distribution is governed by the laws of classical statistical mechanics, and they undergo collisions caused by thermal effects or structural imperfections in the lattice. In the absence of any external forces their average velocity is

$$\vec{v}_a = \frac{1}{N} \sum_{i=1}^{N} \vec{v}_i \tag{14}$$

At equilibrium, $\vec{v}_a$ will be zero since there will be just as many electrons moving in one direction as in the opposite direction.

Because of the collisions which occur one must introduce a relaxation time into the equations of motion of the electrons. This relaxation time, τ, will be closely related to the average time of flight between collisions and appears as a damping term in the equations.

The equation of motion for a free electron in the presence of an electric field is

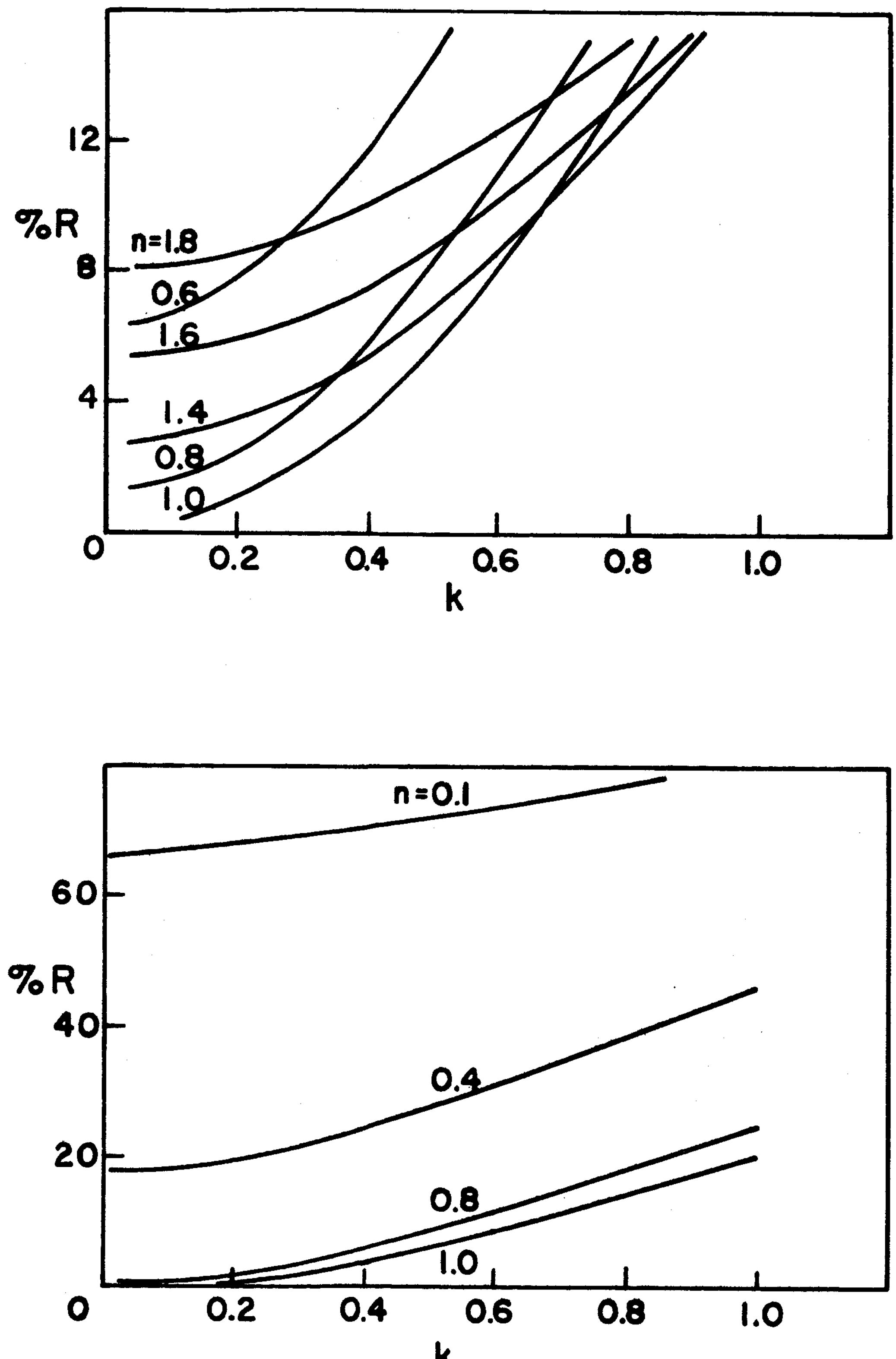

Figure 2
Reflectivity vs. Extinction Coefficient
at Normal Incidence.

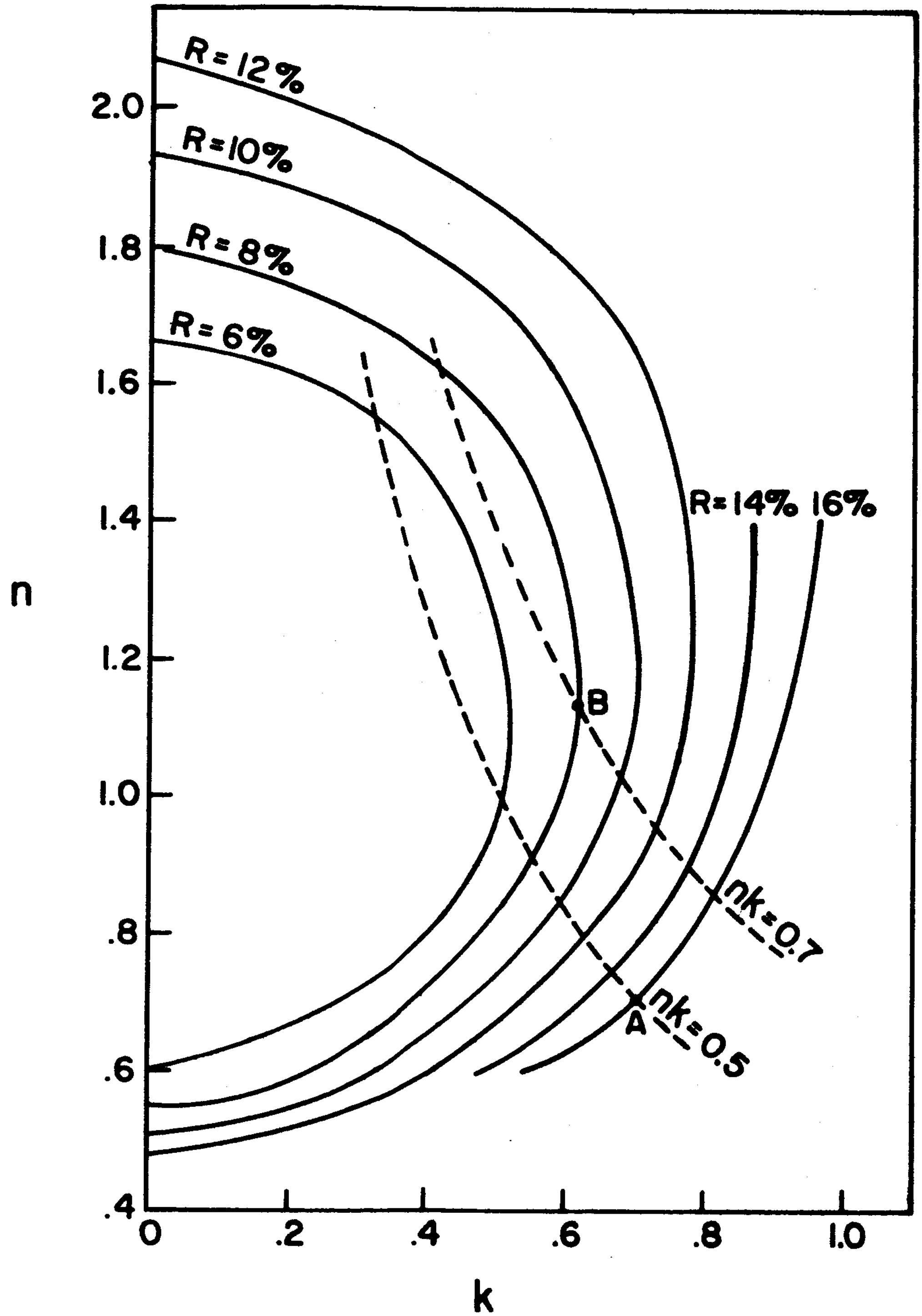

Figure 3
Relation between n and k for constant reflectivity and normal incidence .

(15) $$m \frac{d^2x}{dt^2} + \frac{m}{\tau} \frac{dx}{dt} = -eE_x \quad .$$

A solution to (14) for a field which varies as $e^{i\omega t}$ is

(16) $$x = \frac{eE_x}{m(4\pi^2\nu^2 - 2\pi i\,\nu/\tau)} \quad .$$

Now, the current density, j_x, is given by

(17) $$j_x = Ne \frac{dx}{dt} = \sigma E_x$$

where

N = number of free electrons per unit volume.

Substituting in the last equation for X, and solving for the real part of σ, we get

(18) $$\sigma = \frac{Ne^2}{m\tau} \cdot \frac{1}{(4\pi^2\nu^2 + \frac{1}{\tau^2})}$$

For the case of a static field, $\nu = 0$, and the expression for σ reduces to

(19) $$\sigma = \frac{Ne^2\tau}{m} \quad .$$

Experimental measurements of conductivity of the noble metals indicate a relaxation time of about 10^{-13} seconds.

The Drude theory has been tested by Hagen and Rubens[4] in the far infrared where $\nu \ll \frac{1}{\tau}$, and in this region there is good agreement between calculated and measured values. In the visible and ultraviolet however, the theory does not agree with experimental results. In this region, $\nu \gg \frac{1}{\tau}$, and the expression for σ reduces to

(20) $$\sigma = \frac{Ne^2}{4\pi^2 m\tau\nu^2}$$

---

[4]E. Hagen and H. Rubens, Ann. Physik, 14, 936, (1904).

Curves of conductivity vs. wavelength in the far ultraviolet, (obtained from n, k measurements), show characteristic humps and valleys with values of conductivity often far exceeding those predicted by the Drude theory. Such discrepancies are to be expected inasmuch as the simple theory does not consider possible transitions between quantum mechanical states. The quantum formulation will be developed in later sections and applied to the problem of optical properties and conductivity.

CHAPTER III

QUANTUM MECHANICAL TREATMENT OF OPTICAL PROPERTIES

A. Free Electron Model

The Schroedinger equation for an electron in free space is[1,2]

(1) $$\frac{-\hbar^2}{2m} \nabla^2 \psi = E \psi$$

and has the normalized solution

(2) $$\psi = \frac{1}{V^{1/2}} e^{i\vec{k}\cdot\vec{r}}$$

where $$k^2 = \frac{2mE}{\hbar^2}$$

and should not be confused with the extinction coefficient derived in Chapter II.

Application of boundary conditions leads to discrete values for the wave vector $\vec{k}$. If we consider the electron to be confined within a cube of edge L and require that

(3) $$\psi(x,y,z) = \psi(x+L,y,z)$$

then the allowed values of k are

(4) $$k_x = \frac{2\pi}{L} n_x , \quad k_y = \frac{2\pi}{L} n_y , \quad k_z = \frac{2\pi}{L} n_z ,$$

where n_x, n_y, and n_z are integers.

The Pauli exclusion principle allows only two electrons in each of the three components of $\vec{k}$, one electron with spin $+\frac{1}{2}$, and one with

---

[1] L. I. Schiff, Quantum Mechanics, McGraw-Hill Book Co., New York, 1955.

[2] C. Kittel, Introduction to Solid State Physics, John Wiley and Sons, Inc., New York.

spin - $\frac{1}{2}$. If N electrons per unit volume are to be confined in the cube and the system is to be at equilibrium, states in $\vec{k}$-space will be filled in such a manner that the energy of the system is at a minimum. Under these conditions the filled states will form a sphere in $\vec{k}$-space with a radius given by

$$k_f = (3\pi^2 N)^{1/3} \quad . \tag{5}$$

Correspondingly, electrons will occupy all energy levels up to

$$E_f = \frac{\hbar^2 k_f^2}{2m} = \frac{\hbar^2}{2m} (3\pi^2 N)^{2/3} \tag{6}$$

at a temperature of absolute zero. E_f is known as the Fermi level and its order of magnitude is 5 ev. for many metals.

The density of states, i.e., the number of states per unit energy range per unit volume, is easily found. Letting g(E) be the density of states, we have

$$\int g(E)dE = N = \frac{1}{3\pi^2} (2mE/\hbar^2)^{3/2} \tag{7}$$

$$g(E) = \frac{1}{2\pi^2} (2m/\hbar^2)^{3/2} E^{1/2} \tag{8}$$

Thus, for a temperature of absolute zero, the density of states rises parabolically until the Fermi level is reached, then drops sharply to zero. Higher temperatures lead to a slight rounding off of the discontinuity at the Fermi level. This rounding off occurs over an energy region of approximately kT, (kT$\sim$0.026 ev. at room temperature), and therefore only a small fraction of the average Fermi level.

The Fermi surface is a boundary in k-space which separates the occupied states from the unoccupied ones. For perfectly free electrons the surface is spherical, but this is an idealized case which exists only when a potential energy term is absent from the Schroedinger equation.

The wave function given in (2) is applicable to one electron only. For the system of N electrons one can approximate the total wave function by use of the one-electron approach. In this scheme a wave function for an N electron system is constructed from N one-electron functions and the Hamiltonian for the system includes the energy of coulomb interaction between electrons. The operator for this energy takes the form

$$\frac{1}{2} \sum_{i,j}{}' \frac{e^2}{r_{ij}} \tag{9}$$

and the prime on the summation indicates omission of terms i = j.

The N-electron wave function must be antisymmetric[3] and can be written as

$$\Psi(1,2,---N) = \sum_{p} (-1)^p \, P \, [\phi_\alpha(1)\phi_\beta(2)-----\phi_\nu(N)] \tag{10}$$

where the permutation operator covers the range of the N! permutations and p is the parity of the p-th permutation. The ϕ_i include a space function, $\psi_i(\vec{r})$, and a spin function, $\psi(s)$. This sum can also be written in a form known as the Slater determinant:

$$\Psi(1,2,---N) = \begin{vmatrix} \phi_\alpha(1) & \phi_\alpha(2) & ---- & \phi_\alpha(N) \\ \phi_\beta(1) & \phi_\beta(2) & ---- & \phi_\beta(N) \\ | & & & \\ | & & & \\ \phi_\nu(1) & \phi_\nu(2) & ---- & \phi_\nu(N) \end{vmatrix} \tag{11}$$

---

[3] L. I. Schiff, <u>op. cit.</u>, p. 224.

This determinant has the interesting property that it vanishes identically if two or more electrons are in the same state and it therefore automatically includes the requirements of the Pauli exclusion principle.

Although (10) is composed of one-electron functions, its antisymmetric character precludes independent motion of the electrons. The motion of each is correlated to the motion of the others and this is the result of the Pauli principle rather than electrostatic effects.

The total kinetic energy operator is now

$$\hat{T} = \frac{\hbar^2}{2m} \sum_{i=1}^{N} \nabla^2_i \quad . \tag{12}$$

Its operation on the function (10) yields a simple sum of energies of the one electron functions

$$-\frac{\hbar^2}{2m} \sum_{i=1}^{N} \int \psi_i^* \nabla^2 \psi_i \, d\tau = \sum_{i=1}^{N} E_i \tag{13}$$

The average kinetic energy is therefore unaffected by the symmetry of the total wave function since the same result would be obtained if Ψ were taken to be a simple product of one electron functions.

The average value of the coulomb interaction term is affected by the symmetry of the wave function. Letting (9) operate on (10) leads to a summation of two sets of terms

$$\frac{e^2}{2} \sum_{i,j}{}' \left[\int \frac{|\phi_i(\vec{r}_1)|^2 \, |\phi_j(\vec{r}_2)|^2}{r_{12}} d\tau'_{12} - \int \frac{\phi_i^*(\vec{r}_1)\phi_j^*(\vec{r}_2)\phi_i(\vec{r}_2)\phi_j(\vec{r}_1)}{r_{12}} d\tau'_{12} \right] . \tag{14}$$

The first set of terms gives the usual coulomb energy; the second set gives the exchange energy which is a direct result of the use of an antisymmetric wave function. Whether the exchange energy will be positive or negative depends on the form of the ϕ_i; no general prediction can be made.

B. Band Theory and Brillouin Zones

In the previous section we were concerned with perfectly free electrons, i.e., those described by a Hamiltonian which contained only kinetic energy and electron-electron interaction energy terms. Let us now introduce a potential energy as viewed by an electron in a perfect, semi-infinite crystal. This potential will be periodic with a period of the lattice such that

$$V(\vec{r}) = V(\vec{r} + \vec{R}_j) \tag{15}$$

where $\vec{R}_j$ is a primitive translation vector of the lattice. Because the potential is periodic, the Hamiltonian operator will also be periodic with

$$\hat{H}(\vec{r}) = \hat{H}(\vec{r} + \vec{R}_j) \quad . \tag{16}$$

Now we introduce a symmetry operator $\hat{T}_j(\vec{r})$, which translates the crystal through the vector $\vec{R}_j$ in the manner

$$\hat{T}_j\vec{r} = \vec{r} + \vec{R}_j \quad . \tag{17}$$

The elements $\hat{T}_j$ belong to the translational group of the crystal and by virtue of the above, they commute with the Hamiltonian. Then, any non-degenerate energy eigenfunction of $\hat{H}$ is also an eigenfunction of $\hat{T}$. If T_o is an eigenvalue of $\hat{T}$, the eigenvalue equation can be written as

$$\hat{T}\psi(\vec{r}) = T_o\psi(\vec{r}) = \psi(\vec{r} + \vec{R}) \quad . \tag{18}$$

Application of the translation operator a second time leads to

$$\hat{T}^2\psi(\vec{r}) = \hat{T}T_o\psi(\vec{r}) = T_o^{\ 2}\psi(\vec{r}) = \psi(\vec{r} + 2\vec{R}) \quad . \tag{19}$$

Repeated application of $\hat{T}$ N times gives the result

$$T_o^N \, \psi(\vec{r}) = \psi(\vec{r} + N\vec{R}) \quad . \tag{20}$$

Now, the periodic boundary conditions imposed earlier required that

$$\psi(\vec{r}) = \psi(\vec{r} + N\vec{R}) \tag{21}$$

and therefore

$$T_o^N = 1 \tag{22}$$

or

$$T_o = 1^{1/N} = e^{\frac{2\pi i l}{N}} \, , \; l = 0, 1, \ldots , N-1 \quad . \tag{23}$$

The eigenfunctions of $\hat{T}$ must change only by the complex phase factor when $\vec{r}$ goes to $(\vec{r} + \vec{R})$ and must be of the form

$$\psi_{\vec{k}}(\vec{r}) = u_{\vec{k}}(\vec{r}) \; e^{i\vec{k}\cdot\vec{r}} \tag{24}$$

with $u_{\vec{k}}(\vec{r})$ possessing the periodicity of the lattice.

Although Bloch was the first person to apply (24) to an electron in a crystal, and this function is known as a Bloch wave, the purely mathematical result had long been known to mathematicians as Floquet's theorem. Details of the theorem may be found in moderately recent literature.[4]

It is interesting to ask what the allowed energy spectrum looks like now that a periodic potential has been included in the Hamiltonian. An often quoted example[5] is the Kronig-Penney one dimensional model. The periodic potential of Figure 4 is postulated with heights V_o and widths b, and regions of zero potential of width a. In the latter regions the general solution to the Schroedinger equation is

---

[4] E. T. Whittaker and G. N. Watson, Modern Analysis, American Ed., p. 412, Cambridge U.P., New York, 1943.

[5] F. Seitz, The Modern Theory of Solids, p. 281, McGraw-Hill Book Co., New York, 1940.

Figure 4
Kronig-Penney one-dimensional model.

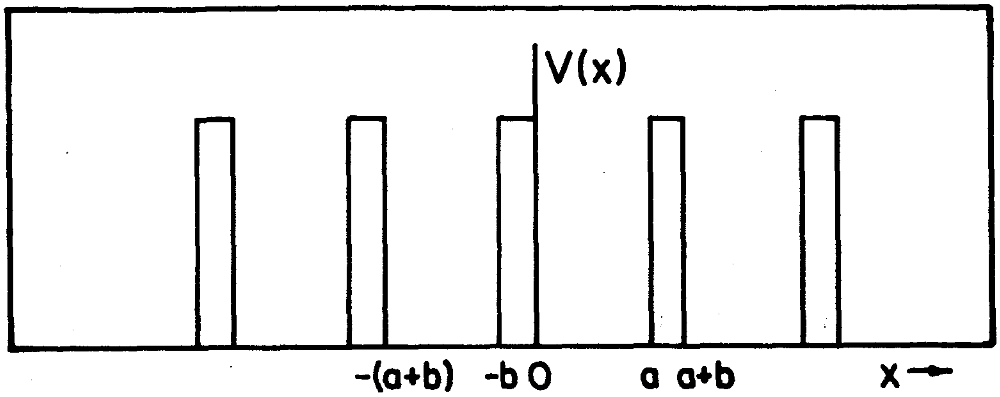

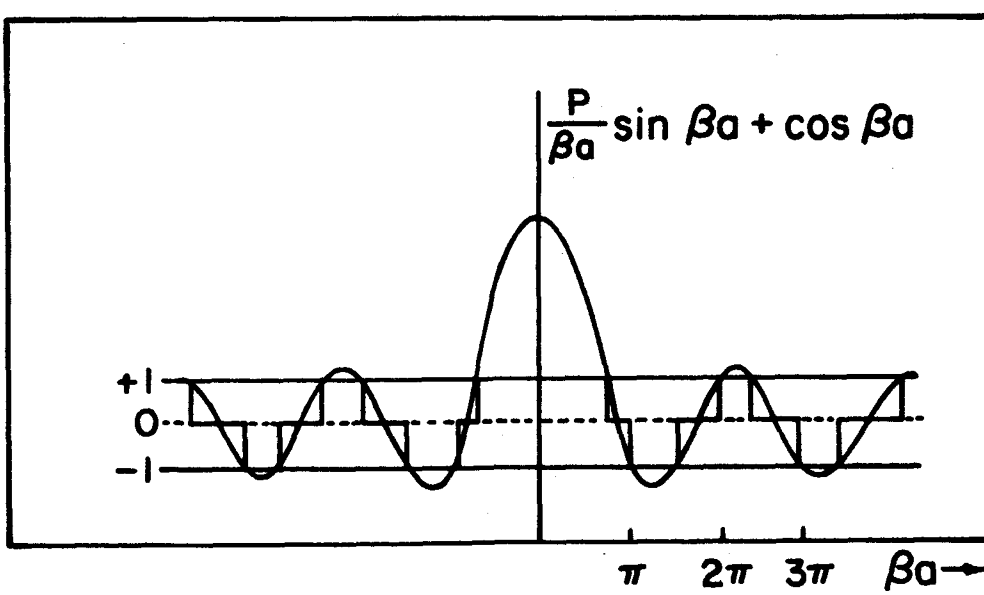

Figure 5
The allowed values of βa given by equation (30) are shown by the heavy line segments on the βa axis.

(25) $\psi_1 = A\cos\beta x + B\sin\beta x; \quad \beta = (2mE/\hbar^2)^{1/2}$.

In the region of constant potential V_o, the solution is

(26) $\psi_2 = C\cosh\gamma x + D\sinh\gamma x; \quad \gamma = [\,2m(V_o - E)/\hbar^2]^{1/2}$.

There is the usual requirement of continuity of wave function and its derivative at $x = a$ and the additional boundary condition because of periodicity that

(27) $$\psi_2\,(a + b) = e^{ik(a + b)}\psi_1(0)$$

$$\psi_2'\,(a + b) = e^{ik(a + b)}\psi_1'(0) \quad .$$

Substitution of (25) and (26) into (27) and solution of the determinantal equation leads to

(28) $\cos k(a + b) = \cos\beta a\,\cosh\gamma b + [\,(\gamma^2 - \beta^2)/2\beta\gamma]\,\sin\beta a\,\sinh\gamma b.$

Equation (28) defines the allowed values of energy, but the example may be simplified by letting V_o approach infinity but in such a way that the product bV_o remains finite. By defining the quantity

(29) $$P = \lim_{\substack{b \to 0 \\ V_o \to \infty}} (mabV_o/\hbar^2)$$

we see that in the limit, (28) approaches

(30) $$\cos ka = (P/\beta a)\sin\beta a + \cos\beta a \quad .$$

Figure 5 is a plot of the right side of (30) as a function of βa with a fixed value of $P = 3\pi/2$. Since the value of the cosine term can only lie between $\pm$ 1, it is seen that only certain bands of energy are allowed and these are separated by regions of forbidden energies. If P is small the forbidden regions disappear, whereas if P approaches infinity, the allowed values of βa reduce to the points $n\pi$, ($n = \pm 1, \pm 2, ---$). P can be considered as indicative of the degree of binding of the electron. With $P = 0$, perfectly free electrons are represented with no forbidden values of energy. As P approaches infinity, there is no energy dependence on k, and the electron is completely bound.

Advancing to a three dimensional lattice we proceed to determine those values of wave vector for which a discontinuity in energy can be expected. To this end it is convenient to work with the reciprocal lattice.

We let the vectors $\vec{a}_1, \vec{b}_1, \vec{c}_1$ be the primitive translations of the crystal lattice. Reciprocal lattice vectors $\vec{a}_2, \vec{b}_2, \vec{c}_2$ are defined by the following relations

$$(31) \qquad \vec{a}_1 \cdot \vec{a}_2 = \vec{b}_1 \cdot \vec{b}_2 = \vec{c}_1 \cdot \vec{c}_2 = 1$$

$$\vec{a}_2 \cdot \vec{b}_1 = \vec{a}_2 \cdot \vec{c}_1 = \vec{b}_2 \cdot \vec{c}_1 = \vec{b}_2 \cdot \vec{a}_1 = \vec{c}_2 \cdot \vec{a}_1 = \vec{c}_2 \cdot \vec{b}_1 = 0$$

The vector $\vec{a}_2$ is perpendicular to the plane of $\vec{b}_1$ and $\vec{c}_1$ and is

$$(32) \qquad \vec{a}_2 = \frac{\vec{b}_1 \times \vec{c}_1}{a_1 \cdot [\vec{b}_1 \times \vec{c}_1]} \quad .$$

Similar relations hold for the other vectors $\vec{b}_2$ and $\vec{c}_2$.

Since these reciprocal lattice vectors have the same dimensions as $\vec{k}$, the electron wave vectors, they may be considered as residing in k-space. If we define a vector $\vec{K}_1$ as

$$(33) \qquad \vec{K}_1 = 2\pi [l\, \vec{a}_2 + m\, \vec{b}_2 + n\, \vec{c}_2] \text{ , } l,m,n \text{ are integers}$$

the Brillouin zone may be found directly from the equation for Bragg reflection from crystalline planes:

$$(34) \qquad 2\, \vec{k} \cdot \vec{K} + K^2 = 0 \quad .$$

Geometrically, the first Brillouin zone (1st B.Z.) is constructed as follows. The center of the zone is symmetrically located at the point

$\vec{k} = 0$. From this point K vectors are drawn and each of these is bisected perpendicularly by a plane. The smallest volume enclosed by the planes is called the 1st B.Z. In this construction any point on the surface of the 1st B.Z. can be reached from one or more other points on the surface by translation through a vector K. The surface of the zone is therefore defined by planes which are mapped by k's which satisfy (34).

It is also possible to reduce all wave vectors to ones which lie in the 1st B.Z., since an appropriate $\vec{K}$ can be added to any $\vec{k}$ to give a $\vec{k}$ lying in the first zone, and still preserve the Bloch form of (24). If

$$\vec{k'} = \vec{k} + \vec{K} \tag{35}$$

then

$$\psi_{\vec{k}}(\vec{r}) = u_{\vec{k}}(\vec{r})\ e^{i\vec{k}\cdot\vec{r}} = u_{\vec{k}}(\vec{r})\ e^{i(\vec{k'} - \vec{K})\cdot\vec{r}} \quad . \tag{36}$$

But the function $\exp(-i\vec{K}\cdot\vec{r})$ has the same periodicity as the lattice and the function $u_{\vec{k}}(\vec{r})$ and may therefore be absorbed in the latter. In this scheme, the wave functions may be taken to be multi-valued functions of the k's in the unit cell of the reciprocal lattice. These results are known as the reduced zone scheme and that volume in k-space in which all the wave functions are considered is called the first Brillouin zone.

For the face-centered cubic lattice, the 1st B.Z. is defined by the following $\vec{K}$ vectors

$$2\pi/a(\pm\hat{i} \pm \hat{j} \pm \hat{k}) \text{ and} \tag{37}$$

$$2\pi/a(\pm 2\hat{i}) \quad , \quad 2\pi/a(\pm 2\hat{j}) \quad , \quad 2\pi/a(\pm 2\hat{k}) \quad .$$

The zone is a truncated octahedron and is shown in Figure 6.

It should be noted that the shape and size of the B.Z. is determined solely by the geometrical parameters of the crystal and is not influenced by the magnitude or form of the periodic lattice potential. The points of symmetry shown in Figure 6 are in accordance with the

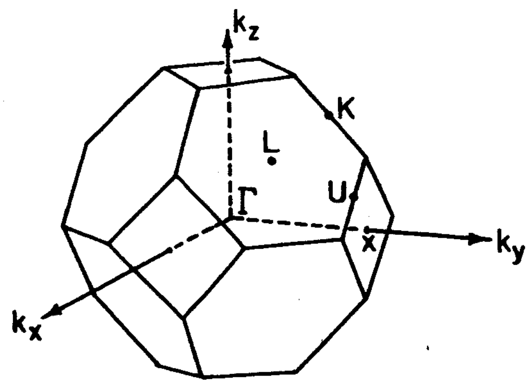

Figure 6

First Brillouin Zone for Face-centered Cubic Lattice

original work of Wigner et.al.[6] Symmetry properties of wave functions at various points in the zone are discussed by Callaway[7] in a survey of electron energy bands in solids.

If the periodic potential is small enough to be treated as a perturbation, the electrons are "almost free", and both the potential and the function $u_{\vec{k}}(\vec{r})$ may be expanded in a Fourier series:

(38) $$V(\vec{r}) = \sum_{\vec{K}_i} v(\vec{K}_i)\, e^{i\vec{K}_i \cdot \vec{r}}$$

(39) $$u_{\vec{k}}(\vec{r}) = \sum_{\vec{K}_i} c(\vec{K}_i)\, e^{i\vec{K}_i \cdot \vec{r}}$$

The coefficients $v(\vec{K}_i)$ and $c(\vec{K}_i)$ may be written as

(40) $$v(\vec{K}_i) = \frac{1}{\Omega} \int V(\vec{r})\, e^{-i\vec{K}_i \cdot \vec{r}}\, d\tau$$

(41) $$c(\vec{K}_i) = \frac{1}{\Omega} \int u_{\vec{k}}(\vec{r})\, e^{-i\vec{K}_i \cdot \vec{r}}\, d\tau$$

---

[6] L. P. Bouckaert, R. Smoluchowski, and E. Wigner, Phys. Rev. 50, 58, (1936).

[7] J. Callaway, Solid State Physics, Vol. 7, Academic Press, New York, 1958.

where the integration is over the unit cell of volume Ω.

Upon substituting this potential, (38), and Bloch function, (39) in the Schroedinger equation one obtains the expression[8]

$$(42)\quad (E_{\vec{k}} - v(0) - \hbar^2 |\vec{k} + \vec{K}_j|^2/2m)\, c(\vec{K}_j) = \sum_{K_m \neq 0} c(\vec{K}_j - \vec{K}_m) v(\vec{K}_m) \quad .$$

The term v(0) denotes the constant term in the potential. If we assume that all the other coefficients of the potential are small in comparison to v(0), then we can expect the expansion of $u_k(r)$ to contain a large c(0) in comparison to the other coefficients. On this assumption we can drop the products of coefficients other than the leading ones and obtain

$$(43)\quad (E_{\vec{k}} - v(0) - \hbar^2 |\vec{k} + \vec{K}_j|^2/2m)\, c(\vec{K}_j) = c(0) v(\vec{K}_j) \text{ for } \vec{K}_j \neq 0$$

and

$$(44)\quad (E_{\vec{k}} - v(0) - \hbar^2 k^2/2m)\, c(0) = 0 \text{ for } \vec{K}_j = 0 \quad .$$

Solution of (44) for $E_{\vec{k}}$ and its substitution in (43) leads to an equation for the coefficients $c(\vec{K}_j)$ in terms of c(0):

$$(45)\quad c(\vec{K}_j) = -c(0)\,[\, 2m\, v(\vec{K}_j)/\hbar^2]/(2\vec{k}\cdot\vec{K}_j - K^2) \quad .$$

The leading coefficient, c(0), is determined by normalization of the Bloch function.

Difficulty arises with this approximation when the value of $\vec{k}$ approaches a zone boundary; at this point the denominator of (45) approaches zero. Prior to but near this point, one of the $c(\vec{K}_j)$ will be large if the corresponding $v(\vec{K}_j)$ does not vanish. Focusing our attention on the particular $v(\vec{K}_i)$ we return to (42) and neglect all coefficients except $v(\vec{K}_i)$ and c(0) and obtain

$$(46)\quad \begin{aligned} &(E_{\vec{k}} - v(0) - \hbar^2 k^2/2m)\, c(0) = c(\vec{K}_i)\, v(-\vec{K}_i) \\ &(E_{\vec{k}} - v(0) - \hbar^2 |\vec{k} + \vec{K}_i|^2/2m)\, c(\vec{K}_i) = c(0) v(\vec{K}_i) \quad . \end{aligned}$$

[8] J. R. Reitz, <u>Solid State Physics</u>, Vol. 1, p. 30, Academic Press, New York, 1955.

A solution for $E_{\vec{k}}$ is

(47) $$E_{\vec{k}} = \frac{1}{2}(E^o_{\vec{k}} + E^o_{\vec{k}'}) \pm \frac{1}{2}[4|v(\vec{K}_i)|^2 + (E^o_{\vec{k}} - E^o_{\vec{k}'})^2]^{1/2}$$

where

(48) $$E^o_{\vec{k}} = v(0) + \hbar^2 k^2/2m \;, \; E^o_{\vec{k}'} = v(0) + \hbar^2 |\vec{k} + \vec{K}_i|^2/2m \;.$$

Equation (48) simply gives the energies of a free electron in a constant potential. Now, if $\vec{k}$ is far from a zone boundary, the term $(E^o_{\vec{k}} - E^o_{\vec{k}'})$ is much larger than $v(\vec{K}_i)$ and (47) has the solutions

(49) $$E_{\vec{k}} = \begin{cases} E^o_{\vec{k}} \\ E^o_{\vec{k}'} \end{cases} .$$

In this region of $\vec{k}$ space, we have essentially free electron energies.

Near a zone boundary, however, $E^o_{\vec{k}} \rightarrow E^o_{\vec{k}'}$, and the roots of (47) are separated by $2|v(\vec{K}_i)|$. Clearly, a gap in energy exists at the zone boundary and its value is twice the Fourier component for this boundary.

It should be pointed out that an energy gap at one boundary does not necessarily lead to a gap in the entire energy spectrum. If the $v(\vec{K}_j)$ are small enough, the gap which occurs for one direction of $\vec{k}$ will not occur over the same energy range for a different direction of $\vec{k}$.

Despite the several approximations which have been made above in deriving wave functions for an "almost free" electron, this type approach has enjoyed remarkable success in the treatment of certain metals. In these cases, the conduction electrons are almost entirely "s" or "p" in character, and there is no overlap of a "d" band with the conduction band. Aluminum, as an example, falls in this category.

On the other hand, elements such as the noble metals, appear to have a "d" band which overlaps the conduction band. Under these conditions, the "d" band interacts strongly with the "s" band giving rise to perturbing potentials sufficiently large that the simple perturbation treatment is no longer applicable. To determine the energy versus wave vector relationship in these cases requires more extended analysis. An excellent summary of methods has been provided by Reitz.[9]

C. Interaction Between Electrons and Electromagnetic Radiation

The semi-classical treatment of radiation is developed in numerous texts[10,11] and will not be repeated here. The use of time dependent perturbation theory leads to the following expression for the transition probability per unit time between states a and b

$$(50)\quad P_{ab} = \frac{4\pi^2 e^2}{m^2 c\omega^2_{ab}} I(\omega_{ab}) \left| \int \Psi_b^* \, e^{i\vec{\eta}\cdot\vec{r}} \, \mathrm{grad}_A \, \Psi_a \, d\tau \right|^2 \delta(\omega_{ab} - \omega)$$

where $I(\omega_{ab})$ represents the intensity of the incident beam of radiation in the immediate region of the energy of transition a-b, and the grad operator is taken in the direction of the radiation vector potential.

Let us consider (50) in the band approximation where Ψ_a and Ψ_b are determinantal wave functions composed of Bloch one-electron functions. Since the integral in (50) consists of individual one-electron operations by the grad operator, the integral vanishes because of orthogonality if Ψ_a and Ψ_b differ by more than one Bloch function. The integral also vanishes if the electron spins in the two Bloch functions differ. Therefore, the absorption or emission of a photon can change the state of only one electron in the system but cannot change its spin.

If the two Bloch functions which differ in (50) are labelled $\psi_{\vec{k}}$ and $\psi_{\vec{k}'}$, the integral reduces to

$$(51)\quad \int u_k^* \, e^{-i\vec{k}\cdot\vec{r}} \, e^{i\vec{\eta}\cdot\vec{r}} \, \mathrm{grad}\, u_{\vec{k}'} \, e^{i\vec{k}'\cdot\vec{r}} \, d\tau$$

$$= \int u_k^* \, e^{i(\vec{k}' - \vec{k})\cdot\vec{r}} \, [\mathrm{grad}\, u_{\vec{k}'} + i\vec{k}' u_{\vec{k}'}] \, e^{i\vec{\eta}\cdot\vec{r}} \quad .$$

---

[9] J. R. Reitz, op. cit.

[10] L. I. Schiff, op. cit.

[11] D. Bohm, Quantum Theory, Prentice-Hill, Inc., Englewood Cliffs, N. J.

All the terms in (51) have the periodicity of the lattice except the exponential term, so the expression may be written:

$$(52)\quad \sum_{r_i} e^{i(\vec{k}'-\vec{k}+\vec{\eta})\cdot\vec{r}_i} \int_i e^{i(\vec{k}'+\vec{\eta}-\vec{k})\cdot(\vec{r}-\vec{r}_i)} u^*_{\vec{k}} \left[\text{grad } u_{\vec{k}'} + i\vec{k}' u_{\vec{k}'}\right] d\vec{\tau}_i$$

where each integral covers one unit cell of the lattice and $\vec{\tau}_i$ connects a corner of this cell with the origin of coordinates. But the exponential term in the sum, $\exp i(\vec{k}' + \vec{\eta} - \vec{k})\cdot\vec{r}_i$, vanishes unless

$$(53)\qquad \vec{k}' + \vec{\eta} - \vec{k} = \vec{K} \quad .$$

Now, even at wavelengths as short as 100 A the magnitude of η is only 6×10^6 whereas a typical value for K is 3×10^8, so η can be neglected, and we are left with the requirement that the transition probability vanishes unless

$$(54)\qquad \vec{k}' - \vec{k} = \vec{K} \quad .$$

This result restricts all transitions to "vertical" ones in the reduced zone scheme as shown in Figure 7.

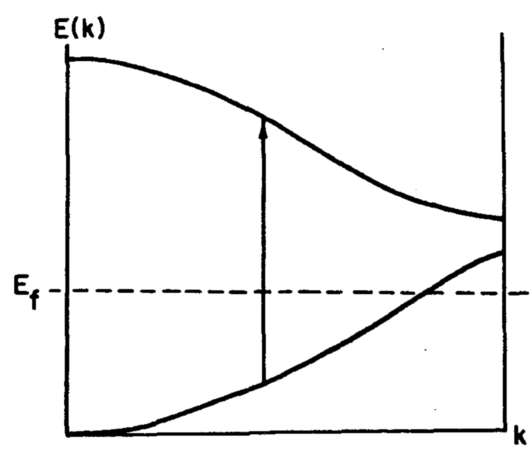

Figure 7

"Vertical" Transitions in Reduced Zone Scheme

Thus far we have assumed that the incident radiation is polarized and incident upon a single crystal. The grad operator of (50) is that component of the gradient operator which lies in the direction of the vector potential $\vec{A}$. Let us now consider the case of unpolarized radiation where the direction of $\vec{A}$ is randomly oriented in a plane which lies at right angles to the direction of the propagation vector $\vec{\eta}$.

We make the dipole approximation by equating $\exp(i\vec{\eta}\cdot\vec{r})$ with unity and rewrite the integral of (50) as a matrix element of momentum:

$$(55)\qquad \int \Psi_b^* \,\mathrm{grad}_A\, \Psi_a d\tau = \frac{i}{\hbar} \int \Psi_b^* \hat{p}_A \Psi_a d\tau = \frac{i}{\hbar} (\vec{p}_A)_{ab} \quad .$$

From matrix theory we have the result that

$$(56)\qquad (\vec{p})_{ab} = im\omega_{ab} (\vec{r})_{ab}$$

and we can write the integral in terms of that component of the radius vector which is in the direction of the vector potential:

$$(57)\qquad \int \Psi_b^* \,\mathrm{grad}_A \Psi_a d\tau = \frac{m}{\hbar}\, \omega_{ab} (\vec{r}_A)_{ab} \quad .$$

In terms of this matrix element, the transition probability becomes

$$(58)\qquad P_{a\to b} = \frac{4e^2\pi^2}{\hbar^2 c}\, I(\omega_{ab})\, |(r_A)_{ab}|^2 \quad .$$

For totally unpolarized radiation, one must consider the angle between the direction of $\vec{A}$ and the vector $(\vec{r})_{ab}$. But in a crystal, the vector $(\vec{r})_{ab}$ can assume all directions, so we can write the matrix element of (58) as

$$(59)\qquad |(\vec{r}_A)_{ab}|^2 = |(\vec{r})_{ab}|^2\, \overline{\cos^2\varphi}$$

where φ is the angle between $\vec{A}$ and $(\vec{r})_{ab}$, and $\cos^2\varphi$ is averaged over all directions in three dimensional space. Under these conditions the transition probability becomes

$$(60)\qquad P_{a\to b} = \frac{4\pi^2 e^2}{3m^2 c\omega^2}\, I(\omega_{ab})\, \left| \int u_{\vec{k}}^*\, e^{-i\vec{k}\cdot\vec{r}}\, \mathrm{grad}\, u_{\vec{k}'}\, e^{i\vec{k}'\cdot\vec{r}} d\tau \right|^2$$

$$\times\ \delta(\omega_{\vec{k},\vec{k}'} - \omega)\ \delta(\vec{k}' - \vec{k} - \vec{K})$$

D. Band Structure and Optical Constants

Given an incident beam of radiation which can produce interband transitions, the rate at which energy is removed from the beam is:

$$\frac{dW}{dt} = \sigma \overline{E^2} = N\hbar\omega P \tag{61}$$

where

σ = that conductivity related to transitions

$\overline{E^2}$ = time average of the square of the electric field

N = number of electrons which are permitted (by delta functions) to make the transitions

P = transition probability per unit time

When the proper substitutions are made in (61), the solution for conductivity is[12]

$$\sigma = \frac{e^2 h}{24\pi^2 \nu m^2 \Omega} \sum_{\vec{k},\vec{K}} \left| \int u^*_{\vec{k}}\, e^{-i\vec{k}\cdot\vec{r}}\, \mathrm{grad}\, u_{\vec{k}'}\, e^{i\vec{k}'\cdot\vec{r}}\, d\tau \right|^2 \delta(\omega_{\vec{k}',\vec{k}} - \omega)\, \delta(\vec{k}' - \vec{k} - \vec{K}) \quad . \tag{62}$$

From Chapter II, Equation (8), we had the result

$$\sigma = nk\nu$$

where n and k are quantities which can be obtained experimentally from reflectivity measurements. Thus, if we concern ourselves with a wavelength region where conductivity is due largely to interband transitions, we have an experimental method of evaluating the sum in (62).

If, however, the transition probability term in (62) is not highly dependent upon $\vec{k}$, we can use the experimentally determined nk product and (62) to ascertain the number of electrons involved in transitions at a given wavelength. With this analysis we can gain some information regarding the band structure of the metal being irradiated.

---

[12] F. Seitz, op. cit., p. 651.

A brief examination will now be made of the consequences of the delta functions found in (62).

As an example let us consider the case of the "almost free" electrons discussed earlier. Let the wave vectors of the ground and excited states be $\vec{k}$ and $\vec{k}'$ respectively, then from (54)

$$\vec{k}' = \vec{k} + \vec{K}.$$

The energy difference between the two states will be very nearly

$$E(\vec{k}')-E(\vec{k}) = \frac{\hbar^2}{2m} (K^2 + 2\vec{k}\cdot\vec{K}) \tag{63}$$

with a corresponding frequency of

$$\nu_{\vec{k}'\vec{k}} = \frac{\hbar}{4\pi m} (K^2 + 2\vec{k}\cdot\vec{K}) = \frac{\hbar}{4\pi m} (K^2 + 2|\vec{k}|\,|\vec{K}| \cos\beta) \ . \tag{64}$$

The angle β is that between $\vec{k}$ and $\vec{K}$. The absolute value of $\vec{k}$ is

$$|\vec{k}| = \frac{\frac{4\pi m\nu}{\hbar} - K^2}{2|\vec{K}| \cos\beta} \ . \tag{65}$$

For a given $\vec{K}$ and ν, β can range from zero, (or π if the numerator of (65) is negative), to a value which produces k_f on the Fermi surface. (Transitions out of ground state cannot occur for states with $k > k_f$ since these are unoccupied.) Clearly, then, states from which transitions can occur lie on a disc in k-space. The vector $\vec{K}$ is perpendicular to this disc and passes through its center. An example of this situation is shown in Figure 8. The figure presents a montage of two cross sections of the 1st B.Z. for the face-centered cubic lattice. Centered in the zone are concentric spheres representing different energy levels. The largest inner sphere denotes the Fermi surface with an energy of 5.5 ev. The volume enclosed by the Fermi surface is one-half the volume of the 1st B.Z. as is the requirement for any mono-valent metal.[13] Three sets of disc radii are drawn, one set for each of the directions (100), (110),

[13] C. Kittel, <u>op. cit.</u>, p. 314.

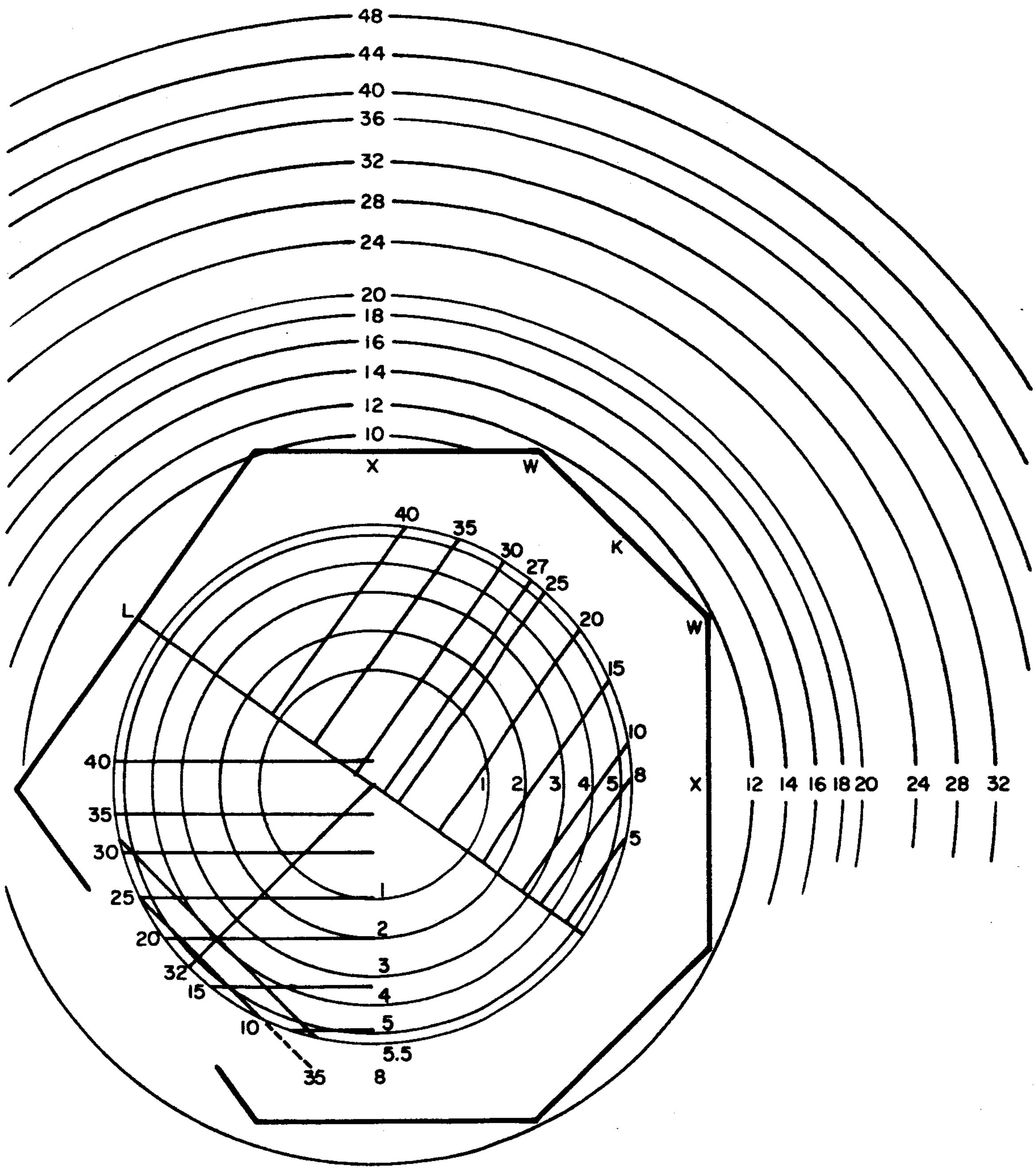

Figure 8
Discs in k-space from which inter-band transitions can occur.
This example is for "almost free" electrons
in a F.C.C. lattice.

and (111). These sets correspond to transitions involving the vectors:

$$\vec{K} = \frac{2\pi}{a} \cdot \begin{cases} \pm 2\hat{i} \\ \pm 2\hat{i} \pm 2\hat{j} \\ \pm \hat{i} \pm \hat{j} \pm \hat{k} \end{cases} \qquad \text{respectively.}$$

Each disc radius is labelled with the energy required for a transition in the appropriate direction. For instance, a 15 ev. photon could produce transitions in the (100) and (111) directions but not in the (110) direction.

In this example, a spherical Fermi surface gives rise to flat discs in $\vec{k}$-space. If, instead, the Fermi surface departs from sphericity because of sizeable energy gaps at the zone faces, the disc will no longer be flat and may become warped.

Evaluation of (62) for conductivity amounts to counting those electrons which are eligible for transitions at a given wavelength and weighting the count by a factor related to the transition probability of each electron. In this interpretation, (62) may be written as:

$$\sigma(\nu) = \frac{e^2 h}{24\pi^2 \nu m^2 \Omega} \sum_{\vec{k},\vec{K}} n_{\vec{k}} P_{\vec{k}'\vec{k}} \tag{66}$$

where

$$\sum_{\vec{k}} n_{\vec{k}} = N = \text{total number on that disc corresponding to a given } \vec{K}$$

$$P_{\vec{k}'\vec{k}} = \left| \int u^*_{\vec{k}}\, e^{-i\vec{k}\cdot\vec{r}} \operatorname{grad} u_{\vec{k}'}\, e^{i\vec{k}'\cdot\vec{r}}\, d\tau \right|^2 .$$

An evaluation of (66) is thus reduced to a measure of N and $P_{\vec{k}'\vec{k}}$. N can be obtained from the areas of the discs and if $P_{\vec{k}'\vec{k}}$ were independent of $\vec{k}$, the problem would be simplified considerably.

If we consider electrons in a single crystal influenced by plane polarized radiation which induces transitions from state $\vec{k}$ to $\vec{k} + \vec{K}$, the effective mass tensor can be written as[14]

(67) $$\left(\frac{m}{m^*}\right)_{ij} = \delta\, ij + \frac{2}{m}\sum_{\vec{K}} \frac{\langle\vec{k}\,|p_i|\,\vec{k}+\vec{K}\rangle\langle\vec{k}+\vec{K}\,|\,p_j\,|\,\vec{k}\rangle}{E_{\vec{k}+\vec{K}} - E_{\vec{k}}} .$$

For an electric field oriented in the x direction (67) becomes:

(68) $$\left(\frac{m}{m^*}\right)_{xx} = 1 - \frac{h}{2\pi^2 m}\sum_{\vec{K}} \frac{\left|\int \psi^*_{\vec{k}}\, \mathrm{grad}_x\, \psi_{\vec{k}'}\, d\tau\right|^2}{\nu_{\vec{k}',\vec{k}}} .$$

But the effective mass is also related to E(k) by

(69) $$\left(\frac{m}{m^*}\right)_{ij} = \frac{m}{\hbar^2}\,\frac{\partial^2 E_k}{\partial k_i \partial k_j}$$

and

(70) $$\left(\frac{m}{m^*}\right)_{xx} = \frac{m}{\hbar^2}\,\frac{\partial^2 E_k}{\partial k_x^2} .$$

Combining (68) and (70) leads to

(71) $$\frac{h}{2\pi^2 m}\sum_{\vec{K}} \frac{\left|\int \psi^*_{\vec{k}}\, \mathrm{grad}_x\, \psi_{\vec{k}'}\, d\tau\right|^2}{\nu_{\vec{k}'\vec{k}}} + \frac{m}{\hbar^2}\,\frac{\partial^2 E_k}{\partial k_x^2} = 1 .$$

In a polycrystalline material with random crystal orientations the grad operator of (71) cannot be taken in the x direction only but must be averaged over all directions as was done in Equation (59), with the result:[15]

(72) $$\frac{h}{6\pi^2 m}\sum_{\vec{K}} \frac{P_{\vec{k}'\vec{k}}}{\nu_{\vec{k}'\vec{k}}} + \frac{m}{3\hbar^2}\,\frac{\partial^2 E}{\partial k^2} = 1 .$$

In this expression, $\frac{\partial^2 E}{\partial k^2}$ is an average value taken over all possible directions of $|\vec{k}|$ and is indicative of the average effective mass of those

---

[14] C. Kittel, op. cit., p. 288.

[15] F. Seitz, op. cit., p. 650.

electrons which lie a distance $|\vec{k}|$ from the center of the Brillouin zone. If we have a situation where this term is independent of $\vec{k}$, then $P_{\vec{k}'\vec{k}}$ will be independent of $\vec{k}$ and the terms of this sum can be assumed to be independent also.

Returning to the example given in Figure 8, we make the assumption that the effective mass of the "almost free" electrons is constant over the range $k = 0$ to $k = k_f$. This assumption is valid if $E(\vec{k})$ goes as k^n in this range of k-space and the value of n is very nearly 2. Under these conditions we can proceed to evaluate (66) as a function of wavelength, keeping $P_{\vec{k}'\vec{k}}$ as an unevaluated constant.

To obtain the total number on a disc we need the area of the disc and the density of states in $\vec{k}$-space. Recalling that $k_x = 2\pi n_x/L$ and $k_y = 2\pi n_y/L$, we can write

$$dk_x dk_y = \frac{4\pi^2}{L^2}\, dn_x dn_y = 2\pi k dk \quad . \tag{73}$$

Since each position in k-space can be occupied by two electrons, one with spin up and one with spin down, the total number will be related to the disc area, A(k), by

$$\frac{N}{L^2} = \frac{k^2}{2\pi} = \frac{A(k)}{2\pi^2} \quad . \tag{74}$$

Since (66) is summed over all K consistent with the delta function one must also consider that there are eight K vectors of length $2\sqrt{3}\,\pi/a$, six of length $4\pi/a$, and twelve of length $2\sqrt{8}\,\pi/a$ for a face-centered cubic lattice, (Equation (34), Chapter III).

With the aid of the above information, the conductivity of the example of Figure 8 was computed for wavelengths of incident radiation from 300A to 2500A. The results are given in Figure 9. The lack of character in this curve is largely due to the fact that a spherical Fermi surface was assumed. If the surface were bulged sufficiently in the L direction, for instance, contact between the surface and zone face would occur. As we shall see later, such a distortion would give rise

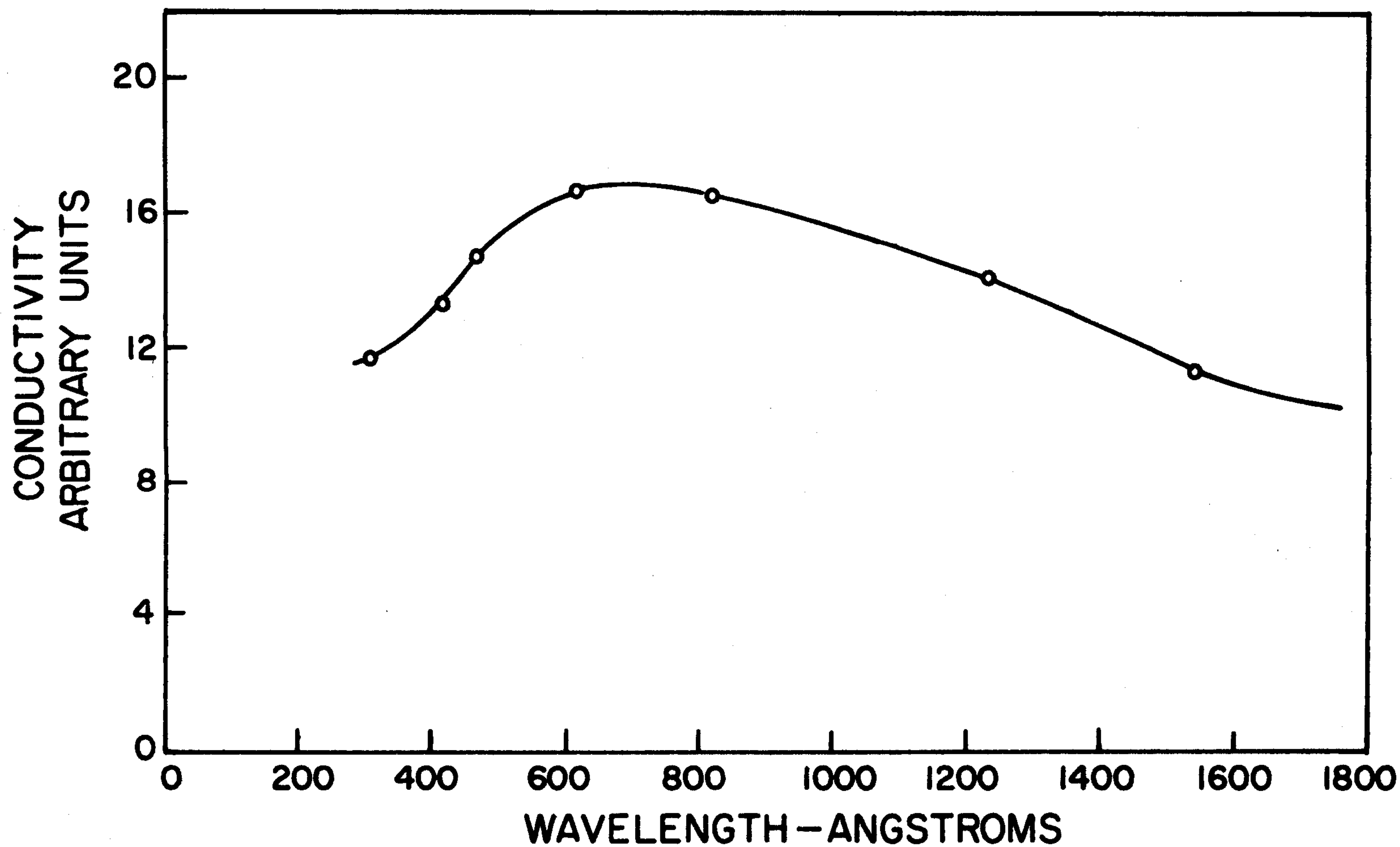

Figure 9
Conductivity vs. wavelength for a monovalent metal having free electrons.

to higher transition probabilities from states near the zone surface and therefore a higher conductivity to photons of energy around 5ev. or 2400A. This effect would also be observed at other wavelengths for which a disc contacted or came near a zone face.

In this respect, therefore, the optical constants, n and k, can be effectively utilized to gain some information as to the band structure of a metal.

CHAPTER IV

EXPERIMENTAL RESULTS AND DISCUSSION

A. Results for Pure Silver

Measurements of reflectivity for four different angles of incidence over the wavelength range 304A to 1671A were made on silver films. Representative results are plotted in Figure 10 and are given in numerical form in Table I.

From these data, the optical constants n and k were determined; these values are also given in Table I. Figure 11 shows the results of using Eqn. (II - 8) to calculate conductivity. In contrast to the free electron conductivity, silver conductivity displays sharp peaks at 600A and at approximately 300A. Since the Drude conductivity in the wavelength range considered here is less 10^{-2} times the observed values, it can be assumed that the effects of interband transitions predominate.

A computation of conductivity for silver was made, using the theory developed in III-D. A Fermi surface and band structure based on the theoretical calculations of Segall[16] were used in this computation. Segall derived the E(k) relationships of silver for two different potentials. One potential was determined from the free ion Ag^- Hartree functions, (no exchange energy considered); the other was derived from the Hartree-Foch free ion functions calculated by Worsley.[17] The first potential gave energy gaps of 5.2 and 4.3 ev. at the points X and L respectively with the p-like states at these zone boundaries lower in

---

[16] B. Segall, "Theoretical Energy Band Structures for the Noble Metals", General Electric Report No. 61-RL-(2785 G), July 1961.

[17] B. H. Worsley, Proc. Roy. Soc., London, A 247, 390, (1958).

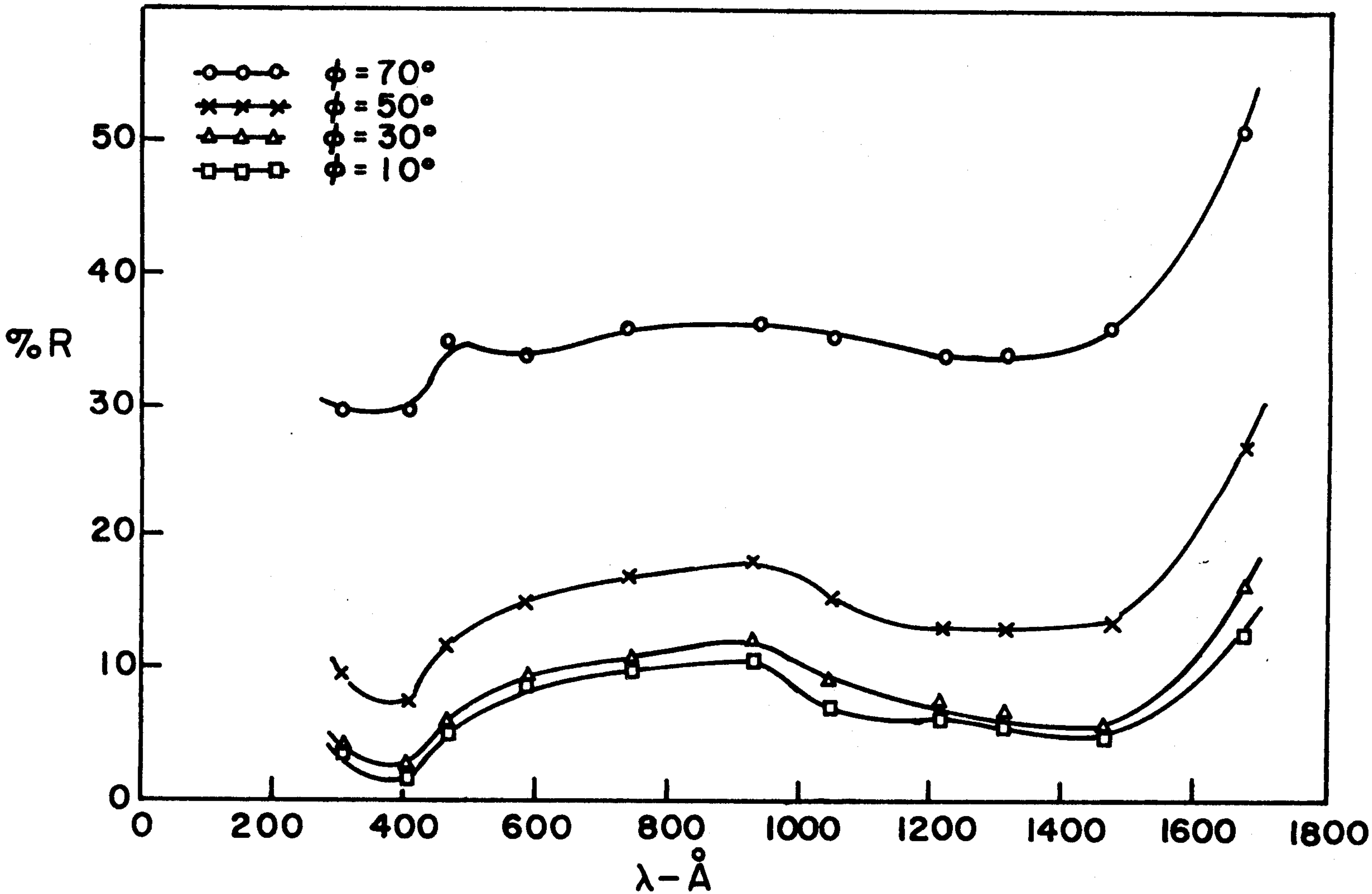

Figure 10
Reflectivity of silver vs. wavelength for four angles of incidence.

TABLE I

SILVER REFLECTIVITY DATA

λ - A	θ	RBm	RBk	%R	n	k
304	D	57.0	35.0		0.93	0.41
	70	38.5	32.0	29.5		
	50	34.1	32.0	9.5		
	30	32.4	31.4	4.6		
	10	32.5	31.5	4.5		
406	D	67.8	43.7		0.88	0.24
	70	48.0	40.9	29.6		
	50	42.2	40.4	7.5		
	30	40.6	40.0	2.5		
	10	40.6	40.2	1.7		
461	D	80.5	21.5		0.90	0.40
	70	41.0	20.4	34.9		
	50	27.0	20.1	11.7		
	30	23.3	20.0	5.6		
	10	23.1	19.8	5.6		
584	D	64.6	2.8		1.10	0.63
	70	23.1	2.2	33.8		
	50	11.4	2.1	15.1		
	30	7.8	5.8	9.4		
	10	7.2	1.8	8.7		
735	D	96.2	4.5		1.10	0.69
	70	36.6	3.6	16.7		
	50	18.9	3.6	16.7		
	30	13.1	3.6	10.4		
	10	12.0	3.6	9.2		
932	D	41.8	7.6		1.18	0.77
	70	19.2	6.8	36.3		
	50	12.5	6.2	18.4		
	30	10.2	6.0	12.3		
	10	9.4	5.9	10.2		

TABLE I (Continued)

SILVER REFLECTIVITY DATA

λ - A	θ	RBm	RBk	%R	n	k
1048	D	68.5	2.1		1.19	0.59
	70	25.0	1.5	35.4		
	50	12.0	1.5	15.8		
	30	7.4	1.5	8.9		
	10	6.1	1.5	6.9		
1216	D	90.5	18.4		1.26	0.49
	70	37.5	13.2	33.7		
	50	21.9	12.3	13.3		
	30	16.9	11.5	7.5		
	10	15.4	11.1	6.0		
1311	D	82.8	21.2		1.09	0.45
	70	38.0	17.0	34.1		
	50	24.1	16.0	13.1		
	30	19.8	15.6	6.8		
	10	18.5	15.0	5.7		
1470	D	62.9	20.0		1.02	0.45
	70	23.0	7.6	35.9		
	50	9.9	4.1	13.5		
	30	5.3	2.9	5.6		
	10	4.1	2.0	4.9		
1671	D	85.0	10.2		0.87	0.67
	70	45.0	6.8	51.1		
	50	25.1	5.0	26.8		
	30	16.2	4.2	16.1		
	10	13.2	3.8	12.6		

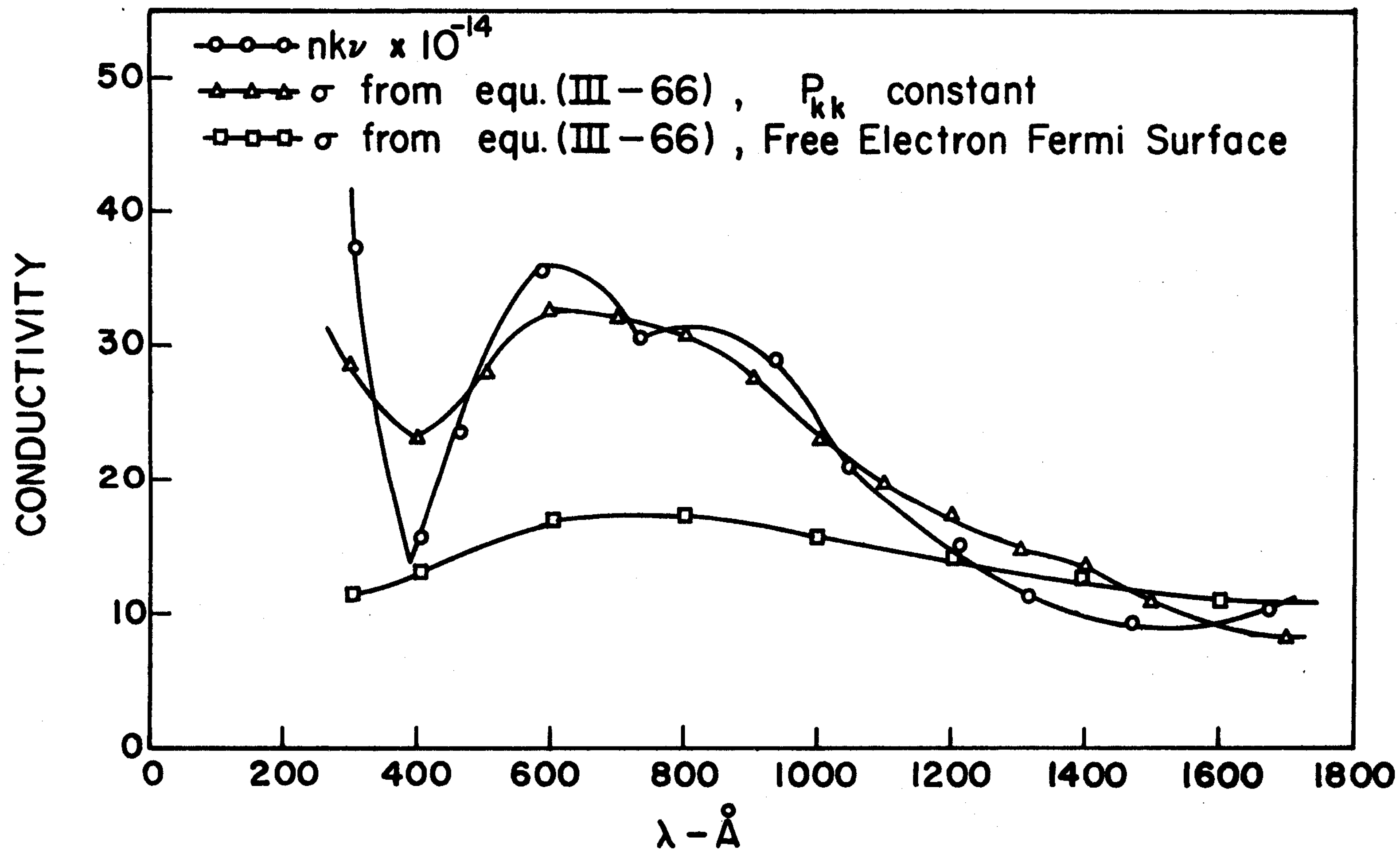

Figure 11
Silver conductivity vs. wavelength.

energy than the s-like states. By adjusting the volume enclosed by the Fermi surface to be one-half the volume of the B.Z., he determined that the Fermi surface of the first potential contacted the zone surface at L but the neck diameter was greater than observed values[18] by about 40 per cent. Also, on the basis of other data, the d-bands appeared too high by about 2 ev. The second potential gave a similar band structure but the gaps at X and L were 3.0 and 2.4 ev., there was no contact at L, and the d-bands appeared to be too low. Segall offered arguments as to why placement of the d-bands approximately midway between the two calculated positions should yield the correct E(k) structure. We have therefore used an E(k) which is an average of the two determined by Segall.

Since there are no theoretical calculations or other evidence available for the higher energy region, we have assumed free electron energies above 20 ev. and let the gaps approach zero at high energies. Justification for these two assumptions will be made later. The E(k) adopted for this computation is shown in Figure 12 and the Fermi surface compatible with this E(k) is given in Figure 13.

A computation was first made in which $P_{\vec{k}',\vec{k}}$ was assumed to be constant over all occupied states including those immediately adjacent to the zone faces. Disc areas were determined graphically in the following manner. First, a $\vec{K}$ vector which could be associated with a transition was selected. Then, for a given wavelength, two values of $\vec{k}$ were located which differed by $\vec{K}$ and which were separated in energy by an amount corresponding to the given wavelength. Selection of sufficient pairs of $\vec{k}$'s which satisfied these requirements defined the area in k-space from which transitions could occur. This process was repeated for different wavelengths over the region of interest and for a

---

[18] The Fermi Surface, edited by W. A. Harrison and M. B. Webb, John Wiley and Sons, Inc., New York, 1960.

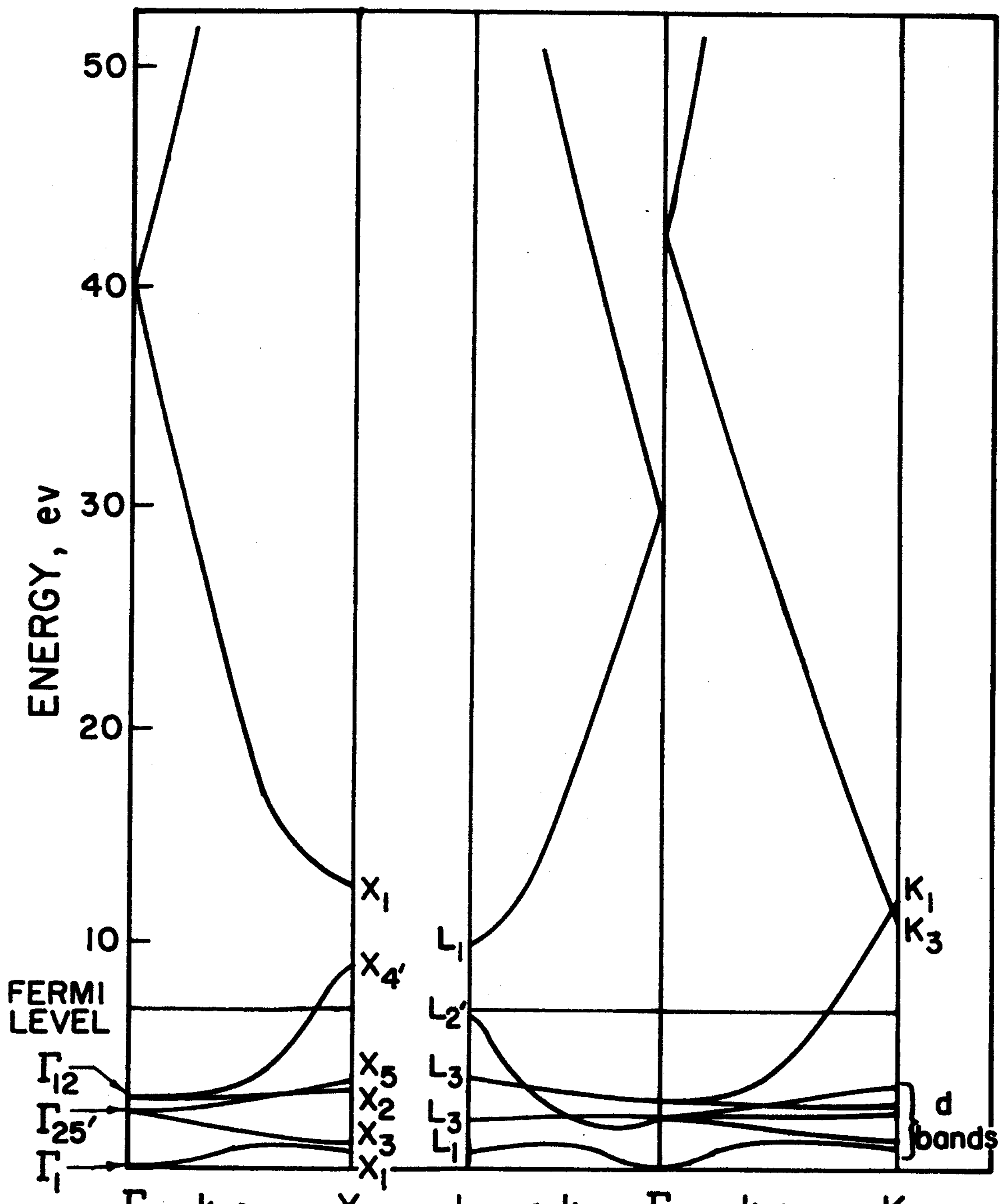

Figure 12
Energy band structure for silver.
(Average value of Segall's calculations)

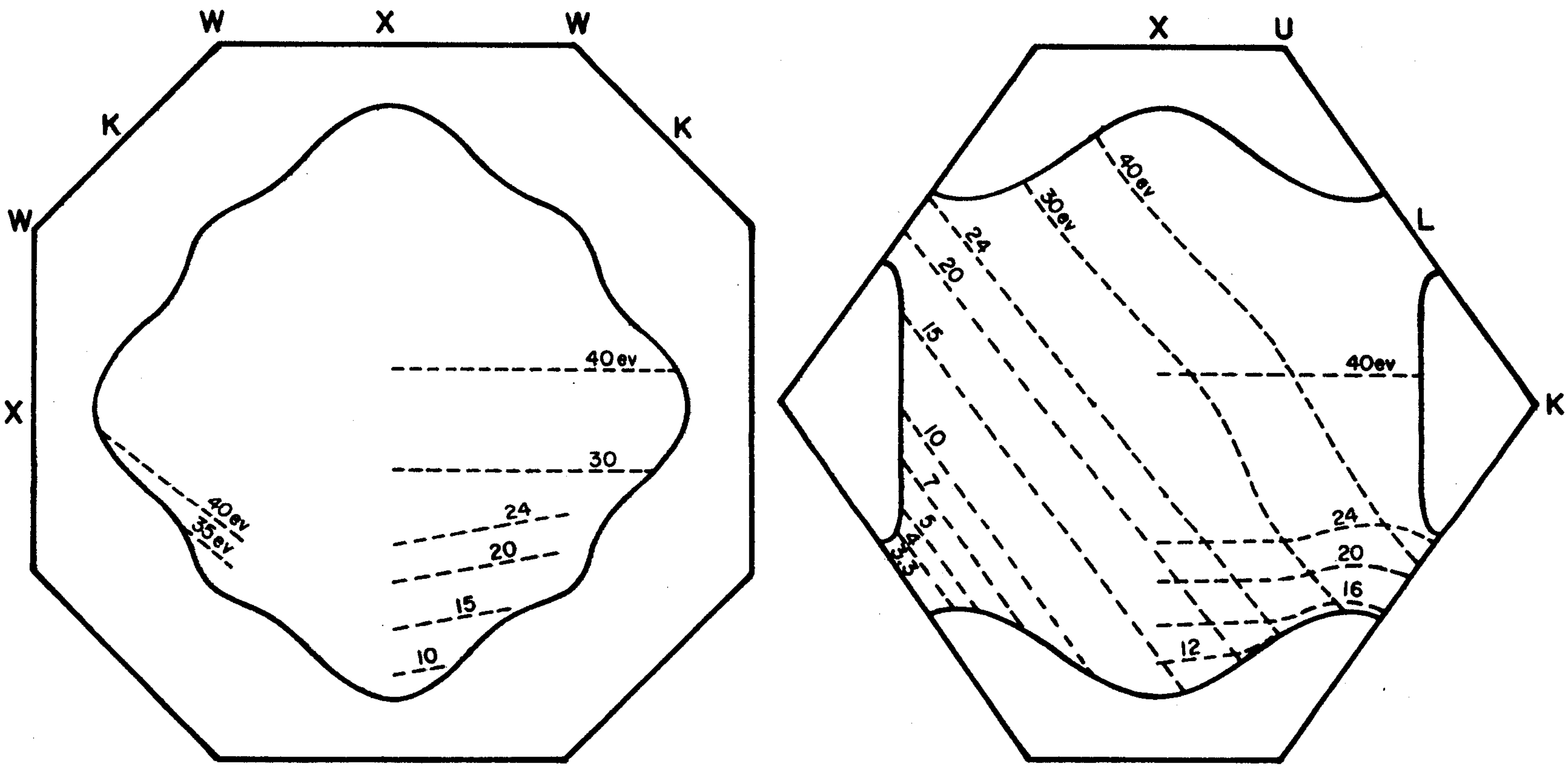

Figure 13
Fermi surface for silver from Segall's calculations.

Dotted lines and accompanying number indicate regions in k-space from which transitions can occur for indicated photon energy.

fixed $\vec{K}$. Next, a different $\vec{K}$ was selected and different areas were again determined for the various wavelengths. This procedure was continued until the supply of $\vec{K}$'s which could satisfy the delta function was exhausted. Examples of the areas so delineated can be seen in Figure 13. Each dotted line indicates the area from which transitions can occur for the photon energy given immediately above the dotted line. It should be noted that only transitions from conduction to excited bands was considered.

In this first computation, therefore, all the areas determined in this manner at a particular wavelength were simply summed, i.e., a count was made of all electrons eligible for transitions at a given photon energy. This sum was used in Equation (66) and a solution for σ was obtained with $P_{\vec{k}'\vec{k}}$ held constant. The results of this approach are given in Figure 11 and Table II for comparison with the measured conductivity.

It is seen that general agreement is obtained in this case if $P_{\vec{k}'\vec{k}}$ has a value of 10^5 cm^{-2}. This is particularly true in the range of 700 to 1700A or 7.3 to 17.6 ev., and aside from discrepancies in the heights and depths of peaks and valleys, general agreement extends to the shortest wavelength studied, 304A. A look at Figure 13 shows us that the higher energy transitions occur mostly from states near the center of the zone while the lower energy ones occur from states generally farther from the zone center. This condition, though not conclusive in itself, can be taken as evidence that $P_{\vec{k}'\vec{k}}$ is a slowly varying function of $\vec{k}$.

We consider now those discrepancies between theory and experiment in the wavelength region below 700A and attempt to adjust $P_{\vec{k}'\vec{k}}$, using the sum rule given in Equation (68).

Analytic expressions derived for E(k) in the X and L directions are:

TABLE II

DATA USED IN SILVER COMPUTATION
(EQUATION 66)

λ - A	$A(K_X)$	$A(K_L)$	$A(K_K)$	$\sum A(K)$	$\sigma/P \times 10^{-9}$
300	18.2	22.6	17.3	58.1	28.4
400	16.4	19.0	0.2	35.5	23.1
500	13.7	20.5		34.2	27.9
600	12.8	20.5		33.3	32.6
700	11.1	17.6		28.7	32.8
800	8.9	14.8		23.7	31.0
900	6.0	12.8		18.8	27.6
1000	3.1	11.2		14.3	23.3
1100	1.8	9.4		11.2	20.0
1200	0.9	8.0		8.9	17.4
1300	0.5	6.5		7.0	14.8
1400	0.2	5.3		5.5	12.6
1500	0.1	4.4		4.5	11.1
1600		3.5		3.5	9.1
1700		2.9		2.9	8.0

The columns headed A(K) give the area in k-space in units of π^2/a^2.

The subscripts on the K's indicate direction in k-space.

(1) $E(k) = 0.51k^2 + 3.1, \qquad 0<k<1.1$

$E(k) = 1.31k^2 + 2.2k - 0.21, 1.1<k<1.8$ X direction

(2) $E(k) = 2.31k^2 - k + 2.5 - 5.4X10^{-5}k^{17.3}$ L direction

for $0<k<3$.

These E(k) were substituted in Equation (68) to obtain the results of Figure 14 for transitions from the conduction to the excited bands. In this we see that the term which contains the sum of $P_{\vec{k}'\vec{k}}$ over all $\vec{K}'$s is essentially constant over most of the occupied states and shows appreciable change only near the point of contact at the center of the hexagonal face. In a first approximation, then, the sum of $P_{\vec{k}'\vec{k}}$ can be assumed constant for all $\vec{k}'$s except those near the point of contact.

Taking these results into consideration, a second computation of conductivity was made. In this, the second curve of Figure 14 was averaged over the range $1.3<k<1.73$ and the small areas in the "neck" of the Fermi surface were multiplied by this average. As the form of Figure 13 suggests, only transitions involving energies around 40, 20 and less than 7 ev. were affected. The result of this correction was to reduce the discrepancies between calculated and measured conductivity as is indicated in Figure 15. A secondary peak now appears in the theoretical results at 600A in agreement with the measured values. It appears, therefore, that this observed peak is not due to transitions from some other band such as perhaps the d-band, but to a large $P_{\vec{k}'\vec{k}}$ near the zone boundary of the conduction band.

Since the observed and calculated widths of this peak are equal, and since they coincide in wavelength, we have evidence for the validity of 1) the assumed area of contact of the Fermi surface and 2) the assumed E(k) at high energy, i.e., if E(k) at high energy did not go as $\hbar^2k^2/2m$, this secondary peak would be calculated at a different wavelength.

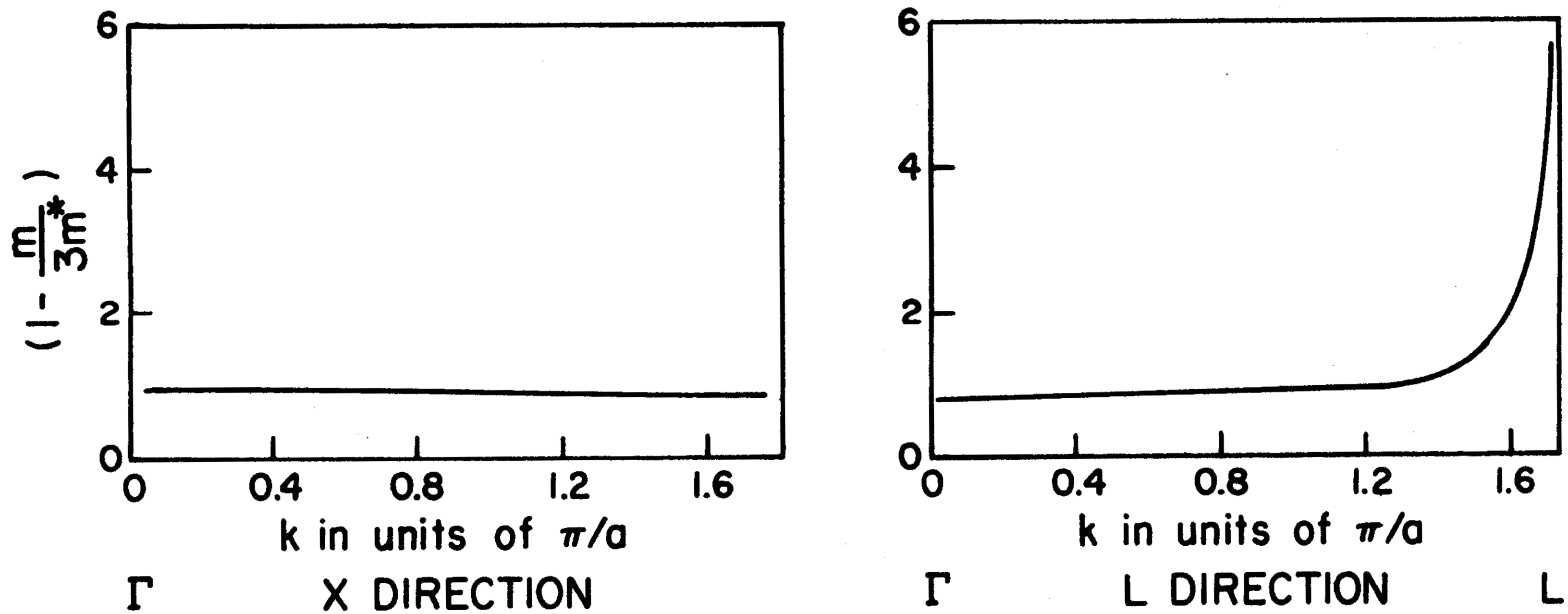

Figure 14

$(1 - \frac{m}{3m^*})$ for two zone directions in silver.

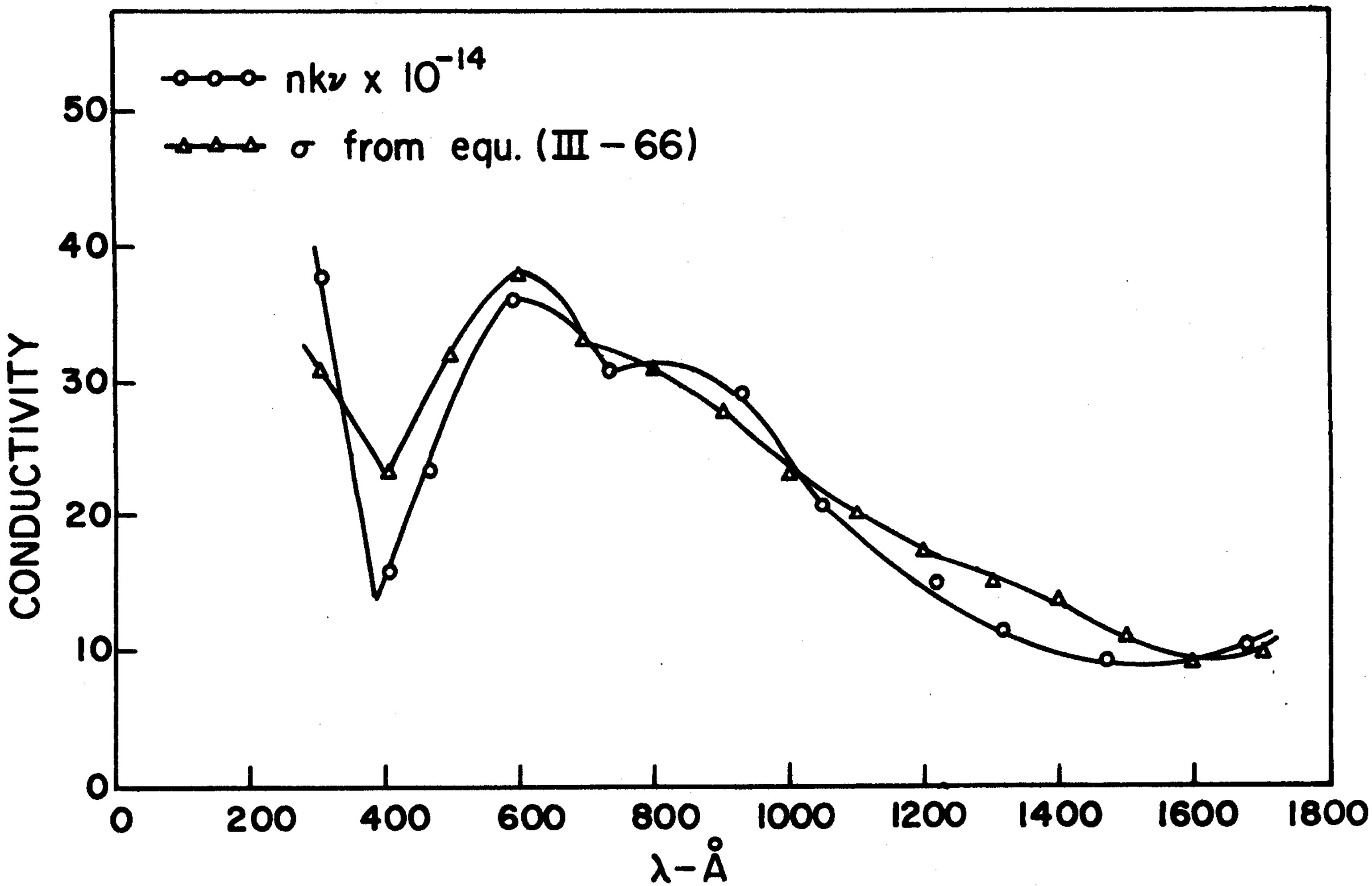

Figure 15
Conductivity of Silver vs. Wavelength.

On the basis of these results, the evidence for the size of gaps at high energy is not clear. The minimum in conductivity between 300 and 400A is at least in part due to the structure of the conduction band; there are simply fewer electrons available for transitions in this energy region. If a gap of a few ev. exists in the X direction at 40 ev. and in the L direction at 30 ev., we can expect minima in conductivity at 330 and 440A. A gap in the K direction at high energy would create effects outside the range of our observation. The fact that the measured minimum at 400A is lower than the calculated value suggests the presence of a high energy gap, but without more experimental data than is now available, nothing quantitative can be deduced. At any rate, the inclusion of a small gap at high energy would not appreciably affect the results considered here.

Although our experimental data ends at 1671A, it is interesting to examine the theoretical model at longer wavelengths. In Figure 13 we see that transitions from conduction to excited band will continue in the L direction down to a photon energy of 3.3 ev. Although these originate from discs of small area, they are in a region of large $P_{\vec{k},\vec{k}}$ and should contribute to another peak in conductivity beginning around 1800 A and ending abruptly at 3700A, (3.3 ev.). In this same range, transitions can occur from the d-bands to unfilled states in the conduction band. The E(k) structure of Figure 12 predicts the following

X_5 to Fermi level - - 3.2 ev., 3850A

L_3 to Fermi level - - 3.1 ev., 3980A

K_2 to Fermi level - - 3.4 ev., 3630A

as the minimum energies associated with these transitions, and very nearly the same limit as conduction to excited band. The maximum energy change to be expected in a d-like to p-like transition should occur at X_3 to X_4, with 8.2 ev., (1500A). Since the upper and lower limits of these two effects very nearly coincide, only one peak should be observed in silver conductivity in the range of 1500 to 4000A. The experimental work of Ehrenreich and Philipp[19] provides corroboration of this extension of the theory. They report a peak in silver conductivity centered at approximately 2000A with edges at 1500 and 3700A, in contrast to copper which has these two peaks well separated in wavelength.

On the basis of these results one can conclude that the E(k) structure and Fermi surface derived from Segall's calculations are essentially correct, and that this approach to the computation of conductivity is basically sound. The use of the disc model reduces much of the ambiguity previously associated with interpretation of the optical constants in the far ultraviolet.

B. Silver-Indium Alloy

To observe the effects of a change in the electron/atom ratio, a film which contained 10.0 at.% indium and 90.0 at.% silver was studied. (The preparation of alloyed films is discussed in Chapter V.) Indium was chosen as the solute because of its proximity to silver in the periodic table and its possession of three valence electrons. With this choice of solute and concentration, current binary alloy data[20] indicate that the alloy retains the f.c.c. structure of silver, and thus, the same Brillouin zone. Under these conditions, it was felt that optical data could be of help in resolving questions regarding the band structure of binary alloys. The history of this problem will be reviewed briefly.

Derivation of the Hume-Rothery rules for alloys is summarized by Kittel.[21] "Hume-Rothery first drew attention to the importance of

---

[19] H. Ehrenreich and H. R. Philipp, Phys. Rev., 128, 1622, (1962).

[20] M. Hansen, Constitution of Binary Alloys, McGraw-Hill Book Co., Inc., New York, 1958.

[21] C. Kittel, op. cit., p. 325.

the average valence electron/atom ratio as a kind of universal parameter in the description of the properties of alloys. He was concerned with the occurrence of certain alloy structures at a definite electron/atom ratio... ".

Table III gives representative data concerning these remarks.

TABLE III

ELECTRON/ATOM RATIO AT α-PHASE BOUNDARY FOR SEVERAL ALLOYS

Alloy	e/a
CuZn	1.38
CuAl	1.41
CuGa	1.41
CuSi	1.42
CuGe	1.36
AgZn	1.38
AgCd	1.42
AgAl	1.41
AgIn	1.36

"The Hume-Rothery rules find a simple explanation on band theory in the approximation of nearly free electrons. Jones pointed out that the observed limit of the α-phase (fcc) occurs very close to the electron concentration of 1.36 for which the inscribed Fermi sphere makes contact with the Brillouin zone surface for the fcc lattice. The observed electron concentration of the β-phase (bcc) is close to the concentration, 1.48, for which the inscribed Fermi sphere makes contact with the Brillouin zone surface for the bcc lattice....

"It is apparent that there is an intimate connection between the electron concentration at which a new phase appears and the electron concentration at which the Fermi surface makes contact with the

Brillouin zone boundary. The general explanation of the association is that it is expensive energetically to add further electrons once the filled states contact the boundary. Additional electrons can be accommodated only in states above the energy gap characterizing the boundary or in the states near the corners of the first zone. The number of states near the corners falls off markedly as a function of energy. In this circumstance it is often energetically favorable for the crystal structure to change, the final structure being one which contains a larger Fermi surface.

"The transformation from fcc to bcc is illustrated by Figure 16 showing the number of states per unit energy range as a function of energy, for the fcc and bcc structures. It is seen that as the number of electrons is increased, a point is reached above which it is easier to accommodate additional electrons in the bcc lattice."

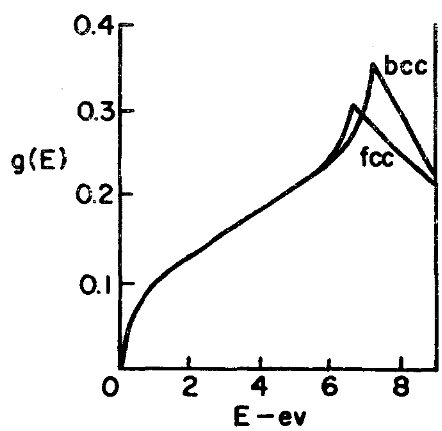

Figure 16

Density of States, g(E), for fcc and bcc Lattices, as a Function of Energy

This simple and elegant explanation of the Hume-Rothery rules had to be either discarded or severely modified when the accumulation of experimental and theoretical work later pointed to the fact that the Fermi surface contacts the zone boundary for many metals in the pure, unalloyed state. It appears almost without question now that contact is achieved at the hexagonal face for the noble metals copper, silver, and gold. Independent measurements and interpretations of the anomalous skin effect, de Haas-van Alphen effect, cyclotron resonance, ultrasonic attenuation, and the optical properties all seem to confirm the latter statement.

At this point a prevailing theory was the one of rigid band structure, i.e., that the E(k) relationships of a metal were unchanged upon alloying with another metal, at least up to those concentrations of solute which precipitated a phase change. In 1958, Cohen and Heine[22] contradicted this concept with the argument that upon alloying: (1) the E(k) must change, (2) the Fermi surface pulls away from the point of contact and becomes more spherical, and (3) the energy gaps at the zone faces either increase or decrease according to whether the s-like state at the face was originally lower or higher than the p-like state. Much of their argument was based on considerations of the s-p excitation energy of the free atom and on the specific heat data of Rayne[23,24]. In particular, they proposed that $E_p < E_s$ for copper and silver but $E_s < E_p$ for gold, and that upon alloying this gap decreases for copper and silver but increases for gold. Their calculations give an energy gap at the point L of 0.10 ev. for silver, in marked disagreement with the value of 3.3 ev. obtained by Segall.

Biondi and Rayne,[25] in 1959, performed optical absorption measurements on a series of α-brasses over the wavelength range 0.23-4.0 microns using electropolished bulk specimens. In the vicinity of 4000A, their data can be interpreted as confirmation of the Cohen-Heine model. Some of their results are reproduced in Figure 17.

---

[22] M. H. Cohen and V. Heine, Adv. in Phys., 7, 395, (1958).

[23] J. A. Rayne, Phys. Rev., 108, 22, (1957).

[24] J. A. Rayne, Phys. Rev., 110, 606, (1958).

[25] M. A. Biondi and J. A. Rayne, Phys. Rev., 115, 1522, (1959).

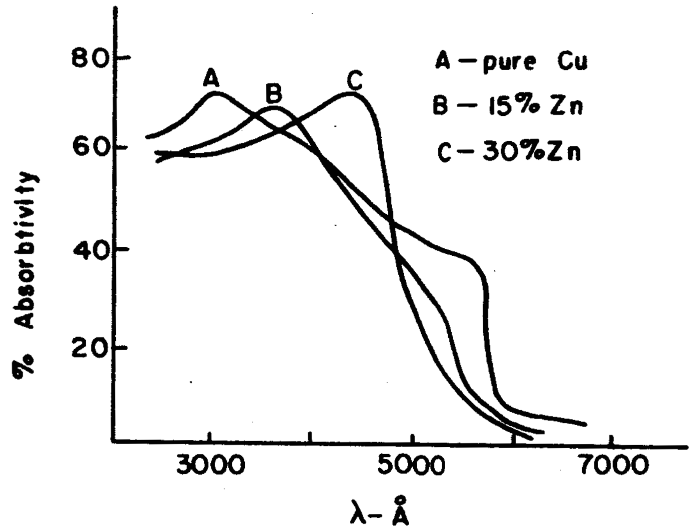

Figure 17

Optical Absorptivity vs. Wavelength
(Biondi, Rayne)

For pure copper, we can attribute the peak at 3000A to transitions from conduction to excited band, L_2' to L_1 and the peak at 5700A to transitions from the d-band to the p-like states immediately above the Fermi level. A shift of this first peak to longer wavelengths as in curves B and C can occur only if the gap, $L_2' - L_1$, decreases as proposed by Cohen and Heine. At the same time, this alloying increases the electron/atom ratio and the Fermi level. Thus, since greater energy is required for d-band transitions, the second peak can be expected to move to shorter wavelengths.

Despite these results, their infrared absorptivity data cause Biondi and Rayne to conclude that the Fermi surface becomes more distorted upon alloying, necessitating an increase in gap.

In 1961, Ziman[26] reviewed the state of affairs and advanced some views of his own. We quote some of his conclusions.

"We have no guarantee that the electronic energy surfaces in k-space remain unchanged when other metals are added to a noble metal.

---

[26] J. M. Ziman, Adv. in Phys. 10, 13, (1961).

...Indeed, Cohen and Heine have specifically proposed that this rigid band hypothesis must be abandoned if we are to understand certain properties of the alloys of the noble metals. It would obviously be valuable to have an independent check on this point."

"...There is no serious inconsistency between the observed transport properties and the assumption that the energy surfaces discovered by the topological techniques remains more or less rigid when the temperature is raised or when the metal is alloyed with other metals. If there is any sphericizing effect of alloying, it does not seem enough to draw the Fermi surface out of contact with the zone boundary."

It was with these questions in mind that the optical properties of an alloy of silver were studied.

Reflectivity of the indium alloy versus wavelength for four angles of incidence is illustrated in Figure 18 and the data are listed in Table IV. Except for a decrease at 304A, the reflectivity curves for the alloy do not differ greatly from those for pure silver. However, the conductivity as obtained from the optical constants shows marked change in several respects. For comparison the conductivity of both silver and its alloy are plotted in Figure 19.

Despite the reduction of reflectivity of the alloy at 304A, conductivity remains about the same; this is another illustration of the shortcomings of using reflectivity alone as a characterizing parameter. The minimum previously observed at 380A has shifted to 450A and from this point on to about 1200A, conductivity has been consistently reduced. Perhaps the most striking change is the loss of the secondary peak at 600A, the one which had been attributed to contact of the Fermi surface with the zone face. Finally, we find the appearance of a broad, low peak between 1200 and 1800A which was not observed for pure silver.

At this juncture we have the opportunity to investigate the validity of the rigid band concept. If, upon alloying, the band structure

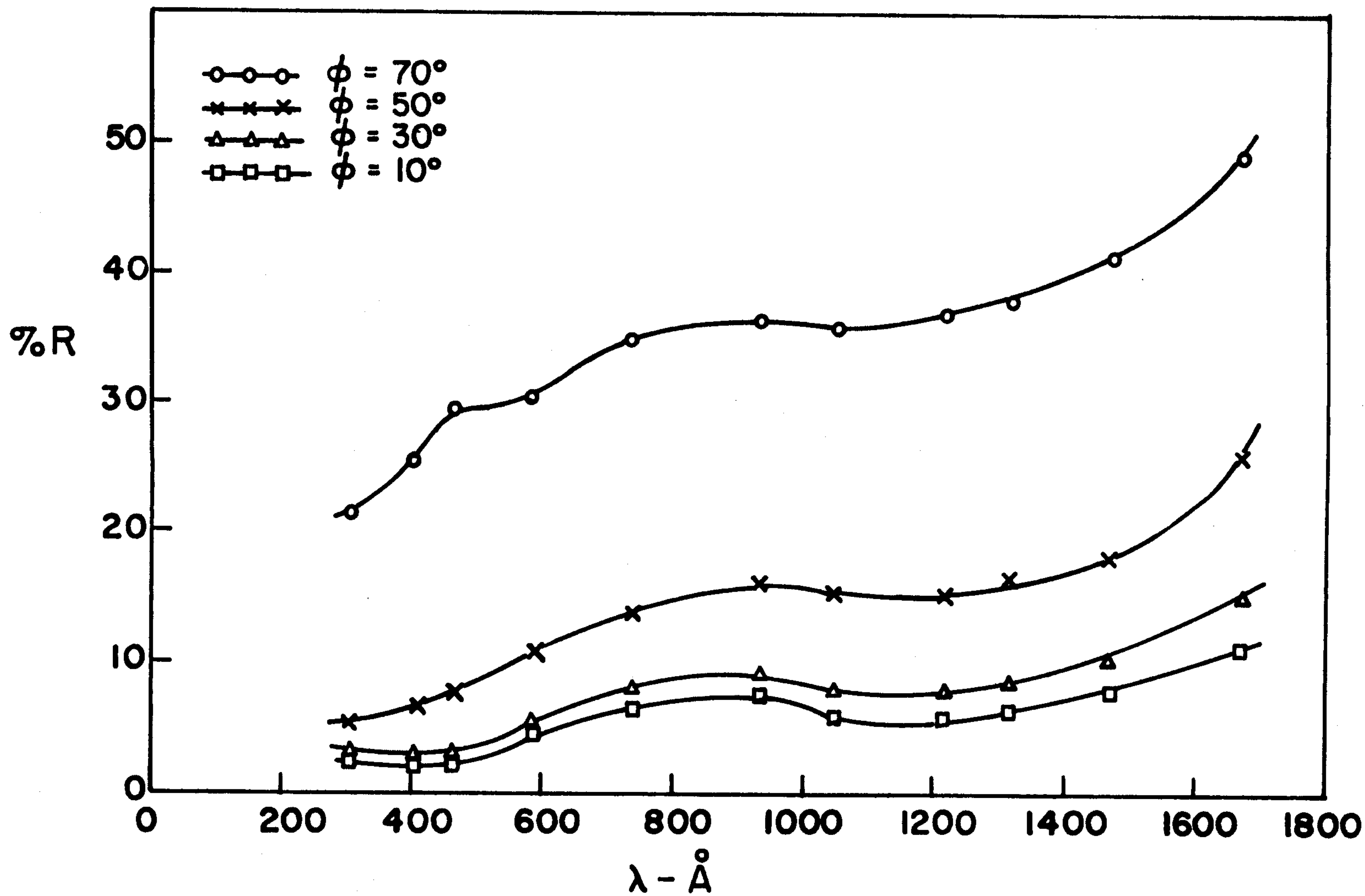

Figure 18
Reflectivity of AgIn alloy (10 at . % In) vs. wavelength.

TABLE IV

SILVER-INDIUM REFLECTIVITY DATA

λ - A	θ	RBm	RBk	%R	n	k
304	D	36.5	20.6		1.04	0.34
	70	22.4	19.0	21.4		
	50	19.5	18.6	5.7		
	30	19.0	18.5	3.1		
	10	18.8	18.4	2.5		
406	D	49.2	19.6		0.95	0.30
	70	25.6	18.0	25.7		
	50	19.5	17.5	6.8		
	30	18.3	17.6	2.4		
	10	18.5	17.9	2.0		
461	D	89.5	15.5		0.92	0.31
	70	32.5	10.6	29.6		
	50	14.6	8.9	7.7		
	30	10.6	8.5	2.8		
	10	10.1	8.4	2.3		
584	D	65.0	1.8		1.00	0.45
	70	20.6	1.4	30.4		
	50	8.3	1.4	10.9		
	30	5.0	1.4	5.7		
	10	4.5	1.4	4.9		
735	D	81.3	1.4		0.98	0.54
	70	29.0	1.0	35.0		
	50	12.1	1.0	13.9		
	30	7.3	1.0	7.9		
	10	6.2	1.0	6.5		
932	D	57.4	7.1		0.97	0.59
	70	24.8	6.5	36.4		
	50	14.5	6.4	16.1		
	30	11.0	6.3	9.3		
	10	10.0	6.2	7.6		

TABLE IV (Continued)

SILVER-INDIUM REFLECTIVITY DATA

λ - A	θ	RBm	RBk	%R	n	k
1048	D	92.2	11.7		1.04	0.54
	70	40.4	11.6	35.8		
	50	23.9	11.6	15.3		
	30	18.1	11.6	8.1		
	10	16.3	11.6	5.8		
1216	D	93.4	4.1		1.05	0.50
	70	36.1	3.2	36.8		
	50	16.8	3.2	15.2		
	30	10.1	3.2	7.7		
	10	8.2	3.2	5.6		
1311	D	66.5	18.0		1.05	0.53
	70	34.4	16.0	37.9		
	50	23.0	15.0	16.5		
	30	19.2	15.0	8.7		
	10	18.1	15.0	6.4		
1470	D	79.0	30.3		1.07	0.58
	70	38.8	18.6	41.5		
	50	23.3	14.5	18.1		
	30	17.6	12.6	10.3		
	10	16.0	12.2	7.8		
1671	D	84.7	10.5		0.85	0.64
	70	43.8	7.4	49.1		
	50	25.0	5.7	26.0		
	30	16.3	5.0	15.2		
	10	13.1	4.8	11.2		

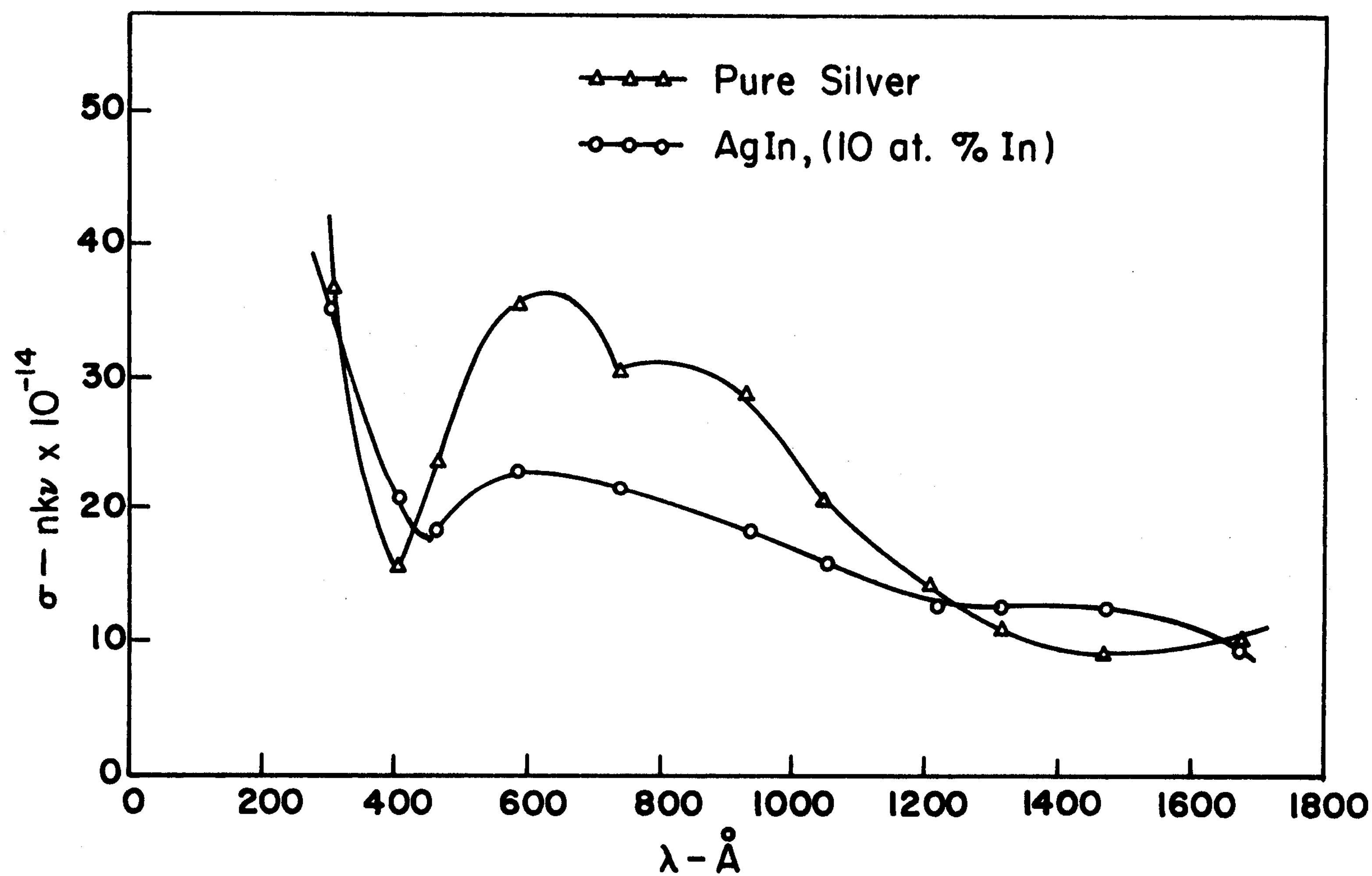

Figure 19
Conductivity of Ag and AgIn Alloy vs. Wavelength.

does not change, we would expect a simple growth in all directions of the Fermi surface adopted for pure silver. The area of contact at the hexagonal face would increase and there would be a greater number of electrons eligible for transitions at all wavelengths. The increased e/a would raise the Fermi level and, as a result, cause the "d to conduction" band transitions to appear at shorter wavelengths. With this model, the observed conductivity should be slightly greater at all wavelengths and the secondary peak at 600A should be retained, though broadened.

With one exception, the experimental data do not confirm any of these predictions. The exception is the appearance of the broad peak between 1200 and 1800A which suggests the shift of d-band transitions to shorter wavelengths, but this could be simply a result of raising E_f.

It appears that the alloy data cannot be explained on the basis of the rigid band model.

Let us now consider the Cohen-Heine (hereafter referred to as C-H) hypothesis and its consequences. The C-H Fermi surface would pull away from the zone face, perhaps to the extreme of losing contact entirely. Energy gaps at B. Z. boundaries would decrease and the Fermi surface would approach a spherical shape. These features seem to be the requirements for explanation of the experimental data. Reduction or loss of contact at the zone face would indeed require that the 600A peak either diminish or vanish. Also, a result of sphericizing the Fermi surface would be a conductivity curve more like the free electron curve of Figure 9. That the trend is in this direction is demonstrated by a comparison of the free electron and the alloy data in Figure 20. Although the alloy curve has assumed some of the character of the free electron curve, there is sufficient discrepancy to warrant the assumption of a Fermi surface which is still distorted but to a lesser degree than that for silver.

Utilizing these features of the C-H theory, a Fermi surface was estimated for the AgIn alloy. In conformity with the alloy e/a of 1.2,

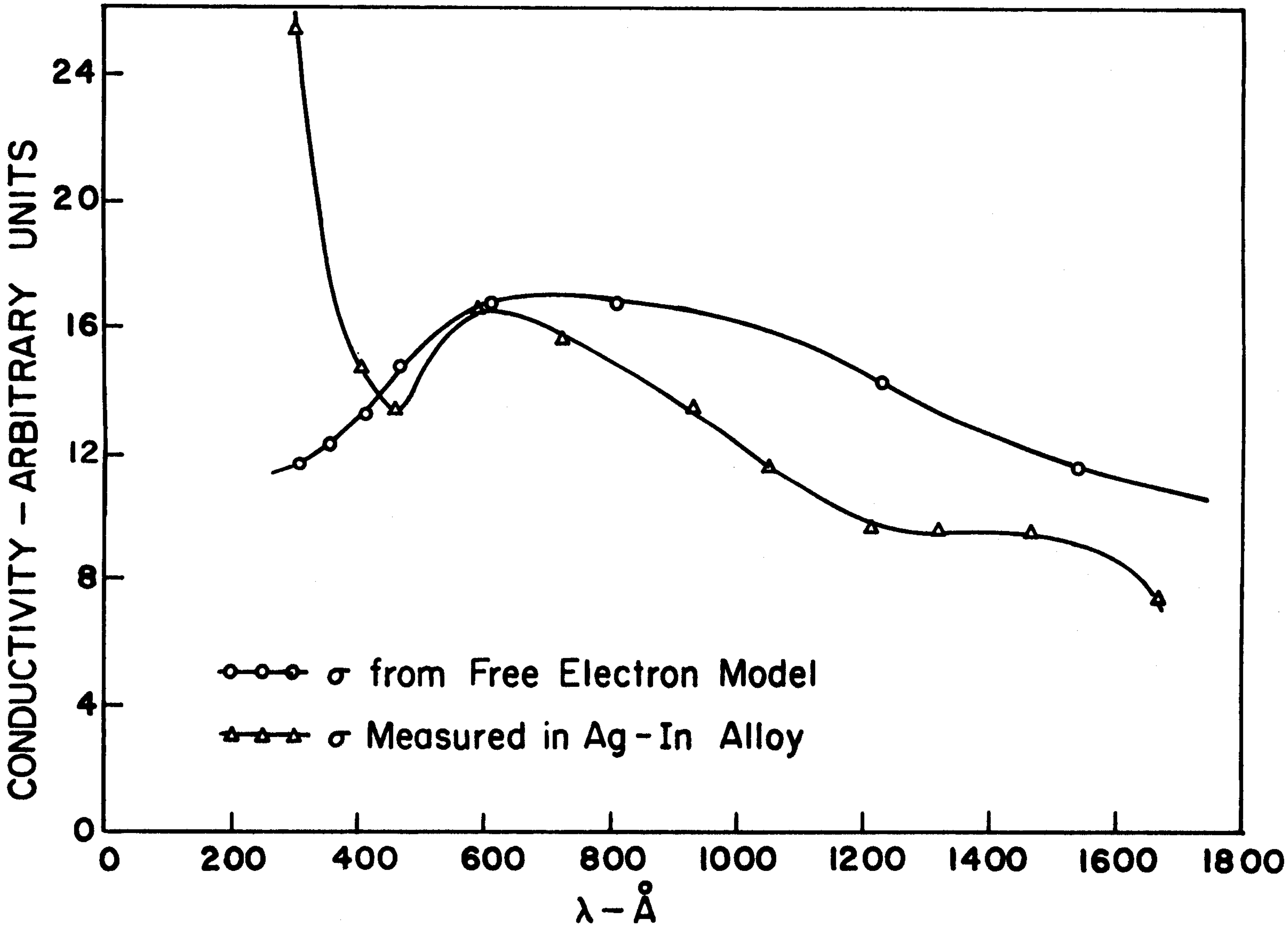

Figure 20
Conductivity of AgIn alloy and free electron model.

the volume enclosed by this surface was adjusted to be 20 per cent greater than the volume used for silver. Only a point contact was retained at the hexagonal zone face as is illustrated in Figure 21. The E(k) were adjusted for decreased gap using the formula proposed by C-H:[27]

$$(3)\qquad \overline{\Delta sp} = \frac{(e/a - 1)}{e/a} \cdot \left(1 - \frac{1}{z - 1}\right)\left[(\Delta sp)_{solute} - (\Delta sp)_{solvent} \right] .$$

This formula gives the average change in the gap size at the zone faces. The terms in the brackets are obtained from the atomic term values, several of which are listed in their report, e.g., Ag: 3.75 ev, In: 7.5 ev, Au: 4.75 ev, and Al: 6.9 ev. The symbol z in the formula is used to denote the valence of the solute. Upon substitution of the values for silver and indium in their formula, an average change of gap of 0.94 ev was obtained and the E(k) were corrected by this amount.

Using this modified Fermi surface and E(k), a computation of conductivity for the alloy was performed in the same manner as outlined earlier for silver; these results are presented in Figure 22 and Table V. A comparison of the experimental and calculated curves indicate that this choice of modified Fermi surface is not a bad one, inasmuch as there is quite good agreement in the wavelengths at which the maxima and minima occur. Small changes in the area of contact of the Fermi surface have a pronounced effect on the calculated results in the range of 500 to 700A. Despite the few experimental points available in this range, one can conclude that the area of contact for the alloy does not exceed 10 per cent of that for silver.

To make the magnitudes of the computed and measured conductivities coincide over the range studied requires a value of $P_{\vec{k}'\vec{k}}$ of 0.6×10^5 cm^{-2} in contrast with the value of 1.0×10^5 obtained for silver. Thus it would appear that an effect of alloying at this

---

[27] M. H. Cohen and V. Heine, op. cit.

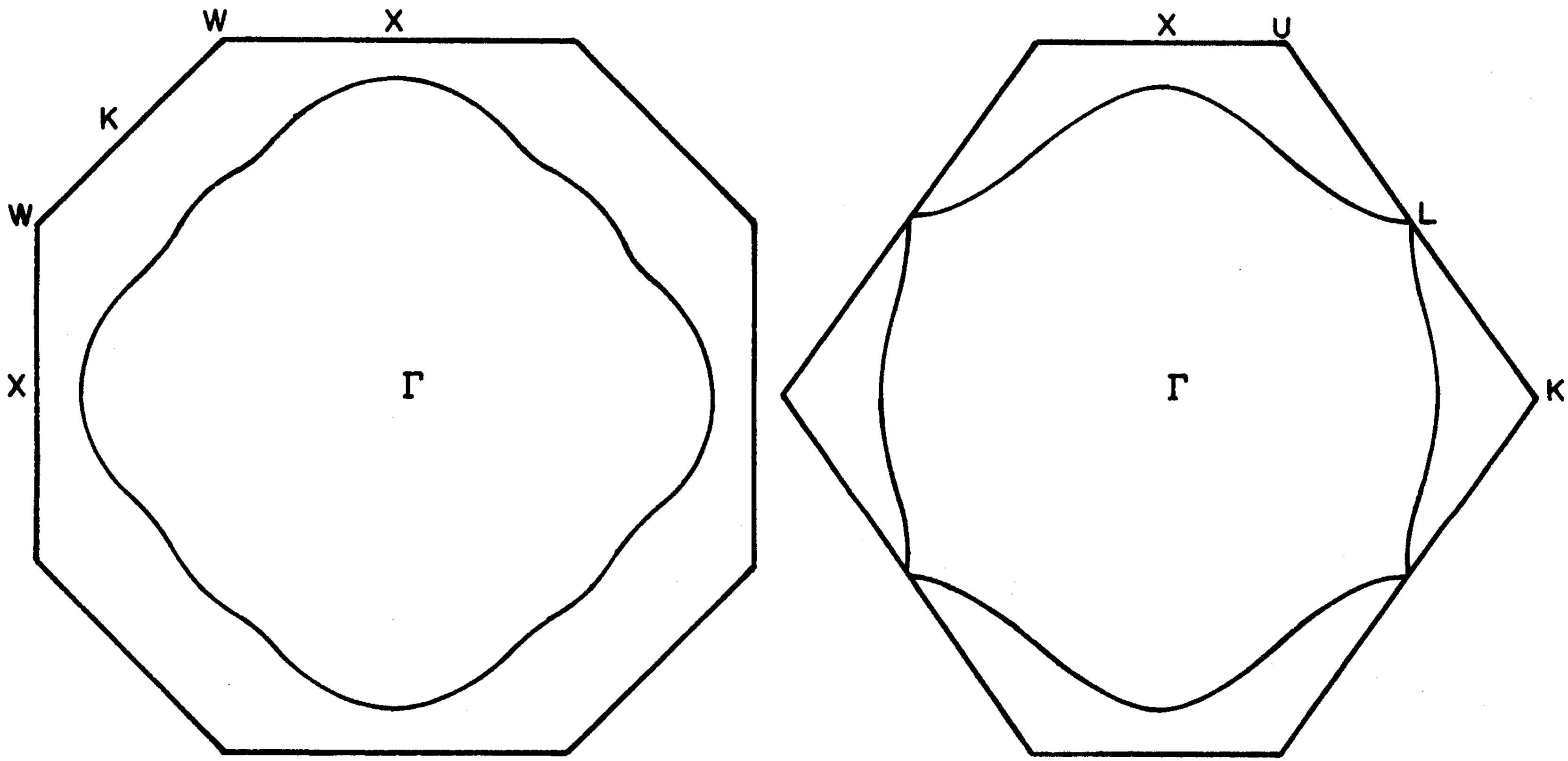

Figure 21
Estimated Fermi surface for AgIn alloy.

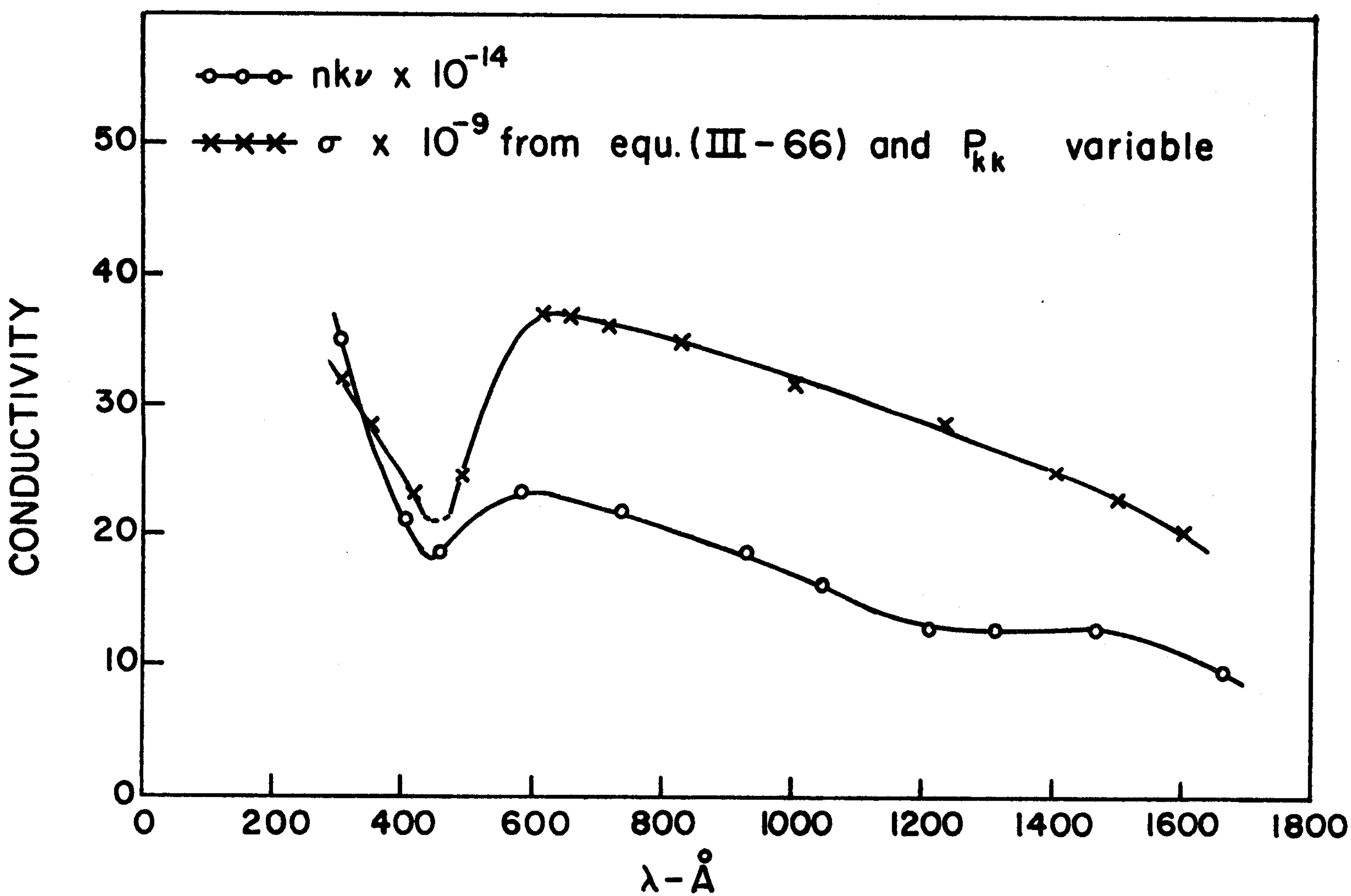

Figure 22
AgIn Conductivity vs. wavelength.

TABLE V

DATA USED IN AG-IN COMPUTATION
(EQUATION 66)

λ - A	$A(K_X)$	$A(K_L)$	$A(K_K)$	$\sum A(K)$	$\sigma/P \times 10^{-9}$
309	16.3	16.1	30.7	63.1	31.8
352	16.7	18.7	14.6	50.0	28.7
412	16.2	18.0	0	34.2	23.0
493	12.6	18.0		30.6	24.6
617	10.6	19.4		30.0	37.5
650	10.8	19.9		30.7	36.7
714	8.1	20.5		28.6	36.5
825	6.0	18.0		24.0	35.0
1000	3.8	15.7		19.5	31.8
1230	2.5	11.9		14.4	28.9
1400	1.6	9.3		10.9	25.0
1500	1.3	8.0		9.3	22.9
1600	1.0	6.8		7.8	20.2

concentration is to reduce the transition probability between conduction and excited band by a factor of almost two. This effect appears to be primarily due to the decrease of energy gap at the zone faces and can be qualitatively predicted by the "almost free" electron approach of Chapter III.

Recalling equations (39) and (45), we write the Bloch function for the case of a small perturbing potential

$$(4) \qquad \psi_{\vec{k}} = e^{i\vec{k}\cdot\vec{r}} \sum_{\vec{K}_i} c(\vec{K}_i) e^{i\vec{K}_i\cdot\vec{r}}$$

$$\psi_{\vec{k}} = c(0) \left\{ \sum_{\vec{K}_i} \frac{2m}{\hbar^2} \frac{V(\vec{K}_i)}{2\vec{k}\cdot\vec{K}_i - K^2_1} \right\} e^{i\vec{k}\cdot\vec{r}} \; .$$

Use of this expression to derive $P_{\vec{k}',\vec{k}}$ gives the result

$$(5) \qquad P_{k',k} = \left| \int \psi_{\vec{k}} \, \mathrm{grad}_x \, \psi_{\vec{k}'} \, d\tau \right|^2 = \left| -\frac{2im}{\hbar^2} \frac{K_x V(\vec{K})}{2\vec{k}\cdot\vec{K} + K^2} \right|^2 ,$$

which shows that $P_{\vec{k}',\vec{k}}$ should go as the square of the Fourier term, $V(\vec{K})$, or as $|E_{sp}/2|^2$. $P_{\vec{k}'\vec{k}}$ can now be written in terms of energy gaps in the form

$$(6) \qquad P_{\vec{k}'\vec{k}}(AgIn) = P_{\vec{k}'\vec{k}}(Ag) \left[\frac{E_{sp}(AgIn)}{E_{sp}(Ag)} \right]^2 .$$

The average value of $E_{sp}(Ag)$, from Figure 12 is 3.6 ev.; this value was reduced by the C-H formula to 2.7 ev. for $E_{sp}(AgIn)$. Equation (6) therefore predicts the transition probability for theAgIn alloy to be less than that for silver by a factor of 0.56, in agreement with the computed factor of 0.60 derived from Figure 22. This close agreement is no doubt in part fortuitous. If it is assumed that the d-band produces distortions in E(k) of the conduction band in the alloy also, then the simple approach used above cannot be expected to apply exactly. But this approach does show the general dependence of $P_{\vec{k}'\vec{k}}$ on E_{sp} and the results lend further support to the C-H theory for alloys.

To summarize, we can say that the major effects observed as a result of alloying silver with indium are (1) the transition probability between conduction and excited bands is reduced by a factor of 0.6 for 10 at .% In, (2) a Fermi surface having reduced contact at the zone boundary provides the proper basis for interpretation of the optical data, and (3) energy gaps at the zone boundaries diminish. These effects suggest a breakdown of the rigid band concept and support the theory advanced by Cohen and Heine.

C. Results for Gold

At the present time only a limited amount of theoretical information is available for the gold band structure. The work of Segall[28] includes a calculation for gold, but in this, he determined the energy at the symmetry points X, Γ, and L only. He points out that one should expect considerably more uncertainty in the potential he has constructed for gold than in the potential used for copper and silver. Since gold is a much heavier atom than the other two, the non-relativistic wave functions and the potential based on them will be less accurate, and, at present, only Hartree functions are available. Segall's results place the p-like states at the gaps at X and L lower in energy than the s-like states, as for silver, but the d-bands fall below even the Γ_1 state. The energies below 24 ev. at the symmetry points Γ, X, and L in Figure 25 are those obtained by Segall.

The calculations of Cohen and Heine[29] predict a differently ordered band structure. Although they make no estimate of the relative positions of the d-bands, their results place the p-like states at X and

---

[28] B. Segall, op. cit.

[29] M. Cohen and V. Heine, op. cit.

L higher in energy than the s-like states. In their band model, the conduction and excited bands overlap near L and the gap at L is only -0.75 ev. They also offer the suggestion, "...The optical constants and electronic heat of gold indicate considerable distortion of the Fermi surface but little, if any contact." No further reference is made to the optical constants used in this conclusion, but they were undoubtedly not ones obtained in the far ultraviolet.

Morse et al.,[30] recently reported on Fermi surface shapes as determined by the method of ultrasonic attenuation in a magnetic field. For gold, they report a radius of contact of 0.24×10^{-19} g-cm/sec at the point L, in partial confirmation of Segall's results. Their data for other directions in k-space are reproduced in Figure 26.

It was with this background of meager and contradictory information that the optical properties of gold were studied and efforts were made to interpret them in terms of band structure.

Representative reflectivity measurements on gold films at four angles of incidence and over the wavelength range 304 to 1671A are summarized in Figure 23 and Table VI. Gold conductivity as determined from n and k is plotted as a function of wavelength in Figure 24.

A conductivity computation was made from a band structure based on the Fermi surface reported by Morse, the symmetry point energies calculated by Segall, and an estimated E(k) between these symmetry points as shown in Figure 25. An E_f was chosen which was compatible with the Morse shape and volume. The results of this computation are compared with experimental data in Figure 24 and are reported in Table VII.

The computed peak at 500A has an origin different from the similar one observed in silver. Because of the highly distorted Fermi surface of gold, Figure 26 shows that there is a pronounced increase

---

[30] R. W. Morse, A. Myers, C. T. Walker, J. Accoustical Soc. Am., <u>33</u>, 699 (1961).

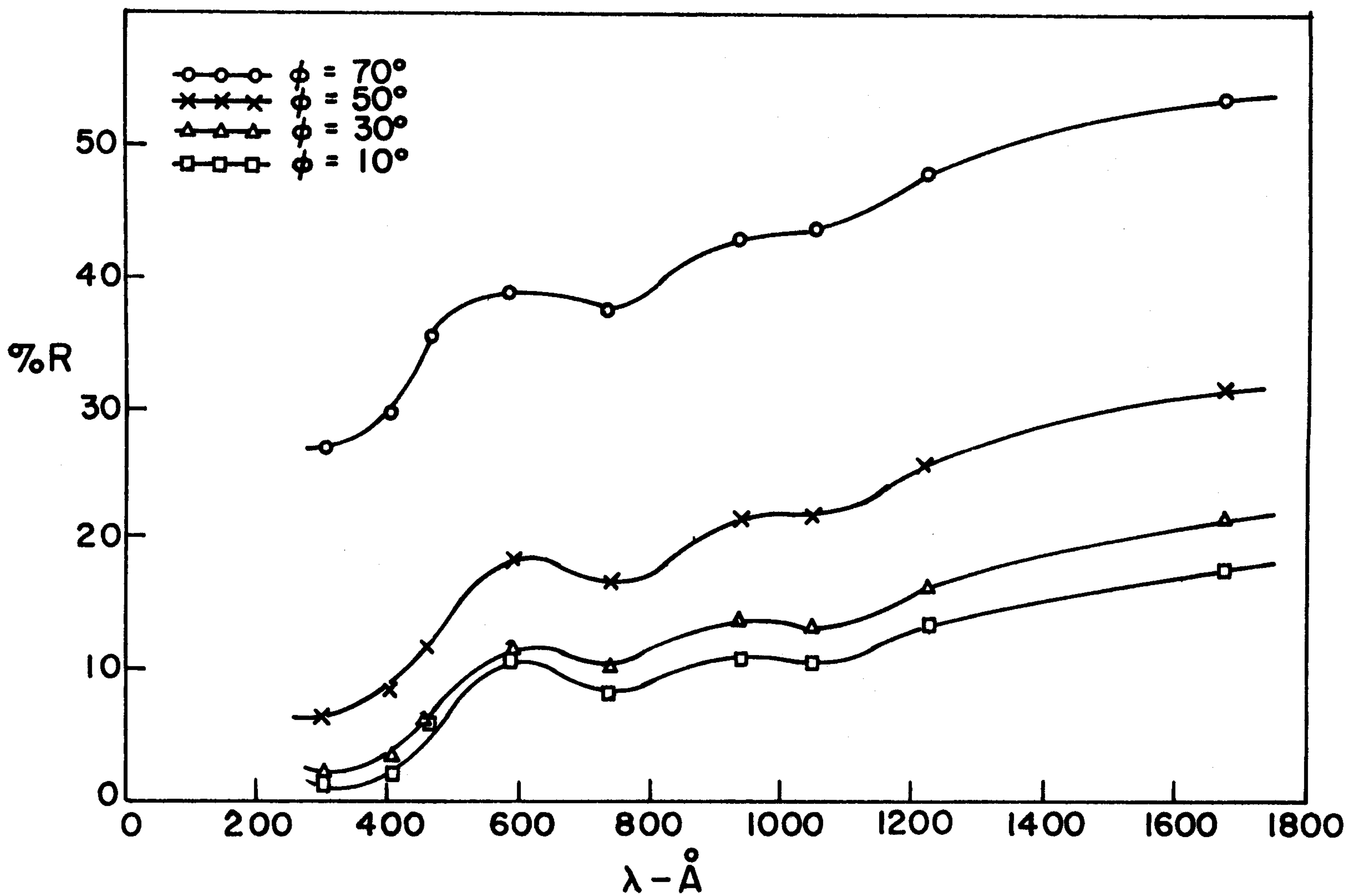

Figure 23
Reflectivity of gold vs. wavelength.

TABLE VI

GOLD REFLECTIVITY DATA

λ - A	θ	RBm	RBk	%R	n	k
304	D	66.0	40.0		0.89	0.23
	70	41.0	34.0	26.9		
	50	32.9	31.3	6.2		
	30	30.0	29.5	1.9		
	10	29.0	28.6	1.5		
406	D	66.0	41.6		0.91	0.31
	70	45.6	38.4	29.5		
	50	39.9	37.9	8.2		
	30	38.1	37.3	3.3		
	10	37.9	37.5	1.6		
461	D	87.8	29.5		0.91	0.39
	70	46.0	25.6	35.0		
	50	31.3	24.5	11.6		
	30	26.5	23.0	6.0		
	10	26.0	22.5	6.0		
584	D	75.5	3.0		0.98	0.67
	70	30.5	2.5	38.6		
	50	15.4	2.0	18.5		
	30	10.6	2.0	11.7		
	10	9.6	2.0	10.5		
735	D	97.0	6.4		0.93	0.58
	70	38.4	4.3	37.6		
	50	19.2	4.2	16.5		
	30	13.1	4.0	10.0		
	10	11.3	4.0	8.0		
932	D	71.7	4.5		0.98	0.71
	70	32.0	3.1	43.0		
	50	17.8	3.1	21.7		
	30	12.3	3.1	13.7		
	10	10.4	3.1	10.9		

TABLE VI (Continued)

GOLD REFLECTIVITY DATA

λ - A	θ	RBm	RBk	%R	n	k
1048	D	92.0	2.0		1.05	0.69
	70	40.0	0.9	43.5		
	50	20.5	0.9	21.8		
	30	12.8	0.9	13.2		
	10	10.4	0.9	10.5		
1216	D	89.5	1.2		1.12	0.80
	70	42.5	1.0	47.0		
	50	23.5	1.0	25.4		
	30	15.0	1.0	15.8		
	10	12.1	1.0	12.6		
1671	D	51.5	6.0		1.04	0.94
	70	28.6	4.2	53.6		
	50	18.0	3.5	31.9		
	30	12.9	3.1	21.5		
	10	10.8	2.8	17.6		

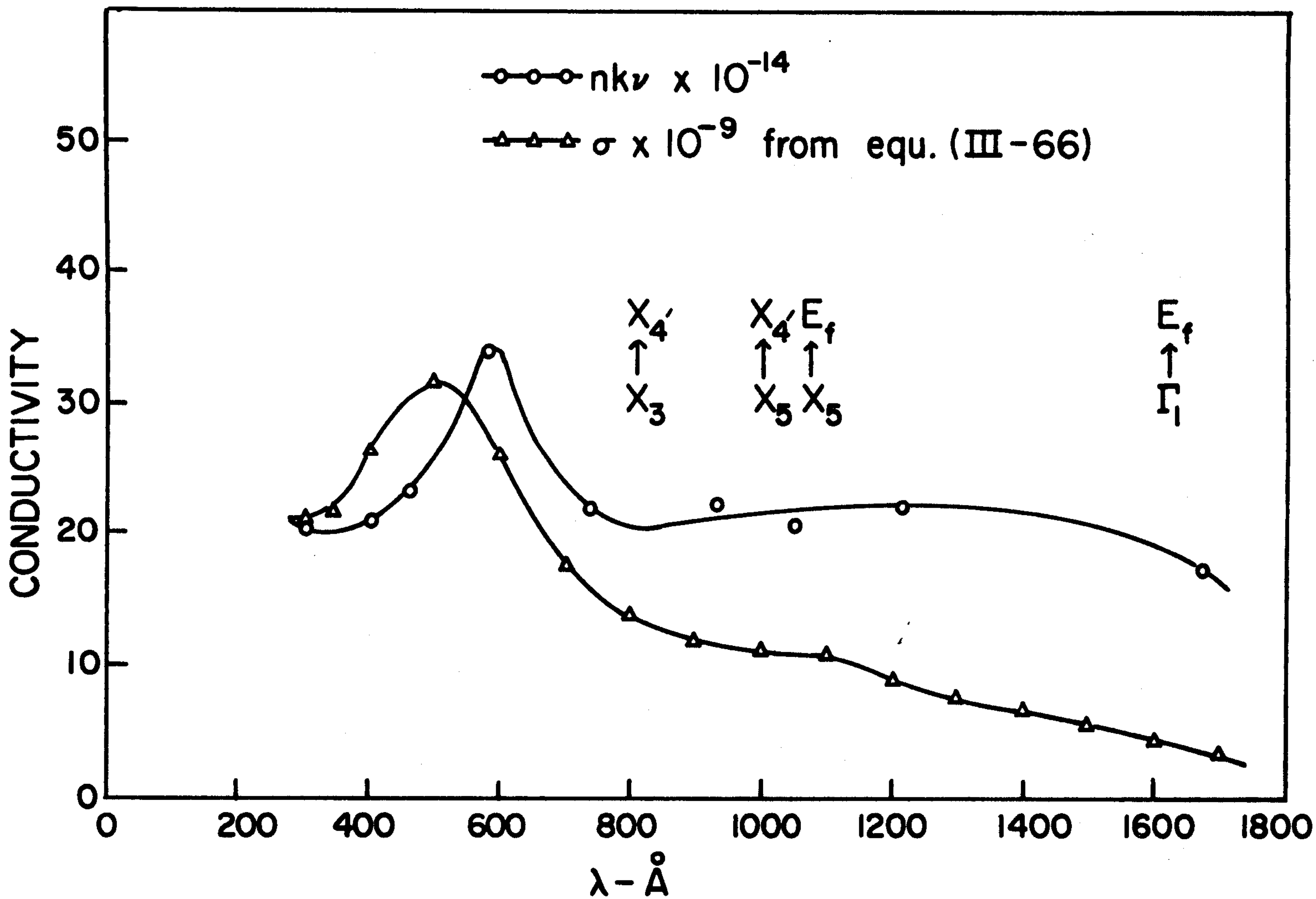

Figure 24
Conductivity of Gold vs. Wavelength.

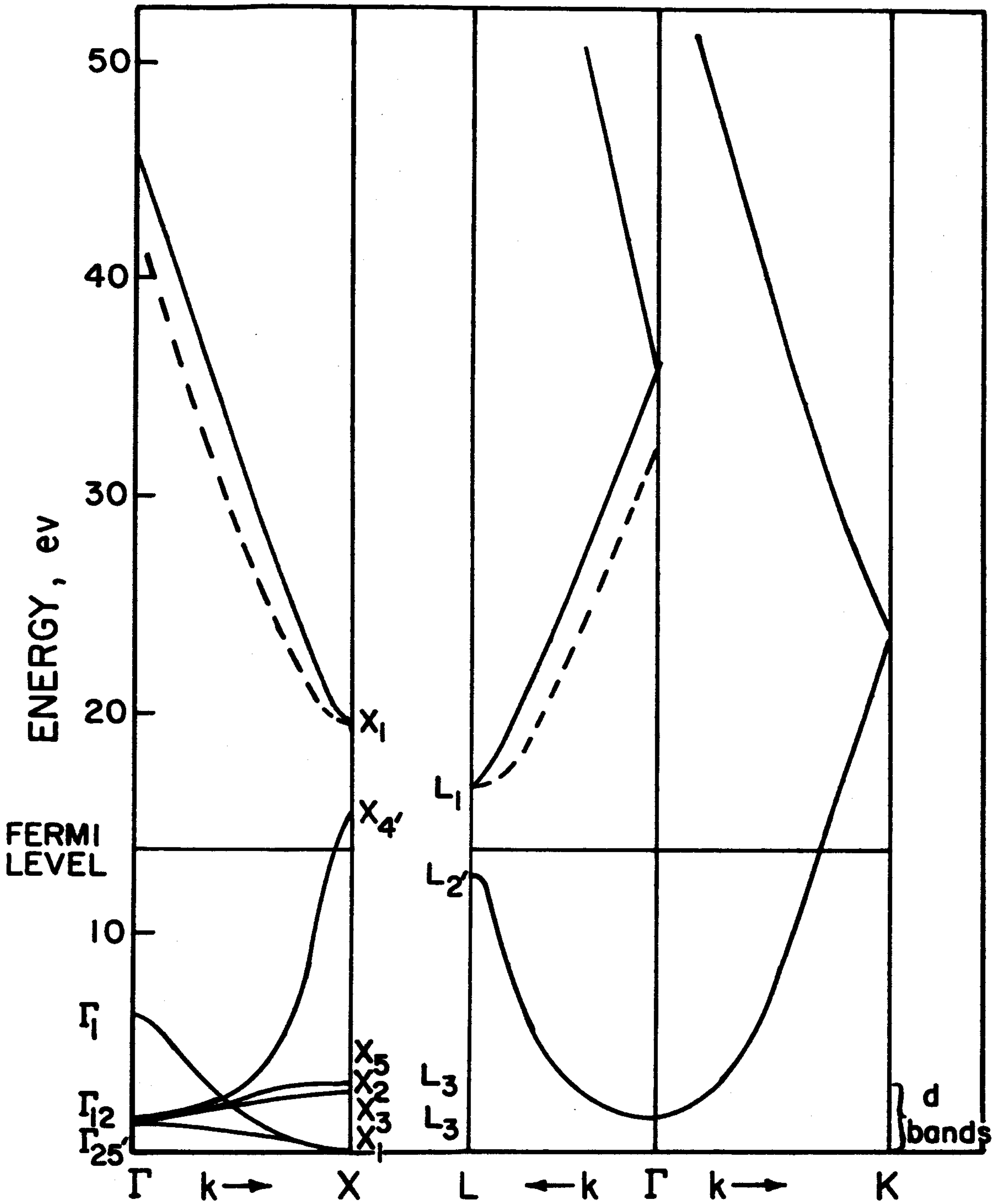

Figure 25
Energy band structure for gold. Energy values at symmetry points are from Segall's calculations; the E(k) values between symmetry points are estimated.

TABLE VII

DATA USED FOR GOLD COMPUTATION
(EQUATION 66, FIGURE 23)

λ - A	$A(K_X)$	$A(K_L)$	$A(K_K)$	$\sum A(K)$	$\sigma/PX10^{-9}$
300	19.1	20.5	3.5	43.1	21.0
350	17.7	20.5	0	38.2	21.8
400	16.2	20.5		36.7	26.4
500	12.8	19.6		32.4	31.8
600	9.0	15.1		24.1	26.1
700	4.9	10.8		15.7	18.0
800	2.3	8.6		10.9	14.2
900	1.5	6.8		8.3	12.2
1000	1.2	5.7		6.9	11.3
1100	1.0	4.6		5.6	11.1
1200	0.8	3.7		4.5	8.8
1300	0.5	3.1		3.6	7.7
1400	0.4	2.5		2.9	6.7
1500	0.1	2.2		2.3	5.7
1600	0	1.7		1.7	4.4
1700		1.3		1.3	3.6
1800		1.0		1.0	2.9

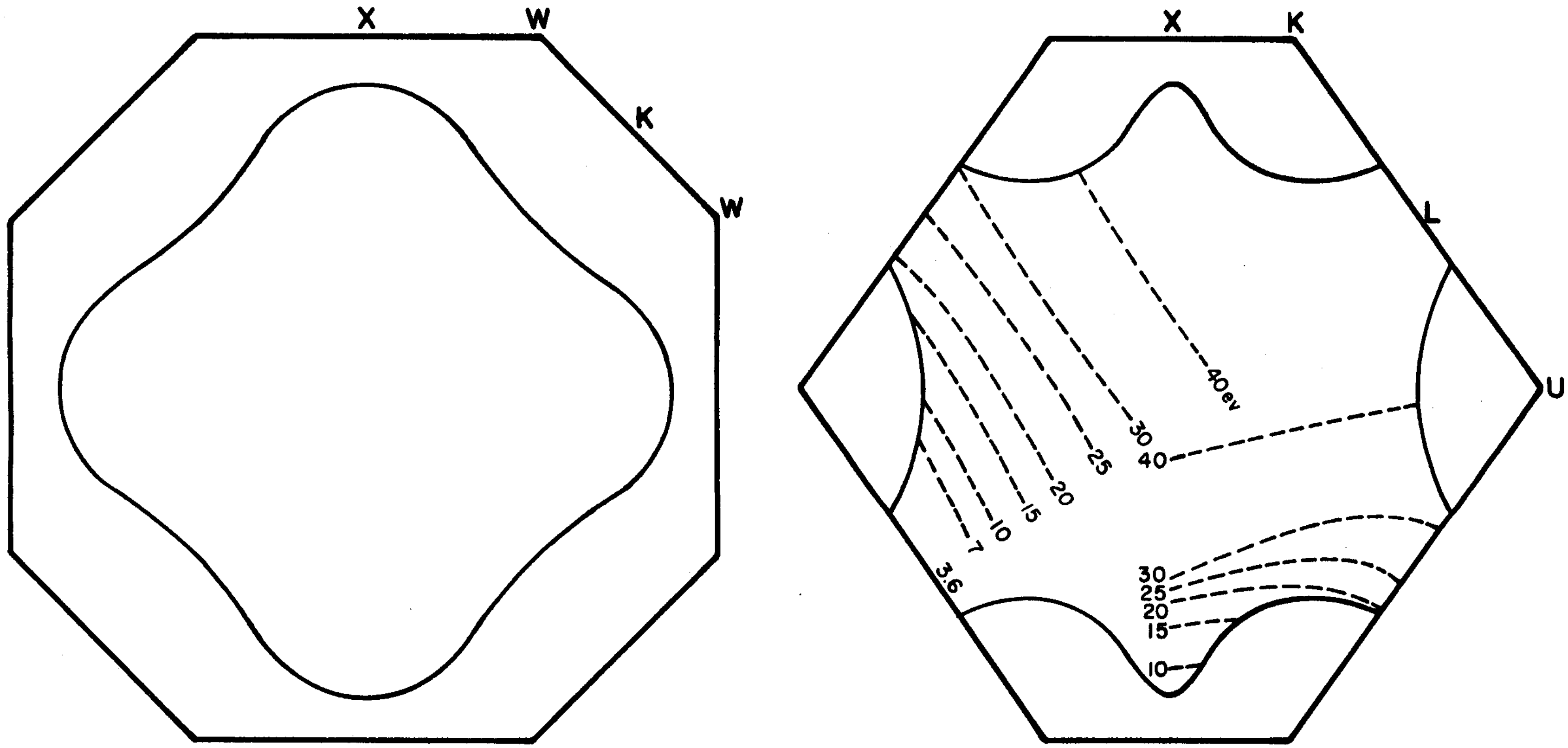

Figure 26
Fermi surface for gold from ultrasonic attenuation measurements of Morse. Discs shown are for E(k) of Figure 24.

in the number of electrons available for transitions in the energy range 20 to 30 ev. Thus, part of this peak would appear even if the increased $P_{\vec{k}'\vec{k}}$ had not been considered in this region. To shift this peak to 600A requires that those discs which touch the zone face near L be associated with lower energy transitions than presently assumed; a decrease of about 4 ev. would be satisfactory. The desired change cannot be effected by simply raising the level of Γ_{12} since this would still allow the 25 ev. disc to contact the zone face at L. The only change in band structure which can bring these peaks into coincidence is one which lowers the energy levels above L_1 and X_1. The dotted E(k) in Figure 25 performs this function while retaining the gaps prescribed by Segall.

In the range of 300 to 800A the magnitudes of computed and measured conductivity are equal if an average value of $P_{\vec{k}'\vec{k}}$ of 10^5 cm^{-2} is assumed. This value is the same as for silver and would indicate that the transition probability between conduction and excited bands is the same for both metals in this wavelength range.

Between 800 and 1800A we find a divergence of computed and measured values; the experimental data suggest the presence of transitions in this range which were not accounted for in the computation. Figure 25 indicates the possibility of the following transitions from the d-bands:

X_3 to $X_{4'}$: 15.2 ev, 810A
X_5 to $X_{4'}$: 12.3 ev, 1000A
X_5 to E_f : 11.5 ev, 1070A
Γ_1 to E_f : 7.6 ev, 1620A.

The first three transitions go from d-like to p-like states near the Fermi level and the last goes from s-like states to the p-like states, thus the probability should be relatively high for these four possibilities. It seems not unlikely, therefore, that conductivity in the 800 to 1800A range is due to transitions of the two types: (1) conduction to excited band and (2) d and s states to unfilled states near the Fermi level.

In a discussion of nk curves for the noble metals, Seitz[31] argues that the peak in nk observed for silver at 2500A can be attributed to transitions from conduction to excited bands. He then supposes that silver and gold have similar valence electron structures and anticipates a peak in the gold nk curve at the same wavelength and for the same reason. He thus infers that the peak for gold at 4000A arises from d-band to Fermi level transitions. In our interpretation which is based on the Segall, Morse and optical data, the inverse situation is demanded. Indeed, if our model is extended to longer wavelengths, it predicts the observed conductivity peak at 3700A and attributes it to transitions in the L direction which originate from the neck areas near L, for example, the 3.6 ev. disc in Figure 26.

As a result of these studies one can conclude that the theoretical calculations of Segall are in accord with the accoustical attenuation measurements of Morse and with the optical constant data obtained in the far ultraviolet. Furthermore, the use of the disc model can be of great value in the interpretation of optical data particularly when the energies between sets of bands overlap as in gold.

D. Gold-Aluminum Alloys

In the course of measuring reflectivity of AuAl films it was noticed that at a critical concentration of aluminum, reflectivity at 304A and near normal incidence increased by a factor of approximately three. Several films were prepared and studied to determine as closely as possible the concentration at which this effect occurs. The data in Table VIII show that the onset of this increase is associated with an aluminum concentration of between 22.6 and 24.6 at.%, or an electron per atom ratio of about 1.47.

Reflectivity and conductivity data for films with concentrations slightly above and below the critical one are given in Figures 27, 28 and

---

[31] F. Seitz, op. cit. p. 655.

TABLE VIII

GOLD REFLECTIVITY AT 304A, $\phi = 10°$, FOR VARIOUS CONCENTRATIONS OF ALUMINUM

FILM #	wt.% Al	at.% Al	e/a	%R
Au-3	0	0	1.0	1.5
Au-Al-8	3.4	20.4	1.41	2.2
Au-Al-9	3.8	22.6	1.45	2.0
Au-Al-10	4.3	24.6	1.49	6.9
Au-Al-7	4.9	27.4	1.55	6.1
Au-Al-6	6.6	34.1	1.68	4.9
Au-Al-1	7.5	37.2	1.75	6.2

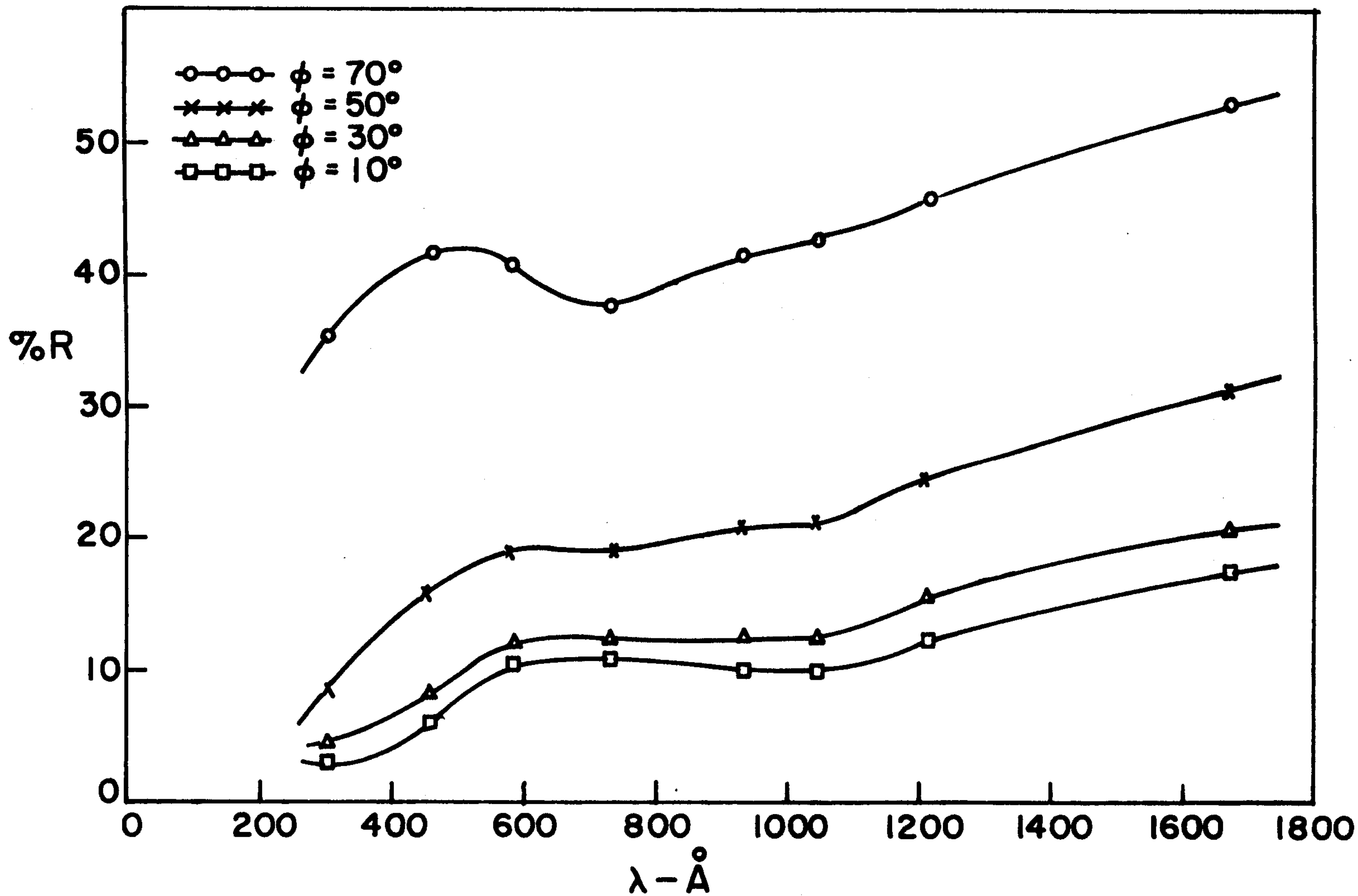

Figure 27
Reflectivity of film #AuAl-8,(22.6 at .%Al) vs. wavelength.

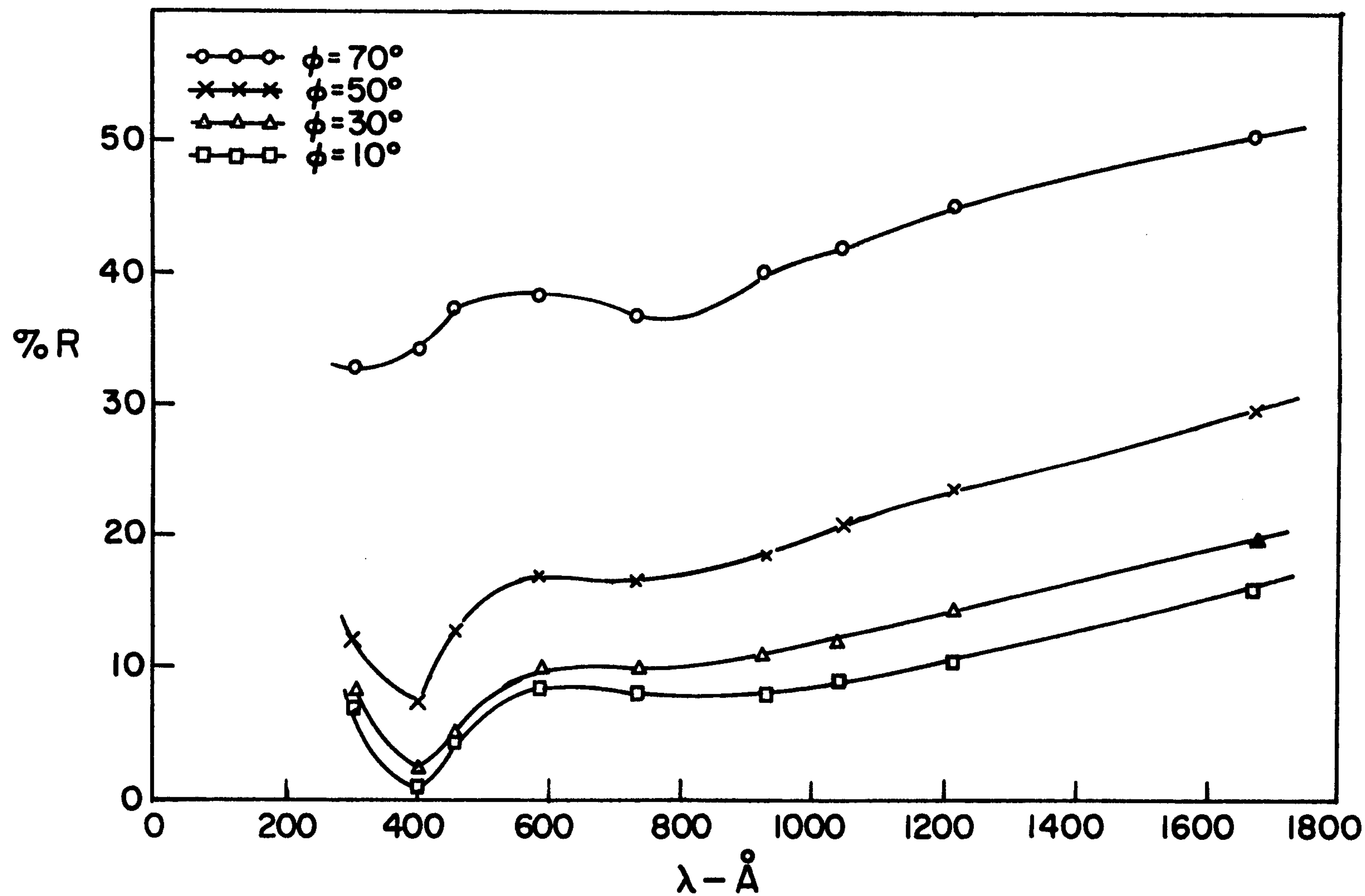

Figure 28
Reflectivity of film #AuAl-10 (24.6 at . %Al) vs. wavelength.

29 and Tables IX and X.

Somewhere in this range of concentrations a phase change apparently occurs but at the present time, metallurgical information is not complete enough to clarify the problem. We quote from a publication as recent as Hansen's,[32] (1958): "In spite of quite extensive investigation by thermal and some micrographic analysis as well as X-ray studies, the composition of some of the intermediate phases and the phase relations in the range 70-90 at.% Au are still not fully known. On the basis of X-ray work, (8) asserted that in the neighborhood of 75 at.% Au a phase, not found by others, (1,7), is formed peritectically, but there is no indication of a peritectic reaction in this range. On the other hand, the occurrence of Au_3Al (95.64 wt.%Au) has been reported on the basis of X-ray studies (3,13) which revealed the existence of a phase with the structure β-Mn.---However, it was shown that a phase of the composition Au_3Al does not exist, (9), and that the phase with the structure of β-Mn has the composition of Au_4Al rather than Au_3Al (7,9). Also, (1) and (8) have claimed the compound Au_4Al to exist. Its structure was found to be similar to, but not completely identical with that of β-Mn (8,9)." (The references in parentheses are Hansen's.)

Since the concentration at which this large change in reflectivity and conductivity occurs, (4.3 wt.%), is very near that of Au_3Al, (4.36 wt.%), it is possible that our data are evidence for the existence of this phase.

The β-Mn structure has 20 atoms per unit cell, but it is of the cubic system and could possibly possess a Brillouin zone similar to the face-centered cubic system of gold. If such were the case, we would have an explanation for the similarity of conductivity curves for Au and the Au-Al alloys. This point must be left open for future study, however, since the space group of the β-Mn structure is also not fully known.

---

[32] M. Hansen, op. cit.

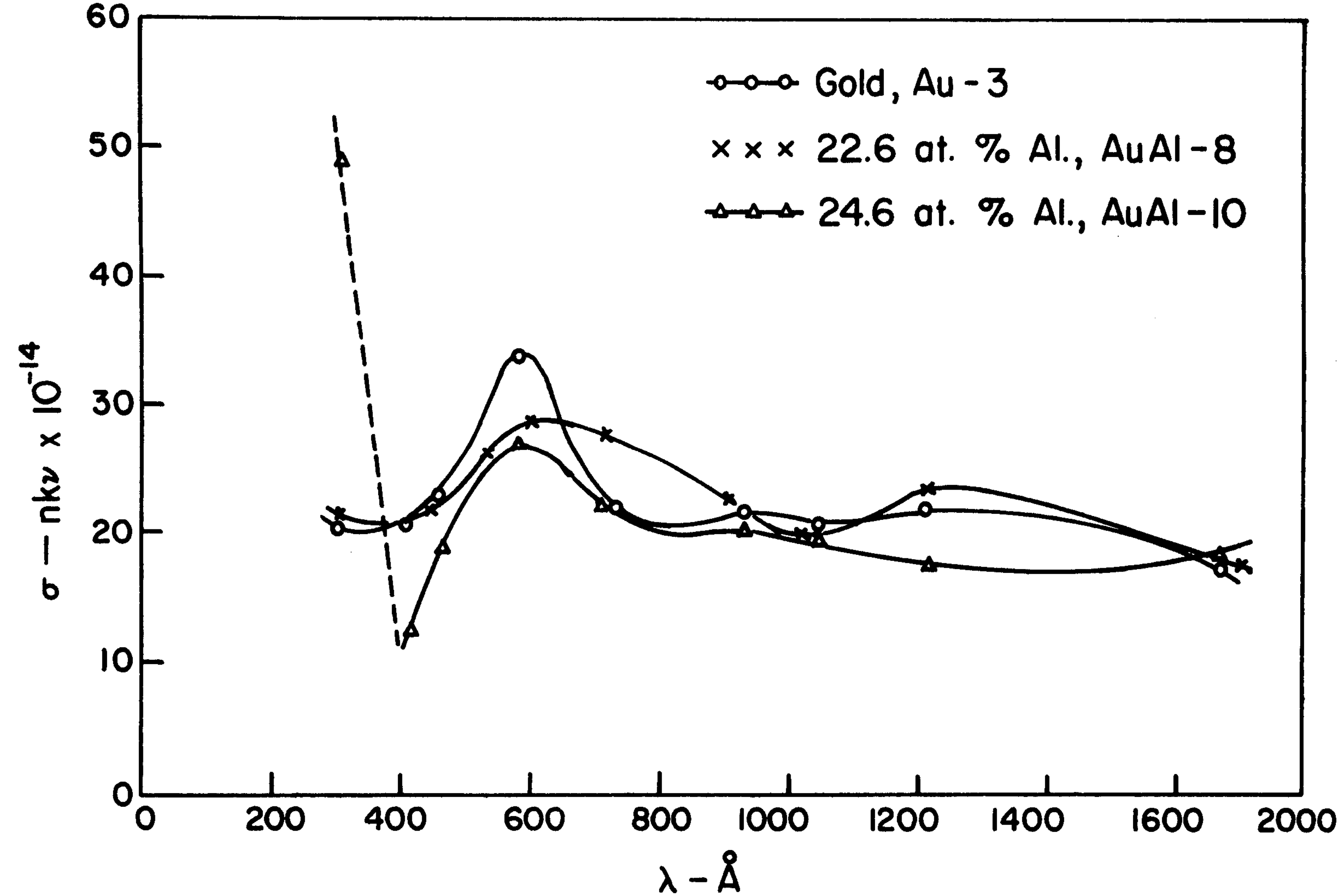

Figure 29
Conductivity of Au and AuAl alloy vs. wavelength.

TABLE IX

GOLD-ALUMINUM REFLECTIVITY DATA
(Au-Al-8, 3.38 wt % Al)

λ - A	θ	RBm	RBk	%R	n	k
304	D	49.5	27.0		0.83	0.27
	70	30.3	22.4	35.1		
	50	22.4	20.5	8.5		
	30	21.0	20.0	4.5		
	10	20.5	20.0	2.2		
461	D	90.7	31.0		0.81	0.41
	70	48.8	23.8	41.9		
	50	32.0	22.6	15.7		
	30	26.8	22.0	8.0		
	10	25.0	21.6	5.7		
584	D	50.5	3.8		0.90	0.63
	70	22.6	3.5	40.9		
	50	12.3	3.5	18.9		
	30	9.1	3.5	12.0		
	10	8.4	3.5	10.5		
735	D	93.5	5.4		0.99	0.69
	70	37.6	4.2	37.8		
	50	20.0	3.6	18.7		
	30	14.2	3.4	12.2		
	10	13.0	3.4	10.9		
932	D	91.2	14.8		1.01	0.68
	70	45.0	13.1	41.8		
	50	29.0	13.1	20.8		
	30	22.8	13.1	12.7		
	10	20.8	13.1	10.2		
1048	D	58.2	2.0		1.04	0.67
	70	25.8	1.7	42.9		
	50	13.6	1.7	21.2		
	30	8.8	1.7	12.6		
	10	7.1	1.7	9.6		

TABLE IX (Continued)

GOLD-ALUMINUM REFLECTIVITY DATA
(Au-Al-8, 3.38 wt % Al)

λ - A	θ	RBm	RBk	%R	n	k
1216	D	71.5	6.2		1.24	0.79
	70	35.5	5.5	45.9		
	50	21.6	5.5	24.6		
	30	15.7	5.5	15.6		
	10	13.6	5.5	12.4		
1671	D	47.4	6.2		1.02	0.91
	70	26.8	4.9	53.2		
	50	17.2	4.2	31.6		
	30	12.5	3.9	20.9		
	10	10.8	3.6	17.5		

TABLE X

GOLD-ALUMINUM REFLECTIVITY DATA
(Au-Al-10, 4.3 wt % Al)

λ - A	θ	RBm	RBk	%R	n	k
304	D	72.0	56.1		0.94	0.53
	70	46.4	41.2	32.7		
	50	40.9	39.0	12.0		
	30	39.0	37.7	8.2		
	10	38.5	37.4	6.9		
406	D	66.2	43.3		0.85	0.20
	70	45.8	38.0	34.1		
	50	38.5	36.8	7.4		
	30	36.5	36.0	2.2		
	10	36.1	35.9	0.9		
461	D	89.8	32.0		0.83	0.35
	70	45.7	24.0	37.5		
	50	30.5	23.0	12.9		
	30	25.2	22.2	5.2		
	10	24.5	21.7	4.8		
584	D	74.2	3.9		0.92	0.58
	70	29.5	2.5	38.4		
	50	14.2	1.8	17.3		
	30	9.0	1.8	10.2		
	10	7.8	1.8	8.5		
735	D	80.6	3.6		0.93	0.59
	70	30.9	2.5	36.8		
	50	15.0	2.1	16.8		
	30	9.6	2.0	9.9		
	10	8.0	1.8	8.0		

TABLE X (Continued)

GOLD-ALUMINUM REFLECTIVITY DATA
(Au-Al-10, 4.3 wt % Al)

λ - A	θ	RBm	RBk	%R	n	k
932	D	79.5	19.6		1.00	0.64
	70	41.2	17.1	40.2		
	50	27.8	16.6	18.7		
	30	23.0	16.3	11.2		
	10	21.0	16.2	8.0		
1048	D	94.0	4.8		1.03	0.66
	70	40.8	3.2	42.3		
	50	21.9	3.2	21.0		
	30	14.1	3.2	12.2		
	10	11.6	3.2	9.4		
1216	D	61.7	8.6		1.05	0.69
	70	31.2	7.1	45.4		
	50	19.6	6.9	23.9		
	30	14.5	6.8	14.5		
	10	12.9	6.7	10.7		
1671	D	85.3	12.3		1.14	0.92
	70	44.5	7.5	50.5		
	50	27.5	5.6	30.0		
	30	19.4	4.9	19.9		
	10	16.4	4.6	16.2		

E. Results for Aluminum

The band structure of aluminum has received considerable attention and is now fairly well understood. Heine[33] has calculated the energy gaps at zone faces using the orthogonalized-plane-wave method, (OPW), and Harrison[34] has shown the effectiveness of a single OPW approximation. Since the gaps at the boundary of the first B.Z. are much smaller than the Fermi level energy, the method of Harrison amounts to the "nearly free electron" approximation. The calculations of Segall[35] produce a band structure not unlike Harrison's. All these calculations point to the fact that the free electron E(k) prevails at all places in the zone with the one exception of points very near the zone faces, and in these areas, the distortion of the free electron E(k) is not great.

A model, (Figures 30 and 31), has been constructed which displays those states in the first B.Z. from which optical transitions to the second zone can originate. The presence of occupied states in the second zone negates transitions from a considerable volume of the first zone. Since transitions from occupied states of the second zone to states in the third zone occur at energies greater than those of our immediate interest, they will not be considered here. The same remark applies to those states which are negated in zone one to zone two transitions.

Following methods outlined earlier, a conductivity computation was made with the use of this model. The results as shown in Figure 32 is a curve whose character is radically different from that obtained for

---

[33] V. Heine, Proc. Roy. Soc. London, <u>A240</u>, 361, (1957).

[34] W. A. Harrison, Phys. Rev., <u>118</u>, 1182, (1960).

[35] B. Segall, *op. cit.*

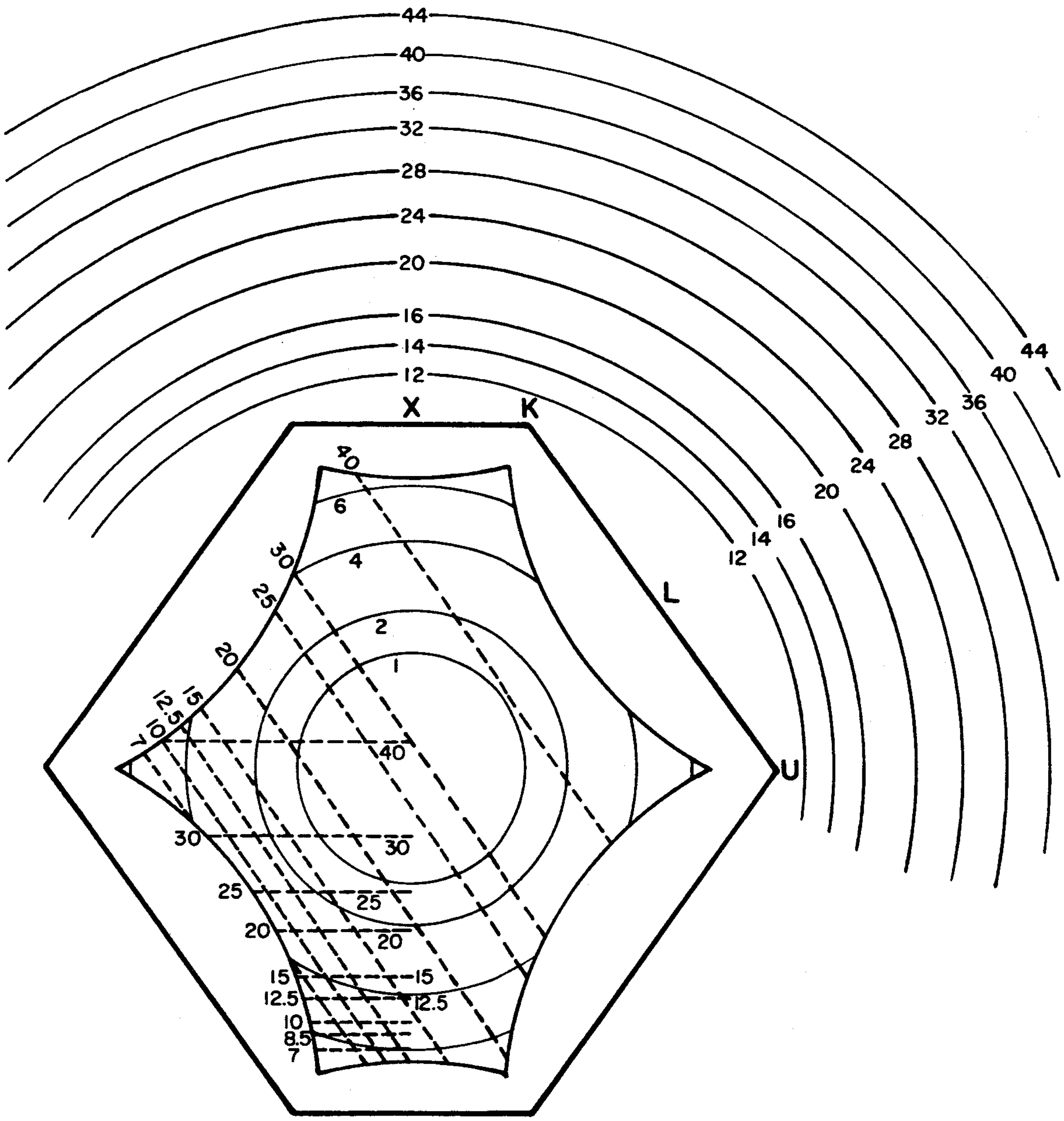

Figure 30
Fermi surface for aluminum.

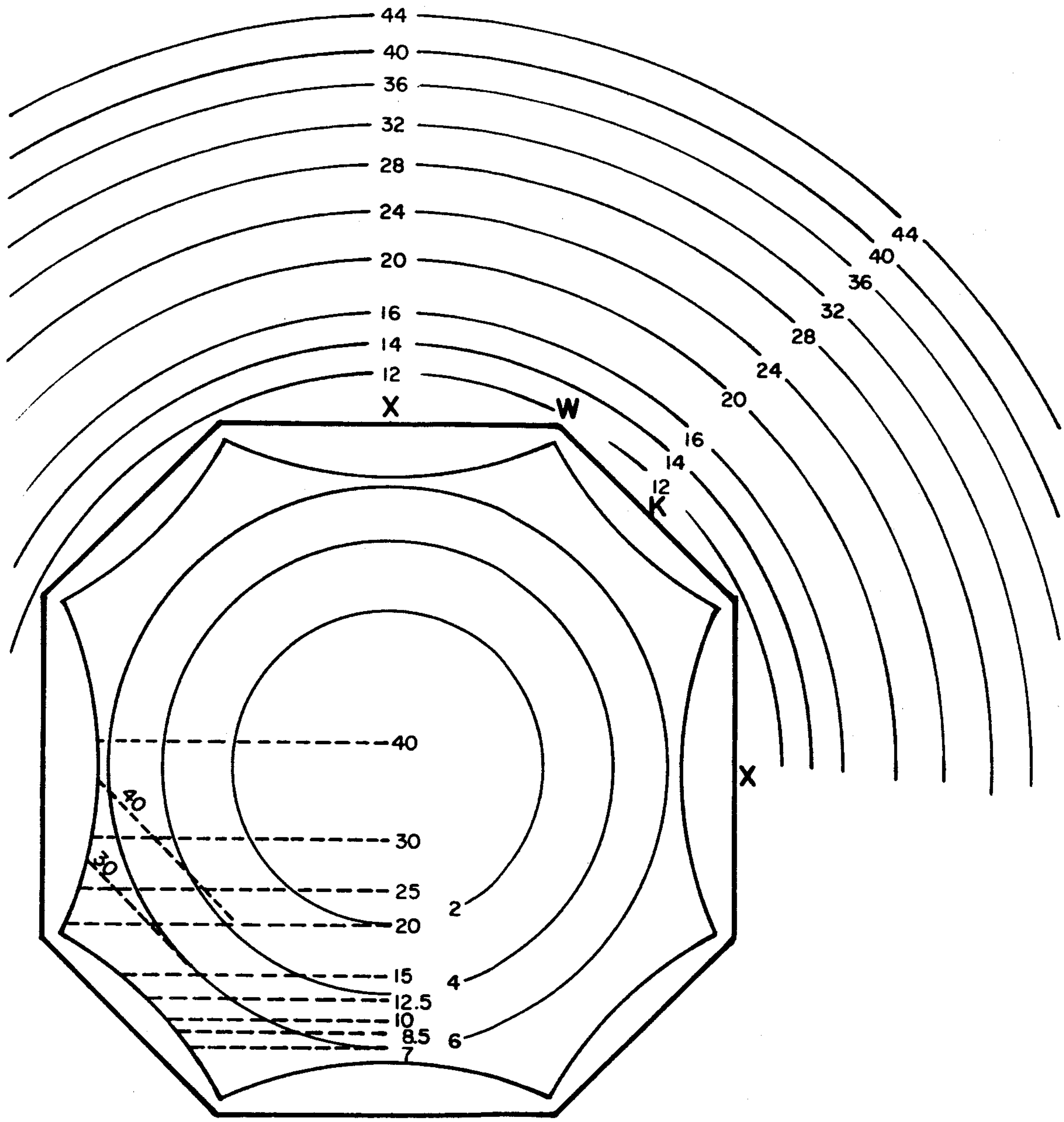

Figure 31
Fermi surface for aluminum.

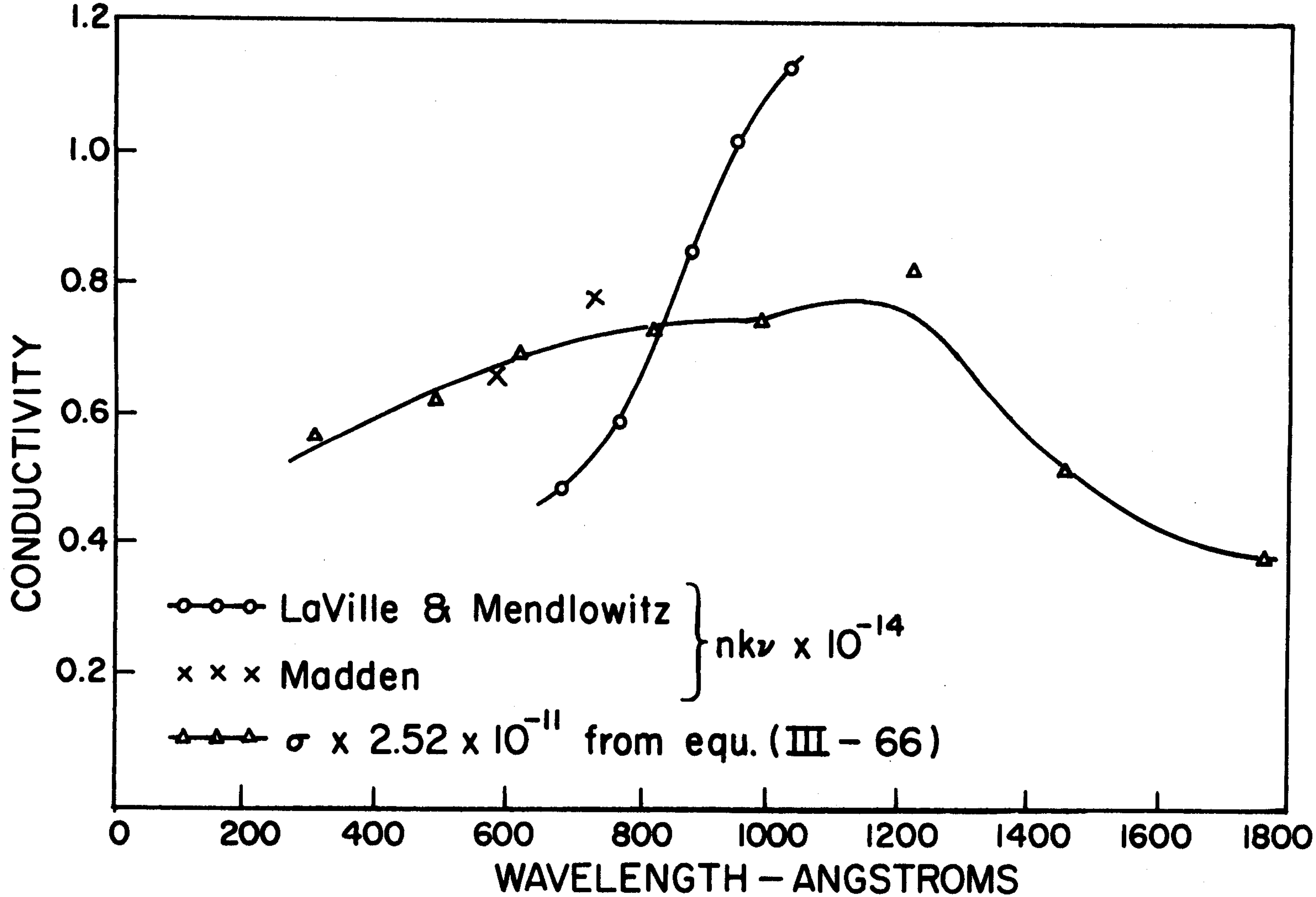

Figure 32

Conductivity of aluminum vs. wavelength.

TABLE XI

DATA USED IN ALUMINUM COMPUTATION
(EQUATION 66)

λ	$A(K_X)$	$A(K_L)$	$A(K_K)$	$\sum A(K)$	$\sigma/P \times 10^{-9}$
300	14.6	13.9	15.0	43.5	21.8
410	12.5	13.1	8.5	31.6	21.2
490	10.7	13.1	0.0	29.8	24.0
615	10.7	15.8		26.5	26.8
820	8.0	13.1		21.1	28.2
990	7.0	10.8		17.8	28.7
1230	6.0	10.0		16.0	32.1
1450	5.5	2.9		8.4	19.9
1760	5.1	0.0		5.1	14.7

silver and gold. The onset of conductivity attributable to interband transitions appears at approximately 2000A and there is no extension into the visible region.

It is difficult to appraise these calculations on the basis of experimental data. The difficulties associated with reflectivity measurements in the far ultraviolet are many[36,37] and the few results reported are not in harmony. The chief problem encountered in these measurements in the inclusion of oxygen atoms in the film during the process of evaporation and the rapid rate of surface oxidation of the film after evaporation of the aluminum. Results of the second effect are illustrated in Figure 33 where we see the rapid increase of the optical constants as the film ages in a vacuum chamber. An interesting aspect of these data is that although both n and k, and thus conductivity, increases with time, reflectivity decreases; these conditions are analogous to the example cited in Chapter II-A.

Included for comparison in Figure 32 are data obtained by LaVille and Mendlowitz[38] and by Madden.[39] If we use Madden's data as reference, a value for $P_{\vec{k}',\vec{k}}$ of 2.5×10^3 cm^{-2} is obtained, indeed a value much smaller than the 10^5 which resulted for silver and gold. If we apply Equation (6) in the form

$$E_{sp}(Al) = E_{sp}(Ag) \frac{P_{\vec{k}',\vec{k}}(Al)}{P_{\vec{k}',\vec{k}}(Ag)} \tag{7}$$

and use the average value of 3.7 ev. for $E_{sp}(Ag)$, we obtain an average $E_{sp}(Al)$ of 0.58 ev, which is in favorable comparison with 0.66 ev. as

---

[36] G. Hass, W. R. Hunter, and R. Tousey, J.O.S.A., 47, 1070, (1957).

[37] G. Hass, and J. E. Waylonis, J.O.S.A., 51, 719, (1961).

[38] R. LaVille and H. Mendlowitz, Phys. Rev. Lttrs., 9, 149, (1962).

[39] R. P. Madden, Private Communication.

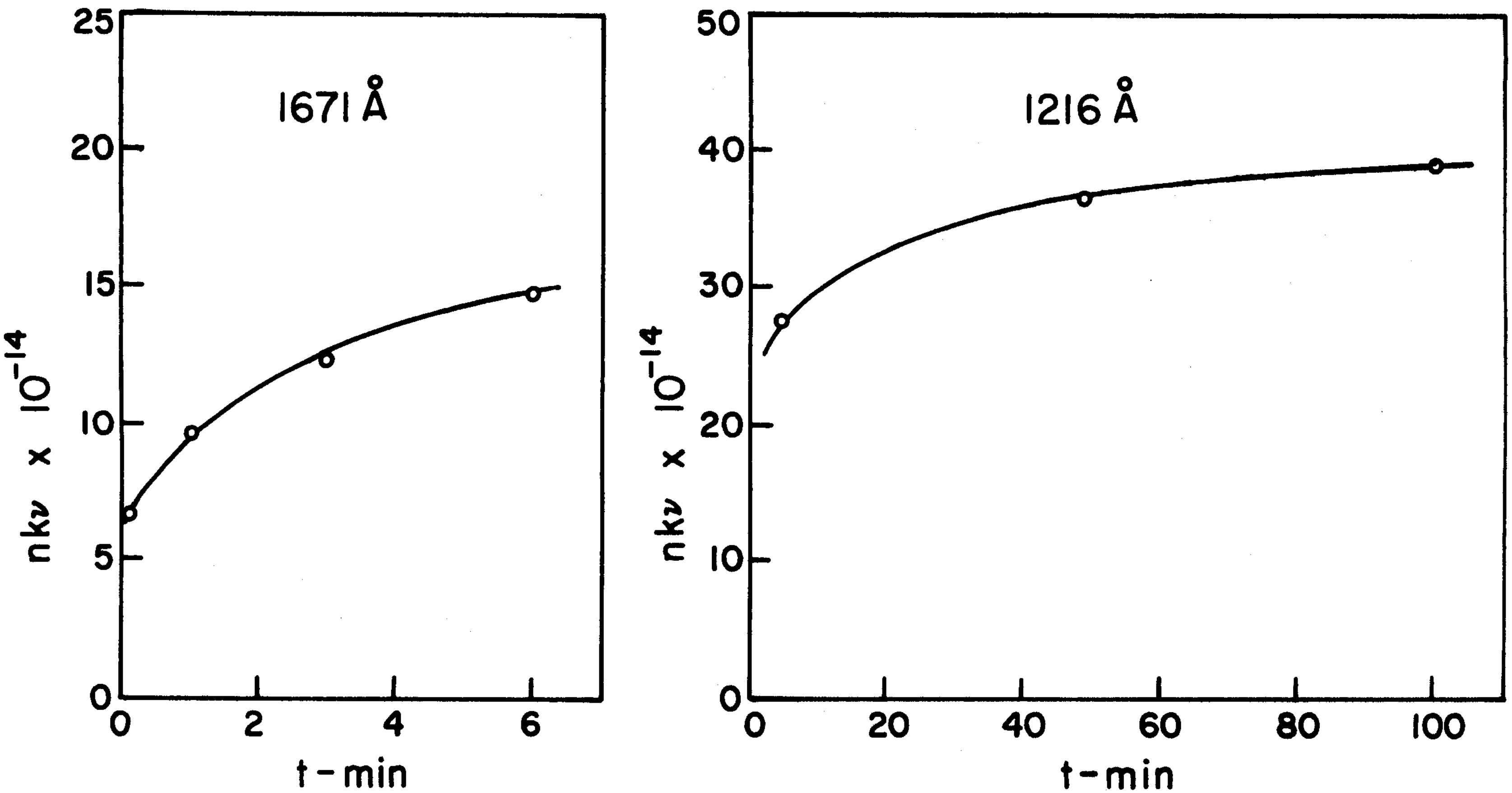

Figure 33
Conductivity of Aluminum film as a function of age of film.
Vacuum chamber pressure = 10^{-5} mm Hg.

calculated by Heine. Thus, it again appears that gap size is a major factor in the determination of interband transition probability.

F. Possible Future Work

Since so few metals have been studied in the far ultraviolet, future research in this area may proceed in several directions. It would be fruitful to measure the optical constants of other metals for which band structure calculations have been made and to continue the conductivity correlations made thus far. Improvement and refinement of experimental technique and equipment such that data could be obtained at many more wavelengths in the far ultraviolet would permit finer resolution of conductivity and band structure. Optical data can be a powerful tool when applied in this direction.

A continuation of the study of alloys is recommended. Many questions concerning the nature of metallic phase changes remain, but the use of optical properties and band structure analysis can provide further understanding of these problems. Since it appears that one effect of alloying is to modify the band structure, more information regarding this effect could lead to effective methods of varying and controlling reflectivity in the far ultraviolet. Applied to the design of optical instruments, such results would be of immediate importance.

CHAPTER V

EXPERIMENTAL APPARATUS AND METHODS

A. Monochromator and Reflectometer

The ultraviolet monochromator used in this work was constructed by Ball Brothers Research Corporation of Boulder, Colorado. The light source is a glow discharge between a hollow aluminum cathode and a copper slit anode, and the output consists of lines characteristic of the source gas used. Helium, neon, argon and hydrogen were used for the spectral lines reported. Mechanical details and photographs of this equipment are included in the thesis by Cole.[40]

Early in the course of these experiments it was discovered that a film of oil was being deposited on the diffraction grating and causing a reduction of output intensity and resolution. To reduce this problem the baffle immediately above the monochromator diffusion pump was fitted with a water jacket for cooling. This modification greatly reduced the grating problem but did not solve it completely.

Several modifications were made in the reflectometer and in its use. A large, semi-circular 35 mm film holder and its associated motor drive mechanism was removed from the reflectometer chamber in an effort to achieve lower pressures in the chamber. The automatic drive mechanism which had been used to move both the film under study and the detector in unison was disconnected and not used. It was felt that since data were needed at only four angles of incidence, greater precision would be obtained if the film and detector were positioned manually. In this manner, the metallic film was brought to the desired angle of

---

[40] T. T. Cole, Thesis, University of Colorado, 1961.

incidence, then the detector was adjusted to obtain a maximum indication of reflected light. Readings were taken at 70°, 50°, 30° and 10° and then repeated in the opposite order. An average was taken of the two sets of readings but if any two readings at the same angle differed by more than four per cent, the entire series was repeated.

The detector consisted of a nine stage photo-multiplier tube mounted on a movable, radial arm and its distance from the mirror was constant at all angles of reflection. The outer surface of the phototube envelope was coated with a solution of sodium salicilate in alcohol. After evaporation of the alcohol, a thin film of the phosphor remained on the envelope and converted the high energy u.v. photons to lower energy ones which could penetrate the glass envelope and reach the photocathode.

Other than the relocation of electrical ground points to reduce the noise level, no changes were made in the signal amplifier and recorder.

The physical geometry of the incident beam and detector assembly were such that a constant area, 25 mm by 6 mm, of the mirror was sampled for all the data reported.

B. Thin Film Production

Holland[41] discusses in considerable detail the effect of the rate of deposition on film homogeniety. He includes micro-photographs to show that a slowly deposited silver film, for instance, does not have a fully connected structure. At a deposition rate of 25A per minute a silver film displays discontinuities and fissures on its surface and these are separated by approximately 0.1 microns. However, for deposition rates of 100A per second, very few of these discontinuities appear and a more uniform surface results. In all cases, photographs and x-ray

---

[41] L. Holland, Vacuum Deposition of Thin Films, John Wiley and Sons, New York, 1950.

studies indicate that thin films made by evaporation techniques consist of an aggregate of microcrystals, randomly oriented. Thus, even a beam of plane polarized radiation incident upon such a surface meets crystal structure with a random assortment of angles.

To meet the requirements of deposition rate suggested by Holland, a high speed evaporation system, which approached "flash" evaporation, was devised. The heat source consisted of braided 15 mil, tungsten wires or a small molybdenum boat through which a large electrical current was passed. The sources were supplied by a 5 volt, 110 ampere transformer whose primary was excited by a Variac. Temperatures on the order of 2500°C could be achieved with this apparatus, and deposition rates of 1000A per second.

Gold, aluminum, and the gold-aluminum alloys were evaporated from the tungsten filaments since both these metals wet tungsten when in their melted state. Silver, however, forms a contact angle greater than 90° with tungsten and must be evaporated from a container such as the molybdenum boats. Purity of all metals used exceeded 99.95%.

Normal procedure in all evaporations was to slowly increase heater temperature until the melting point of the metal or both components of the alloy was reached; sputtering of the evaporant was avoided by this precaution. After the metals were completely melted, full power was applied to the heater and maintained until all the evaporant had left the heater. An opaque film at least 2000A thick could be produced in two seconds with this technique. Film thickness was determined from a measure of the weight of evaporant placed in the heater and relative distances between heater and film.

The data presented by Holland show that at these high rates of evaporation, both phases of the Au-Al and Ag-In alloys leave the heater at approximately the same rate and produce a homogeneous film. To be assured of this feature, reflectivity measurements were made immediately after evaporation of the alloys, the films were then annealed in situ at approximately 400°C for three hours, and reflectivity measurements were repeated. Deviations between measurements before and after annealing did not exceed the normal experimental error of measurement, and it was assumed that homogeneous films had been attained.

All the data reported here were taken immediately after evaporation in situ, and evaporations were conducted at chamber pressures between $8X10^{-6}$ and 10^{-5} mm Hg.

C. Data Reduction and Analysis

Determination of n and k from the reflectivity data was made with the use of the charts prepared by Cole and based on the graphical method suggested by Tousey.[42] (This method is discussed in Chapter I.) The degree of polarization of the incident beam at various wavelengths was in agreement with that encountered by Cole.

A reflectivity measurement in situ was found to be reproducible to within ± 2% for intense source lines and ± 3% for the weaker lines. Comparison between measurements of two different films of the same material and at the same wavelength indicate an element of error of the same order of magnitude.

To investigate the effect of errors in reflectivity on the nk product and conductivity, the reflectivity data for silver at 1671A were adjusted by ± 5% and a family of n-k curves was obtained for both adjustments as shown in Figure 34. It is seen that the effect of introducing such an error in the reflectivity data is to greatly increase the spread of intersections of these curves. The average nk product was also changed as shown and the errors introduced in conductivity were - 6.9% and + 3.5% for the + 5% and the - 5% changes in reflectivity respectively. Had an error been made in reflectivity at only one angle of incidence, three of the n-k curves would still have intersected at a

---

[42] R. Tousey, op. cit.

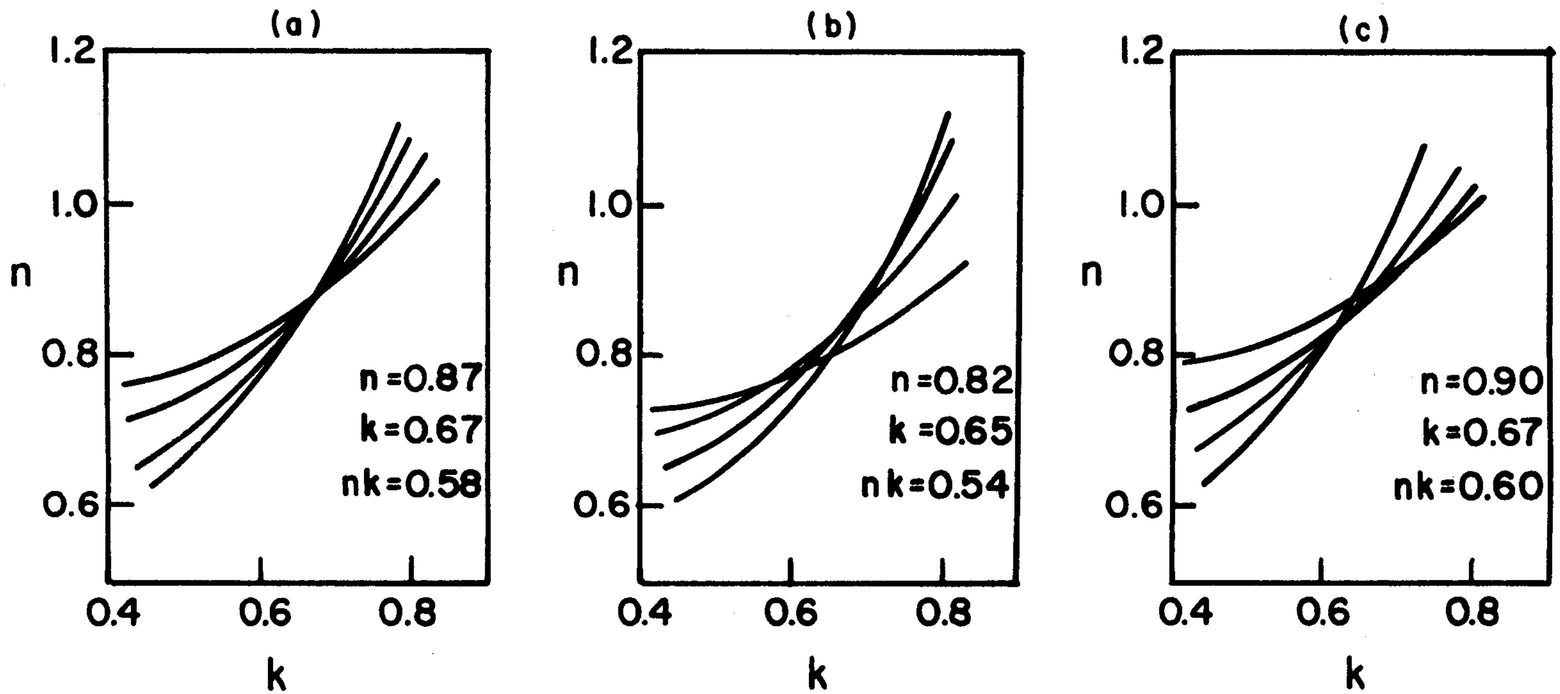

Figure 34
Effect of errors in reflectivity on n-k curves for silver at 1671A.
(a) n-k from measured reflectivity data
(b) n-k from reflectivity adjusted + 5%
(c) n-k from reflectivity adjusted - 5%

near common point as in Figure 34-a. It is apparent that such errors in reflectivity lead to multiple solutions of the Fresnel equations for n and k.

To minimize such errors, reflectivity data had to meet the following criterion to be considered valid for calculation of conductivity. The nk product was determined for each of the six possible intersections of the four n-k curves. These products were averaged arithmetically and the deviation of each product from the average was calculated. If the deviation for any one intersection exceeded 5% of the mean, these reflectivity measurements were discarded. With these restrictions and with the reproducibility of measurements given earlier, the error in conductivity at any wavelength does not exceed 5% of the reported value. It should be noted that of approximately one hundred nk products determined in this manner, only six had to be rejected as possibly invalid.

BIBLIOGRAPHY

Biondi, M. A. and Rayne, J. A., Phys. Rev., 115, 1522 (1959).

Bohm, D., Quantum Theory, Prentice-Hall, Inc., Englewood Cliffs, N. J.

Bouckaert, L. P., Smoluchowski, R., Wigner, E., Phys. Rev., 50, 58 (1936).

Callaway, J., Solid State Physics, Vol. 7, Academic Press, New York, 1958.

Cohen, M. H. and Heine, V., Adv. in Phys., 7, 395 (1958).

Cole, T. T., Thesis, University of Colorado (1961).

Ehrenreich, H. and Philipp, H. R., Phys. Rev., 128, 1622 (1962).

Hagen, E. and Rubens, H., Ann. Physik, 14, 936 (1904).

Hansen, M., Constitution of Binary Alloys, McGraw-Hill Book Co., Inc., New York, 1958.

Harrison, W. A. and Webb, M. B., The Fermi Surface, John Wiley and Sons, Inc., New York, 1960.

Harrison, W. A., Phys. Rev., 118, 1182 (1960).

Hass, G., Hunter, W. R. and Tousey, R., Jour. Opt. Soc. Amer., 47, 1070 (1957).

Hass, G. and Waylonis, J. E., Jour. Opt. Soc. Amer., 51, 719 (1961).

Heine, V., Proc. Roy. Soc. London, A240, 361 (1957).

Kittel, C., Introduction to Solid State Physics, John Wiley and Sons, Inc., New York, 1956.

LaVille, R. and Mendlowitz, H., Phys. Rev. Letters, 9, 149 (1962).

Madden, R. P., private communication.

Morse, R. W., Myers, A. and Walker, C. T., J. Accous. Soc. Amer., 33, 699 (1961).

Panofsky, W. K. H. and Phillips, M., Classical Electricity and Magnetism, Addison-Wesley Pub. Co., Reading, Mass., 1955.

Rayne, J. A., Phys. Rev., 108, 22 (1957).

Rayne, J. A., Phys. Rev., 110, 606 (1958).

Reitz, J. R., Solid State Physics, Vol. 1, p. 30, Academic Press, New York, 1955.

Segall, B., General Electric Report No. 61-RL-(2785 G), 1961.

Seitz, F., The Modern Theory of Solids, McGraw-Hill Book Co., New York, 1940.

Schiff, L. I., Quantum Mechanics, McGraw-Hill Book Co., New York, 1955.

Tousey, R. J., Jour. Opt. Soc. Amer., 29, 235 (1939).

Whittaker, E. T. and Watson, G. N., Modern Analysis, Amer. Ed., Cambridge U.P., New York, 1943.

Wilson, A. H., The Theory of Metals, Cambridge University Press, 1936.

Worsley, B. H., Proc. Roy. Soc. London, A247, 390 (1958).

Ziman, J. M., Adv. in Phys., 10, 13 (1961).